République algérienne démocratique et populaire

Ministère de l'Enseignement supérieur et de la Recherche scientifique

Université d'El Oued

Faculté de technologie

Laboratoire de génie électrique et des énergies renouvelables d'El-Oued

(LGEERE)

Thèse de doctorat

Soumise en vue de l'obtention du doctorat (LMD)

Domaine : Génie électrique

Spécialisation : Réseaux électriques

Etude des techniques de contrôle dédiées aux systèmes micro-réseaux en présence des sources d'énergies renouvelables

Présenté par :OUASSA Mohammed Lamine

Soutenue le [Jour/Mois/Année], en présence du Jury d'Examen :

Nom	Rang	Affiliation	Rôle
LABBI Yacine	MCA	Université d'El Oued	Président
BESSOUS Noureddine	Professeur	Université d'El Oued	Directeur de thèse
BORNI Abdelhalim	Directeur de recherche	Centre de recherche Ghardaia	Co-Directeur
SERHOUD Hichem	Professeur	Université d'El Oued	Examinateur
RACHEDI Mohamed Yacine	MCA	Université Ouargla	Examinateur
MEGHERBI Ahmed Chaouki	Professeur	Université de Biskra	Examinateur
MIDA DRIS	MCA	Université d'El Oued	Examinateur
MAMMERI Oussama	MAA	Université d'El Oued	invitée

Année académique : 2025-2026 / 1447-1448 AH

People's Democratic Republic of Algeria

Ministry of Higher Education and Scientific Research

University of El Oued

Faculty of Technology

Laboratory El-Oued Electrical Engineering and Renewable Energy

(LGEERE)

A Doctoral Thesis

Submitted in Fulfillment of the Requirements for Degree of Doctor (LMD)

Field: Electrical Engineering

Specialization: Electrical Networks

Study of control techniques dedicated to micro-grid systems in the presence of renewable energy sources

Presented by: OUASSA Mohammed Lamine

Defended on [Day/Month/Year], in the presence of the Examination Committee:

Name	Rank	Affiliation	Role
LABBI Yacine	MCA	University of El Oued	Chair
BESSOUS Noureddine	Professor	University of El Oued	Supervisor
BORNI Abdelhalim	Research Director	Ghardaia Research Center	Co- Supervisor
SERHOUD Hichem	Professor	University of El Oued	Examiner
RACHEDI Mohamed Yacine	MCA	University of Ouargla	Examiner
MEGHERBI Ahmed Chaouki	Professor	University of Biskra	Examiner
MIDA DRIS	MCA	University of El Oued	Examiner
MAMMERI Oussama	MAA	University of El Oued	Invited

Academic Year: 2025-2026 / 1447-1448 AH

DEDICATION

I dedicate my dissertation to my friends and family, with a particular sense of appreciation for my parents.

Ouassa Mohammed Lamine

Acknowledgement

In the name of ALLAH, the Most Gracious and the Most Merciful. Thanks to ALLAH who is the source of all the knowledge in this world, for the strengths and guidance in completing this thesis. I express my deep sense of gratitude and heart-felt thanks to my supervisor, Prof. **BESSOUS Noureddine***, and Prof.* **BORNI Abdelhalim** *for invaluable guidance, patience, kindness and consistent encouragement throughout the course of this work. I am very glad that I have pursued my doctoral studies under excellent supervision .*
I would like to express my appreciation to my thesis committee members: Dr. ***LABBI Yacine*** *,*
prof. ***SERHOUD Hichem*** *, Dr.* ***RACHEDI Mohamed Yacine*** *and prof.* **MEGHERBI Ahmed Chaouki** *,*
and Dr. **MIDA DRIS** *for their discussions, suggestions, and feedbacks to improve my thesis.*

I would like to thank Dr. ***MAMMERI Oussama*** *for help and support*

Mohammed Lamine OUASSA

Table of Contents

List of Figures

List of Tables

List of Acronyms

RES	Renewable energy sources
AC	Alternating Current
ANN	Artificial neural network
AI	Artificial intelligence
DC	Direct Current
FLC	Fuzzy logic control (controller)
IGBT	Insulated Gate Bipolar Transistor
INC	Incremental conductance
IncCon	Incremental conductance
MPC	Model Predictive Control
MPP	Maximum Power Point
MPPT	Maximum Power Point Tracking
NPC	Neutral-Point Clamped
P&O	Perturb and observe
VS-INC	Variable step-size incremental conductance
PSO	Particle swarm optimization
PV	Photovoltaic
P-V	Power-voltage
I-V	Current-voltage
P-I	Power -Current
V-I	Voltage - Current
PWM	Pulse Width Modulation
SVM	Space Vector Modulation
THD	Total harmonic distortion
VSI	Voltage Source Inverter
F-INC	Fuzzy logic control and Incremental conductance
F-P&O	Fuzzy logic control and Perturb and observe
MOSFET	Meta-Oxide semiconductor Field-Effect Transistor

List of Symbols

I_{pv} $I_{pv}(k)$	Output current of PV Array
i_{ph}	Photocurrent of the cell.
i_{sd}	Reverse saturation current of the diode.
V_{pv} $V_{pv}(k)$	Output voltage PV
p_{pv} $\mathrm{p}_{pv}(k)$	Output power of PV
$\Delta v_{pv}(k)$	PV voltage variation
$\Delta i_{pv}(k)$	PV current variation
P_A	Anod Pressure
P_C	Cathod pressure
V_{dc}, V_{dc-ref}	Measured DC link voltage & DC link Voltage reference
abc	Natural Frame quantities
$\alpha\beta$	Stationary frame quantities
θ	Grid voltage angle
T_S	Simpling Time
S	Control action of DC-DC converter
$S_{x,i}$	Switching state of phase $x = a,b,c$ $i = 1,2,...$
$i_{g\alpha.\beta-ref}(k+2)$	Predicted grid reference Current
v_g	Grid Voltage
SW_x	Number of switching change in inverter phase $x = a,b,c$
$\frac{d}{dt}$	Derivative operator
V_{dc-bus}	DC bus voltage
D	Duty cycel

General introduction

Like water, energy is a fundamental part of life for all living organisms. There are five main types of energy: mechanical, chemical, thermal, nuclear, and electrical. Among these, electrical energy is often considered the most important today, as it plays a central role in modern human life. Its key advantages lie in how easily it can be stored and transported.

Electricity has dramatically improved the quality of life and has been a driving force behind economic and social progress. As the world has industrialized, global electricity consumption has steadily increased—doubling in recent years. Despite technological advancements and shifting energy goals, fossil fuels such as coal, oil, and natural gas still dominate electricity production, even decades into the 21st century.[8]

These traditional sources of electricity have helped fuel population growth, technological development, and economic expansion. However, their use has also brought serious environmental and health challenges. The burning of fossil fuels releases large amounts of carbon dioxide, contributing to climate change, biodiversity loss, environmental degradation, and an increase in disease.[10]

At the same time, policies aimed at reducing emissions have driven up electricity costs and created imbalances, as efforts to cut carbon emissions are directly tied to how energy is produced and how quickly its demand is rising.

Over the past few decades, there has been a steady increase in the demand for clean, affordable, and renewable energy. This shift is largely driven by ongoing energy crises and growing concerns about environmental issues like global warming and pollution.[12]

Significant progress has been made in the development of sustainable energy sources, including biomass, hydropower, solar photovoltaic (PV) energy, and wind power. According to recent data [2], renewable energy sources now contribute about 29.9% of the world's total electricity generation.

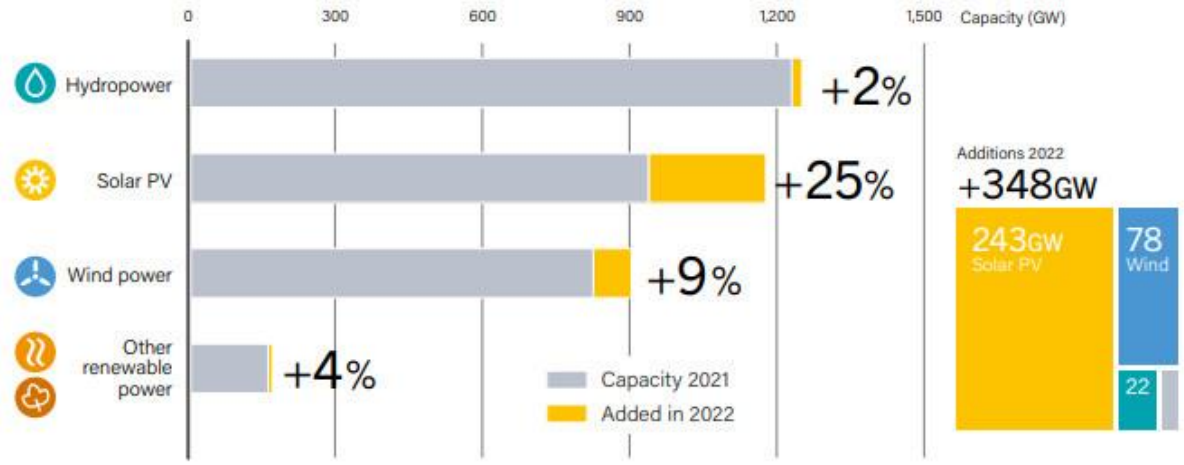

Fig.I.1. Renewable Power Total Installed Capacity and Annual Additions[2]

The global energy transition is not just focused on generating electricity, but also on advancing specific technologies within the power sector. As of 2022, the majority of new renewable energy capacity came from solar PV and wind power together making up 92% of the additions that year. In total, 348 gigawatts (GW) of renewable capacity were added in 2022, which marks a 13% increase compared to the 306 GW added in 2021, as shown in Fig.I.1. [2].

Motivation and objectives of a dissertation

The increasing global demand for renewable and environmentally friendly energy sources has positioned solar energy as a key player in the transition toward sustainable power generation. Among various renewable technologies, photovoltaic (PV) systems have gained widespread attention due to their scalability, low operating costs, and direct conversion of solar radiation into electricity. However, one of the main challenges in optimizing the performance of PV systems lies in efficiently harnessing the available solar energy, which fluctuates with changing environmental conditions such as irradiance and temperature. To address this, maximum power point tracking (MPPT) techniques are employed to ensure that the system continuously operates at its optimal power output.

This thesis focuses on the simulation and evaluation of an advanced MPPT strategy designed to enhance the energy-harvesting efficiency of PV systems. The proposed method integrates the well-established incremental conductance (INC) algorithm with fuzzy logic control, resulting in a hybrid technique referred to as FL-INC. By incorporating fuzzy logic, the system gains the ability to handle uncertainties and nonlinearities more effectively, improving the accuracy and dynamic responsiveness of the MPPT process—especially under rapidly changing atmospheric conditions.

In addition to refining the MPPT mechanism, the study also investigates the downstream power conversion process. The electrical power extracted from the PV panels at the maximum power point is routed to an inverter, which plays a critical role in converting direct current (DC) to alternating current (AC) suitable for grid integration. In this work, the inverter is controlled using a combination of Space Vector Modulation (SVM) and Model Predictive Control (MPC) methods. SVM provides efficient switching control, while MPC offers predictive decision-making capabilities, contributing to enhanced control performance, faster dynamic response, and reduced harmonic distortion.

Following the conversion process, the resulting AC power is transmitted to the electrical grid, making it available for residential, commercial, and industrial use. This step is vital for integrating clean solar energy into the broader energy mix and supporting the decarbonization of the power sector. The complete system—comprising the MPPT controller, inverter, and grid connection—is thoroughly evaluated through detailed simulations. Performance metrics such as energy yield, response to environmental variations, grid compatibility, and overall system stability are analyzed to validate the effectiveness and practicality of the proposed approach in real-world solar energy applications.

Dissertation organization

The present dissertation is structured into four chapters. Each chapter's work is succinctly summarized as follows:

Chapter I

The objective of this chapter is to describe the microgrids are small-scale, flexible power systems capable of operating both in connection with the main grid and independently in island mode. Their control and stability can be complex due to the influence of various dynamic factors. As part of the broader smart grid framework, microgrids contribute to energy resilience by maintaining power supply during grid disruptions. Typically integrated with the main transmission network, they often rely on renewable energy sources such as solar, wind, and biomass, positioning them as a vital component in the transition to sustainable energy systems.

Chapter II

The objective of this chapter is to describe the modeling of a photovoltaic (PV) energy system is fundamental for analyzing and optimizing its performance under varying environmental conditions. A PV system is typically modeled by representing the electrical characteristics of solar cells, which convert solar irradiance into electrical current. By using this equivalent circuit model, the output voltage and current of the PV module can be accurately predicted, enabling better control and integration with power electronics. Complementing the PV system, the boost converter a type of DC/DC converter is modeled to step up the variable DC voltage generated by the solar panels to a higher, regulated DC voltage suitable for load requirements or grid interfacing. Mathematical equations describing the energy storage in the inductor, the switching operation, and the voltage conversion process allow precise simulation of the converter's behavior. Together, these models provide a comprehensive framework for designing and simulating efficient solar power systems.

Chapter III

This chapter highlights the integration of key components in a photovoltaic (PV) energy system. The conventional Incremental Conductance (INC) and the Perturbation and Observation (P&O) methods are used to track the maximum power point (MPP) of the solar panel by continuously adjusting the operating voltage. A DC/DC boost converter follows, stepping up the variable voltage from the PV array to a stable level suitable for further conversion. To manage the final stage of energy delivery, an NPC (Neutral Point Clamped) inverter is employed, controlled by a Space Vector Modulation (SVM) strategy. SVM improves the inverter's switching efficiency and reduces output harmonics, enabling smoother AC power output and reliable grid interaction.

Chapter IV

This chapter outlines the proposed control system for enhancing the performance of a photovoltaic (PV) energy system. At its core is the FL-INC method, which combines fuzzy logic with the traditional Incremental Conductance (INC) algorithm to improve the accuracy and responsiveness of maximum power point tracking (MPPT), particularly under rapidly changing environmental conditions. The output of the PV system is regulated by a DC/DC boost converter, which increases the variable voltage from the solar panels to a stable level suitable for conversion. For the final power stage, a Neutral Point Clamped (NPC) inverter is used, controlled by a Model Predictive Control (MPC) strategy. MPC provides optimal control

decisions based on real-time system modeling, improving dynamic performance and grid compatibility. This integrated system aims to ensure efficient energy extraction, stable voltage regulation, and high-quality AC power delivery to the grid.

General Conclusions

This general conclusion provides a summary of the author's contributions and the general conclusion of the thesis. Furthermore, potential avenues for further research pertaining to the findings presented in this dissertation are proposed.

Chapter I: A micro-grid and renewable energy – A review study

1.Introduction

Microgrids are compact power systems that may operate in both island and grid modes. Controlling their stability and power balance could be challenging because a lot of factors affect them. Think of a microgrid as a self-sufficient power hub that can keep the lights on even if it's cut off from the main grid. It's part of the smart grid but works independently when needed. To stay reliable, it's hooked into the same transmission network as big power plants. Microgrids often use green energy sources like wind, solar, and biomass to generate power, making them a key player in sustainable energy solutions [1, 2].

2.Microgrid

2.1. Definition of micro-network

A microgrid is basically a mini version of a power grid that can operate on its own or stay connected to the main grid. The International Electrotechnical Commission calls it a "local electric power system" with smart features for automatic control. Think of it as a smart, self-managing power setup that can switch between working independently or alongside the larger grid [3].

A microgrid is like a local energy hub that handles generation, demand, and storage on a smaller scale. It usually covers a neighborhood or similar area, working mostly at low voltage but sometimes with high-power options for selling or storing energy [4]. Everything's connected through devices like converters and circuit breakers. It can operate independently if needed, whether for emergencies or planned reasons, and has to keep the power flowing smoothly. Its smart features mean it's designed to meet specific goals, often focusing on minimizing environmental impact Fig.1.1.

Transformation from passive to active control in electrical grids opens up new ways to manage energy. It allows local generation to feed into the main grid and helps balance energy supply with demand right at the user level. Power can flow both ways now: the grid not only supplies energy but can also receive it from microgrids, potentially benefiting economically [4].

Fig.1.1. Sources of power quality disturbances in microgrid [5] .

2.2. Elements of microgrid

2.2.1. Power Elements

In a microgrid, the power elements serve as both the source and the load of the power flow. We'll dive into each element separately to describe what it actually does and how to manage it in an efficient way.

2.2.1.1. Renewable Energy Sources

Microgrids with Renewable Energy Sources (RES), such as wind turbines or solar panels, have their limits because they rely on natural conditions. You can't always control how much energy they generate, which means sometimes energy is wasted. Still, it's useful to manage how much they contribute to avoid overloading the grid.

2.2.1.2. Micro sources

In a microgrid, controlled micro sources serve as the energy sources. They supply electricity to the Microgrid control system when needed. They present a compelling substitute for depending on the main grid during periods of high energy usage. Examples are Combined Heat Power (CPH) Units and Diesel Generators, each of which has inherent behaviors that call for certain control strategies.

Diesel generators take a while to start up because they must wait for the grid to supply the necessary energy. Large amounts of heat are produced by CPH units; this heat needs to be directed and utilized.

2.2.1.3. Storage Units

Storage units in a Microgrid are like your backup battery for power. As production is high, they store excess energy, which they then release as required. Controlling them is key for keeping energy levels balanced both now and later. The big things to watch are how quickly they can start supplying power and how much they can hold. Examples include Lead-Acid Batteries, Flywheels, and Hydrogen fuel cells.

2.2.1.4. Customers

Customers, within a Microgrid environment, are the consumers who the energy produced and regulated by the device is delivered to. They may be households, establishments, or other infrastructures based on the Microgrid as an assured and regular electrical energy source. Managing their needs and preferences is crucial for ensuring the Microgrid operates efficiently and meets demand effectively.

2.2.1.5. Main Grid

A microgrid can be viewed as a type of infinite energy storage because its main grid can act as a source or a load depending on what is most practical for the energy balance.However, the primary drawback of main grids is the associated economic costs, whereas the primary constraint of storage units is their capacity. Conversely, if energy is fed into the grid, less inexpensive revenue can be made available. Controlling the energy flow through the grid is therefore crucial.

2.2.2. Control Elements

A Microgrid's key feature is its capacity to manage power elements as a unified system. It needs a solid setup to handle everything from market transactions to the regulation of voltage and frequency. Regardless of how the Microgrid hierarchy is set up, the control system must typically complete two jobs, which are handled by the different controllers.

- The general distribution system's administration and control
- The control of one or a pack of power devices

2.2.3. Energy Management

Microgrid hierarchy configuration will essentially determine its energy management decision making. When it comes to Centralized control, all decisions are made at the MGCC; whereas in Decentralized control, The local MCs are tasked with the primary duty of moving and coordinating independently of the rest of the microgrid and won't receive the information on the grid. The general microgrid operation forms a very great part of the decision outcome.

2.2.3.1. Centralized Control

A centralized system can be used to manage the microgrid. manner by allocating all the planning to the MGCC which is the only one in charge of all decisions. Data forced to journey from every controller to a virtual mathematical area and as a consequence, it demands an increased infrastructure, also making it more complex due to the addition of the nodes to it. Alternatively, the control system is simple as long as the Decisions are made. with the complete knowledge of all the materials from all the local resources. Thus, the latter is the centralized approach that makes the decision faster and guarantees the efficient operation of the plant because it functions as a single body of many different nodes. The aforementioned data makes it evident that the centralized approach is additional appropriate for Microgrids With the same goal, as the sole entity makes the decisions.

2.2.3.2. Decentralized Control

The use of a Microgrid in a decentralized manner allows the autonomous control of each power element to the local controllers. For the MC, this is considered a “case” [4]. The many-agent system consists first of all of local controllers which are organized to the MC by the data networks. The Systems cooperate. through the communication with a master controller the MGCC concurrently, a task is divided across the agents. Finally, a self-aware will agent can be given a task of physical control, but it can also be something else This implies that it has the authority to decide that next operations are executed the way it wants. An action taken on one part will affect others, which will in turn mean that others have to adjust as well.

2.2.4. Control Algorithms

Control algorithms are the essence of the system which is the main component of the microgrid, as they calculate a solution from the initial data sent from the module. The algorithm is for the best handling of the distribution grid, in the short term or long term, however, the final solution may be not optimal since there are practical limitations of customer limitations, infrastructure, and processing speed, among other factors that might not be fully considered [6].

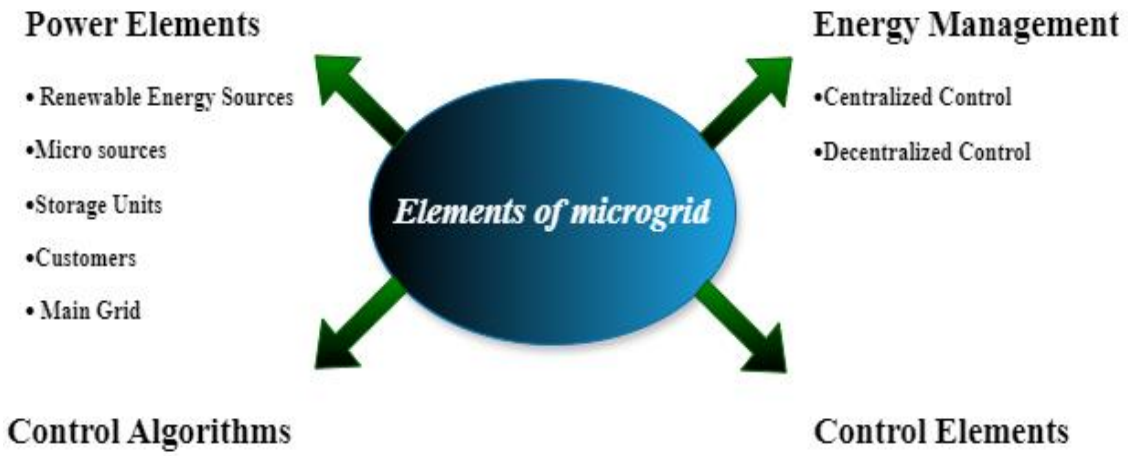

Fig.1.2. Elements of microgrid.

3. Classification of microgrid

Microgrids can be classified based on several criteria including their connection to the main grid, type of energy sources, control architecture, and application domain. Here's a breakdown of the common classifications:

3.1. Classification according to distribution network

DC Microgrid: Monopolar, bipolar or homopolar AC Microgrid: Single phase, three phase 3F or 4F

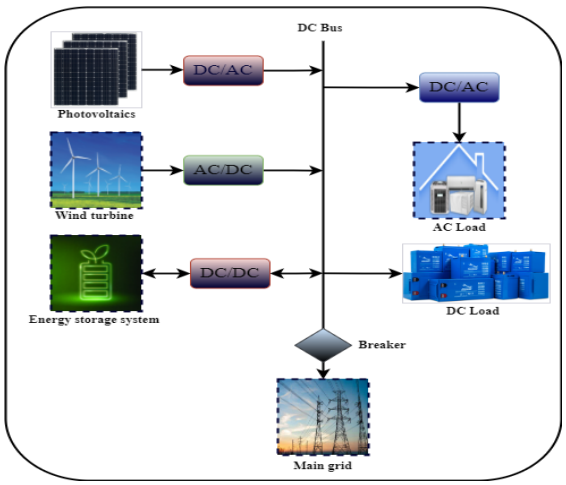

Fig.1.3. DC Microgrid

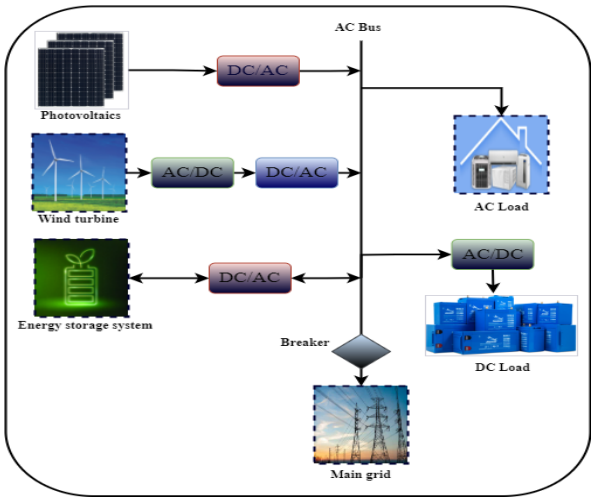

Fig.1.4. AC Microgrid

- Hybrid microgrid, DC and AC

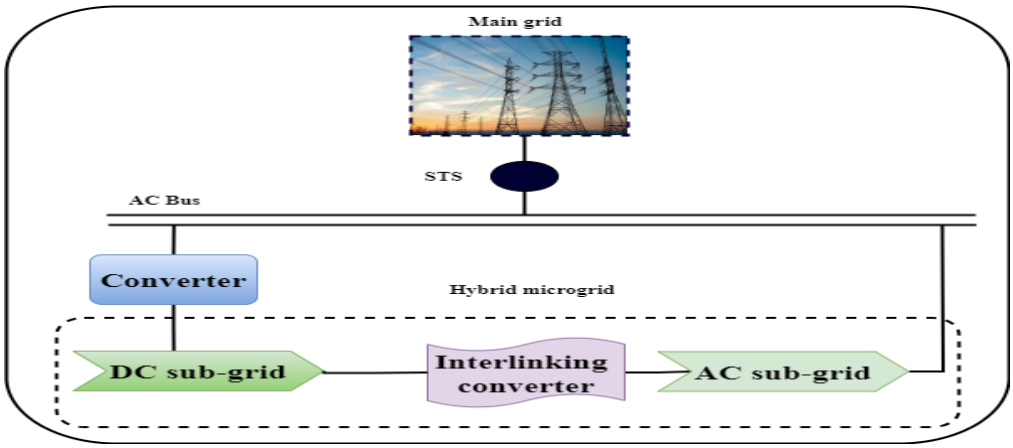

Fig.1.5. Hybrid Microgrid

3.2. Classification: According to size

- Single Plant: <2 MW - Small individual plants with multiple loads, such as schools or hospitals.
- Multiple Plants: 2-5 MW - Small to large traditional plants with local loads exclusively C&I*. [Commercial & Industrial.]
- Feeder: 5-20 MW - Small to large traditional plants with many or large local loads, typically C&I.
- >20 MW substation: a conventional plant with numerous heavy local loads. residential and C&I.
- Rural Electrification: Rural communities throughout North America and Europe, as well as in many rising economies such as China, Brazil, India, and others.

3.3. Classification: According to the "Function" of MG

1: MG for backup only

- only functions while the main grid is unavailable.
- Generation is only sized to handle essential loads.

2: MG to supply an isolated area

- A system that is distant from the main grid, for example, is never connected to it.
- possesses enough local generation to meet all local demands.

3: Hybrid MG for economic reasons

- Operates partly connected to the grid and partly disconnected
- Mode of operation: based on elements like expenses and main grid breakdown, fuel supply, etc.
- possesses enough local generation to meet all of the critical local loads, at a minimum

4. Benefits of microgrids

Customers, utility operators, and the environment all gain from microgrids in a number of ways. Micro-grids were presented as the potential solution for the widespread deployment of more electricity sources with zero emissions that would subsequently bring down emissions of greenhouse gases. Distributed, controllable generation, such natural gas-fueled combustion

turbines, can be balanced with non-controllable renewable power sources, like solar, by using a microgrid manager (local energy management system). Batteries and energy storage in electric cars are other techniques that they can use for balance between production and consumption in the microgrid[7].

Microgrids increase the potential of recovering energy that is normally lost through the line losses and heat that normally rises through exhaust stacks. Distance is power's enemy regarding the transmission of electricity. Almost 6% of the electricity on average is actually wasted during the process of overhead power wiring. Some of it is power cables, but about 2‰ is the meter. For this issue, a dense neighborhood area, the power is readily available only from the neighboring device. Microgrid electricity comes to life just adjacent to its intended application (referred to as scattered generating), therefore, we have hardly any line losses and the most part of the same level demand are met with reduced power. Furthermore, conventional power production that involves fossil generation and nuclear reactors among others causes a significant amount of heat to be released. This is because the electricity is responsible for a significant portion of the heat energy that is released. Generation machines running during these peak load times.

The heat that is produced is typically radiated off into the atmosphere, not used for any productive purposes. As power is produced at the sources near the users, the heat from the power plants can be effectively utilized for several objectives, thereby increasing the total amount of energy use is decreased. The utilization of heat from the power plant at the site powered by the end users overcomes the economic barriers of using heat energy thus, Water may be efficiently heated using it, and space heating in homes and businesses, which will, in turn, reduce greenhouse gas emissions [7].

By enhancing local control over Microgrids can assist utilities in delaying costly investments in new power generation by balancing electricity supply and demand. Microgrids can help control or lessen electricity demand and ease grid congestion when placed strategically inside the electrical system. This lowers electricity rates and lowers the need for peak power. Microgrids can assist delay or prevent investments in additional electric capacity (such as Transmission lines, energy storage, substations, "peaker" plants, and other infrastructure) while also enhancing system efficiency and reliability. When linked to the local transmission or distribution network, microgrids can also trade from a single node to export excess power or import imbalances from the surrounding system[6].

Microgrids can help the power grid deal with more extreme weather and cyber-attacks. The microgrid is the smallest form of power generation, which is continuous power supply on a building, neighborhood, or a city scale, even if the surrounding microgrid goes weak. This describes the microgrid functioned detached from the rest of the system, and the concept is called islanding. An islanded grid can also help to restore a microgrid during a system failure, albeit indirectly, through allowing services needed by the restoration crews, or directly, through re-energizing the grid [8].

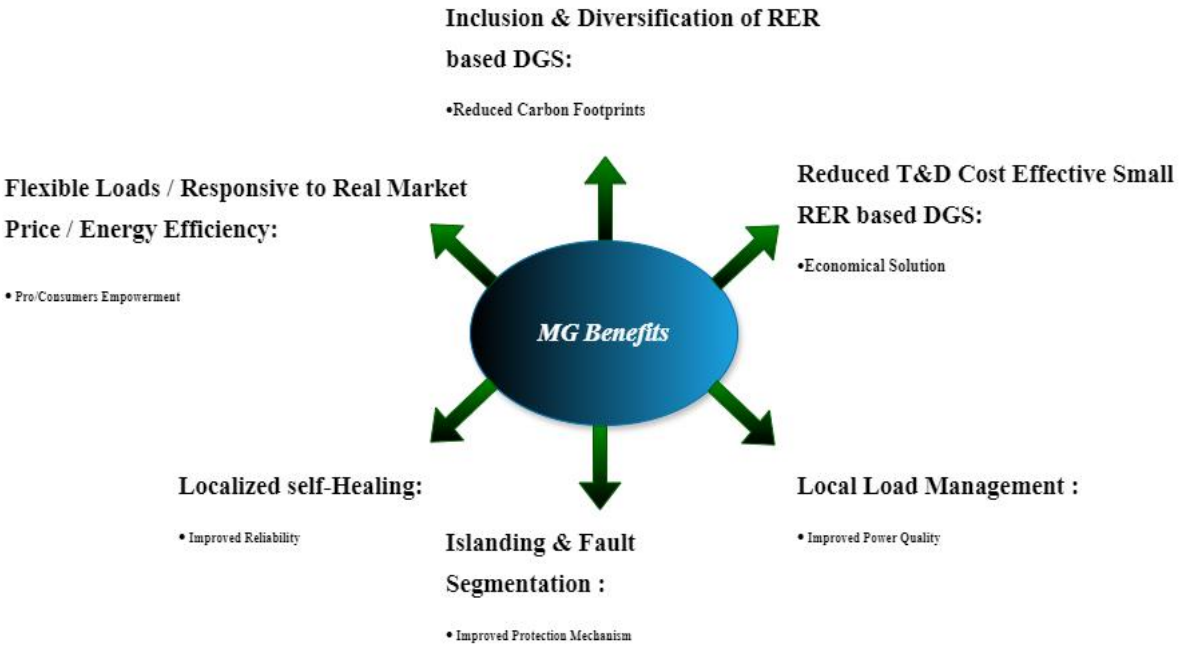

Fig.1.6. Micro-grid benefits.

5. Comparisons of power grid structures

Table.1.1. Advantage and disadvantage of grid [8].

	Advantage	Disadvantage
Conventional grid	• Low capital intensiveness as extra expenses on There are fewer power converters and EMCS devices. • established guidelines and policies for the operation of the system	• The occurrence of fault in transmissions involves the areas of the grid which are in a large scale, and it can cause instability in the system and cause cascading blackouts. • The process of black-start operation, which is laborious and convoluted • Less efficient in the cases of DERS • Given the high operational cost of older power plants for which maintenance is getting more and more expensive • Increase in the complexity of operation coordination • Enough money to be allocated to develop remote areas
Microgrid	• The technique of isolating in the event that the main grid malfunctions is better for the microgrid's resilience and dependability. • Such a function is possible due to drones using renewable energy which makes them highly portable. • Such a system can provide the operator with ancillary services like support for voltage and frequency. • Higher system effectiveness • Better handling of instability caused by quicker dynamic reaction of DER and EMCS • Smaller network and DER, hence cheaper to maintain and faster to restore • High efficiency due to increased system utilization and demand response which is also helped by the deployment of digital transformers and DER.	• Often times it is necessary to use intricate and costly defense tactics. • The ability to be independent during power outages requires an increase in capacity for generating and storage. • Because power converters and controllers are being used more frequently, their cost is rising. • The system operation has relatively fewer well-known standards and other regulations.

6. Renewable energy

6.1. Definition Renewable Energy

Renewable energy comes from the sun, wind, rain, tides, and geothermal heat, among other natural resources. These materials may be found naturally restored and are renewable. As a result, unlike finite traditional fossil fuels, these resources might be regarded as almost limitless.[9]. Clean and renewable energy sources are growing and developing thanks to a renewed push from the global energy crisis.

Worldwide, organizations are adopting Development Mechanisms (CDMs) [10].

The pollution caused by burning fossil fuels is a significant reason opposing fossil fuels, in addition to the world's rapidly depleting fossil fuel sources. On the other hand, compared to its conventional equivalents, Renewable energy sources are known to produce energy without the harmful effects of pollution and to be substantially cleaner.

6.2. Different sources of Renewable Energy

6.2.1. Solar power

The origin of solar power The utilization of solar energy source that British astronomer John Herschel [11] is famous for. Was who, by the way, famously demonstrated the use of solar heat collectors for cooking while in Africa. The sunlight is the most readily available and utilizable form of energy on our planet. The sun's energy resource can be divided into two parts.

Firstly, the heat that comes from solar energy can be utilized to heat spaces using solar thermal energy, for example. In a different way, the solar power plants can convert the sun's light energy into electricity, the most widely used form of energy. Only solar photovoltaic cells [12] or concentrated solar power plants may make this happen. [Exceptional content that adheres closely to all guidelines and focuses on all specified content objectives while maintaining the HTML elements and content structure]

6.2.2. Wind power

Wind turbines are devices that are adapted to utilize the power in breezes. Today’s turbines have a power output of between 600 kW and 5 MW [13] . Given that the third power of the wind speed linearly correlates with the power, it quadruples if the wind is faster by one unit. The Aero Dynamically wind turbines have a smaller drag along with a greater lift as opposed to the earlier wind turbines.

6.2.3. Small hydropower

Hydropower plants with a capacity of up to 10MW are the so-called small hydropower and they are rated as renewable energy sources [14]. These methods involve turning the potential energy of water that is accumulated in dams/barrages/hydropower plants (DHP) into renewable electrical energy via water turbines. Run-of-the-river hydropower generates hydroelectricity that does not require huge energy storage in the form of reservoirs or dams

6.2.4. Biomass

Photosynthesis is the process of plants catching the sun's radiation and turning it into energy. On combustion, these plants release the trapped energy. Thus, biomass energy acts as a natural battery that stores solar energy [15].

6.2.5. Geothermal

The thermal energy known as geothermal energy is expelled below the earth's crust or is stored there. It is this gradient that causes the core of the earth to conduct heat constantly to the earth's surface. Additionally, water may be heated to the point of superheated steam using the gradient, which can then power steam turbines to generate energy. Despite its many benefits, geothermal energy is typically only found in regions close to tectonic plate borders. and only a few regions, but the recent developments in the technology have led to the spreading of the geothermal power plant around the world.

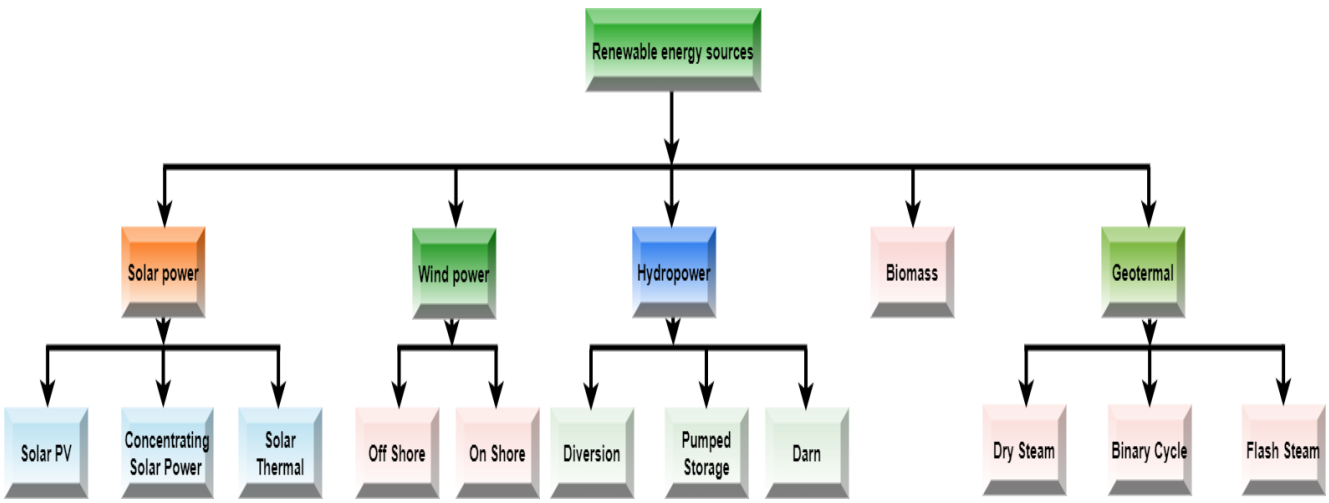

Fig.1.7. Main renewable energy source.

7. Estimated renewable energy share of total final energy consumption

Over the past 30 years, renewable energy systems have significantly improved in terms of efficiency and cost[16]. In present times, a great deal of the global Renewable energy sources are the foundation of new electricity producing capability [17]. Various clean technologies with renewable energy sources, initially the expensive ones such as solar and wind energy, have achieved massive price declines in the last ten years, which allowed them to become eventually cheaper than their fossil fuel competitors [18]. In most of the Currently, the least expensive new-build electricity sources in countries are photovoltaic solar or onshore wind[19]. For the years from 2011 to 2021, the percentage of renewable energy in global electricity production went

from 21.3% to 29.9%. Most of the part was gained from the sun and the wind with the number of both going from a combined 2.8% to 12.1%. The fossil energy consumption fell from 68% to 61% [20]. In 2022, renewable resources captured According to the U.S. Energy Information Administration (EIA) and the International Renewable Energy Agency (IREA), they will account for 30% of the world's energy output and more than 42% by 2028 [21, 22]. Renewable energy sources already account for more than 20% of the energy supply in many nations, with some even generating more than half or all of their electricity resources [23, 24].

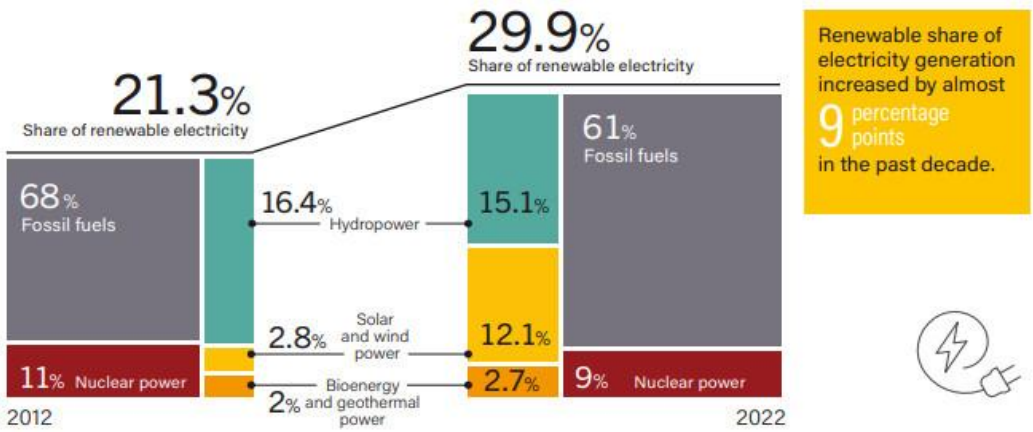

Fig.1.8. Estimated renewable energy share of total final energy consumption [2].

Chapter I: A micro-grid and renewable energy – A review study

8. Comparisons of renewable energy and conventional

Table.1.2. renewable energy and conventional [25].

	Renewable energy supplies (Green)	Convictional energy supplies (Brown)
Examples	Wind, solar, biomass, tidal	Coal, oil, gas, radioactive ore
Source	Natural local environment	Concentrated stock
Normal state	A current or flow of energy. An income	Static store of energy. Capital
Initial average intensity	Low intensity, dispersed: ≤300 W m-2	Released at ≥100kWm-2
Lifetime of supply	Infinite	Finite
Cost at source	Free	Increasingly expensive.
Equipment capital cost perkW capacity	Expensive, commonly ≈US$1000 kW-	Moderate, perhaps $500 kW without emissions control; yet expensive >US$1000 kW with emissions reduction
Variation and control	Fluctuating; best controlled by change of load using positive feedforward control	Steady, best controlled by adjusting source with negative feedback control
Location for use Scale	Site- and society-specific Small and moderate scale often economic, large scale may present difficulties	General and invariant use Increased scale often improves supply costs, large scale frequently favored
Skills	Interdisciplinary and varied. Wide range of skills. Importance of bioscience and agriculture	Strong links with electrical and mechanical engineering. Narrow range of personal skills
Context	Bias to rural, decentralized industry	Bias to urban, centralized industry
Dependence	Self-sufficient and 'islanded' systems supported	Systems dependent on outside inputs
Safety	Local hazards possible in operation: usually safe when out of action	May be shielded and enclosed to lessen great potential dangers; most dangerous when faulty
Pollution and environmental damage	Usually little environmental harm, especially at moderate scale Hazards from excess biomass burning Soil erosion from excessive biofuel use Large hydro reservoirs disruptive Compatible with natural ecology	Environmental pollution intrinsic and common, especially of air and water Permanent damage common from mining and radioactive elements entering water table. Deforestation and ecological sterilization from excessive air pollution Climate change emissions
Aesthetics, visual impact	Local perturbations may be unpopular, but usually acceptable if local need perceived	Usually utilitarian, with centralization and economy of large scale

9. conclusion

Microgrids are becoming essential in today's energy environment, particularly when it comes to advanced energy storage systems, renewable energy sources, and the expanding trend of electrifying transportation. However, ensuring ideal power quality becomes difficult when DG units are included. High PQ is neither a necessity for compliance nor a prerequisite for the proper and effective operation of microgrid electrical systems and devices. The second chapter will cover electricity generation from solar panels and the small-scale integration of solar energy into the microgrid.

Chapter I: A micro-grid and renewable energy – A review study

Reference

[1] O. Palizban and K. Kauhaniemi, "Microgrid control principles in island mode operation," in *2013 IEEE grenoble conference*, 2013: IEEE, pp. 1–6.

[2] W. Al-Saedi, S. W. Lachowicz, D. Habibi, and O. Bass, "Power flow control in grid-connected microgrid operation using Particle Swarm Optimization under variable load conditions," *International Journal of Electrical Power & Energy Systems,* vol. 49, pp. 76–85, 2013.

[3] N. C. V. DUARTE, "Estudos baseados na IEC 61850 90-17 para Monitoramento e Proteção em Eventos de Qualidade de Energia em Geração Distribuída."

[4] N. Hatziargyriou, *Microgrids: architectures and control*. John Wiley & Sons, 2014.

[5] S. Sepasi, C. Talichet, and A. S. Pramanik, "Power quality in microgrids: A critical review of fundamentals, standards, and case studies," *IEEe Access,* vol. 11, pp. 108493–108531, 2023.

[6] A. C. Z. de Souza and M. Castilla, *Microgrids design and implementation*. Springer, 2019.

[7] M. A. Jirdehi, V. S. Tabar, S. Ghassemzadeh, and S. Tohidi, "Different aspects of microgrid management: A comprehensive review," *Journal of Energy Storage,* vol. 30, p. 101457, 2020.

[8] M. Roslan, M. Hannan, P. J. Ker, and M. Uddin, "Microgrid control methods toward achieving sustainable energy management," *Applied Energy,* vol. 240, pp. 583–607, 2019.

[9] A. M. Abdelshafy, J. Jurasz, H. Hassan, and A. M. Mohamed, "Optimized energy management strategy for grid connected double storage (pumped storage-battery) system powered by renewable energy resources," *Energy,* vol. 192, p. 116615, 2020.

[10] M. Alanazi, M. Mahoor, and A. Khodaei, "Co-optimization generation and transmission planning for maximizing large-scale solar PV integration," *International Journal of Electrical Power & Energy Systems,* vol. 118, p. 105723, 2020.

[11] P. Das, P. Mathuria, R. Bhakar, J. Mathur, A. Kanudia, and A. Singh, "Flexibility requirement for large-scale renewable energy integration in Indian power system: Technology, policy and modeling options," *Energy Strategy Reviews,* vol. 29, p. 100482, 2020.

[12] A. A. Mohamed, A. El-Sayed, H. Metwally, and S. I. Selem, "Grid integration of a PV system supporting an EV charging station using Salp Swarm Optimization," *Solar Energy,* vol. 205, pp. 170–182, 2020.

[13] A. Bartolini, F. Carducci, C. B. Muñoz, and G. Comodi, "Energy storage and multi energy systems in local energy communities with high renewable energy penetration," *Renewable Energy,* vol. 159, pp. 595–609, 2020.

[14] M. McPherson, L. D. Harvey, and B. Karney, "System design and operation for integrating variable renewable energy resources through a comprehensive characterization framework," *Renewable Energy,* vol. 113, pp. 1019–1032, 2017.

[15] H. Karbouj, Z. H. Rather, D. Flynn, and H. W. Qazi, "Non-synchronous fast frequency reserves in renewable energy integrated power systems: A critical review," *International Journal of Electrical Power & Energy Systems,* vol. 106, pp. 488–501, 2019.

[16] F. Hua and A. Ezzi, "The Present Trends and Challenges in Renewable Energy Sources Connected to a Grid."

[17] H. M. Dinçer, "The Role of Irena in Global Renewable Energy Policies," Kadir Has Üniversitesi, 2018.

[18] G. Bilicic and S. Scroggins, "2023 levelized cost of energy+," *Lazard, April,* vol. 12, 2023.

[19] R. IEA, "Analysis and forecast to 2026," *Paris: International Energy Agency,* 2021.

[20] R. Imomiddin, "DEVELOPMENT OF CORRECT METHODS OF USING ALTERNATIVE ENERGY," *Research Focus,* vol. 3, no. 7, pp. 34–36, 2024.

[21] И. Рахмонов, "ПРЕИМУЩЕСТВА АЛЬТЕРНАТИВНОЙ ЭНЕРГЕТИКИ," *Research Focus,* vol. 3, no. 7, pp. 58–62, 2024.

[22] M. El Zein and G. Gebresenbet, "Digitalization in the Renewable Energy Sector. Energies 2024, 17, 1985," ed, 2024.

[23] H. Ritchie, M. Roser, and P. Rosado, "Renewable energy. Our World In Data. 2020," ed, 2020.

[24] S. Sharma, "Renewable Energy and Energy Harvesting In Himachal Pradesh and All Over India," *Renewable Energy,* vol. 10, no. 6, 2023.

[25] A. Chatzipanagi *et al.*, "Clean Energy Technology Observatory: Photovoltaics in the European Union-2024 Status Report on Technology Development, Trends, Value Chains and Markets," 2022.

Chapter II: Modeling of photovoltaic System and power converter

1. Introduction

The availability of traditional energy resources diminishes gradually each day, raising concerns among many. Economic factors and apprehensions regarding fossil fuels promote the advancement of photovoltaic (PV) energy systems. Photovoltaic (PV) energy, as a clean and renewable resource, has garnered considerable interest in the past decade, attributed to the escalating energy costs and detrimental environmental effects of traditional fossil fuels [1]. Malaysia's equatorial location facilitates substantial sunshine exposure year-round, rendering photovoltaic energy a highly promising renewable resource.

Photovoltaic technology denotes Direct conversion of solar energy into electrical power via solar cells or other equipment. This technology has been developed during the 20th century. This technology is advancing swiftly and is anticipated to attain full maturity in the 21st century The utilization of this technology is ubiquitous and can be encountered almost universally. An elementary illustration would be calculators in a residence or workplace. The little, dark-hued panels located on the calculator's surface are referred to as solar cells. Additional instances encompass traffic signals, contemporary parking meters, roadside emergency telephones, among others [2] .

The basic unit of a photovoltaic generator, the main part of a solar generator, is a solar cell.

A photovoltaic generator, or photovoltaic array, is the complete system comprising all PV modules interconnected in series or parallel [1].

2. Solar energy

2.1. Definition

The sun's radiant radiation is the source of solar energy, which can be converted into electricity or heat using many technologies. This energy is primarily harnessed by photovoltaic panels or solar thermal power facilities. Photovoltaic panels, typically installed on rooftops, directly use the photoelectric effect to turn sunlight into electricity. Solar thermal power plants utilize lenses or mirrors to focus sunlight, creating steam produced by high temperatures that power turbines and provide energy.

Remarkably, within a mere six hours, the solar radiation that strikes the Earth's deserts

surpasses the total energy consumption of humanity over an entire year. This tremendous potential highlights the extensive magnitude of solar energy available for utilization [3].

Fig.2.1. Fixed photovoltaic field [4].

2.2. Solar potential in the world

One essential renewable resource for decarbonization and the long-term development of human society is solar energy. The efficacy of global governments in the extensive deployment of solar technologies is significantly contingent upon a comprehensive understanding Measuring the distribution and intensity levels of solar radiation worldwide, a difficult undertaking because of the generally limited availability of current global-scale data. This study primarily seeks to analyze the global, continental (excluding Antarctica), and national (194 countries) use data from direct normal irradiation (DNI) and global horizontal irradiation (GHI), which are published in reliable worldwide databases at the highest geographic resolution currently available, to determine the distribution and intensity of solar radiation. A statistical analysis of seven potential classes, defined using established geostatistical methods, revealed six primary There are six different DNI hotspots (southwestern North America, western South America, southwestern Africa, northwestern Arabian Peninsula, Tibetan Plateau, and Australia) with values exceeding 2500 kWh/m², as well as GHI hotspots (western South America, northern, eastern, and southwestern Africa, the Arabian Peninsula, and Australia) with annual values exceeding 2200 kWh/m². The areas with

the strongest solar radiation levels, categorized as the seventh potential class (excellent) for both criteria, which includes most of the world's DNI (about 8 million km2, or 5% of the world's land area) and GHI (roughly 15 million km2, or 10% of the world's land area) superb class regions. Africa has the highest GHI solar resources, with almost 10 million km² of exceptionally high-quality resources, or about one-third of the continent's total area. but Australia has the most extensive DNI resources, spanning around 4 million km², or about 50% of its territory. Within their borders, 12 countries serve as GHI epicenters, with 9 in Africa (Namibia, 96%; Sudan, 86%; Niger, 84%; Egypt, 77%; Western Sahara, 72%; Chad, 69%; Eritrea, 58%; Libya, 56%; and Djibouti, 52%) and 3 in Asia (Oman, 92%; Yemen, 87%; and Saudi Arabia, 74%) having at least a 50% superb potential threshold. Only three nations, however, (Namibia, 77%; Jordan, 53%; and Australia, 51%) reach this percentage criterion for DNI maximum solar potential. These epicenter nations, as well as those with notable absolute GHI and DNI superlative class regions, such as the United States, Mexico, Chile, Peru, Bolivia, Argentina, and China, are among the most favorable for the widespread installation of photovoltaic and concentrating solar power systems, which are currently currently Only three nations, however, (Namibia, 77%; Jordan, 53%; and Australia, 51%) reach this percentage criterion for DNI maximum solar potential. These epicenter nations, as well as those with notable absolute GHI and DNI superlative class regions, such as the United States, Mexico, Chile, Peru, Bolivia, Argentina, and China, are among the most favorable for the widespread installation of photovoltaic and concentrating solar power systems, currently the most common technologies used in solar energy production, according to our findings [5].

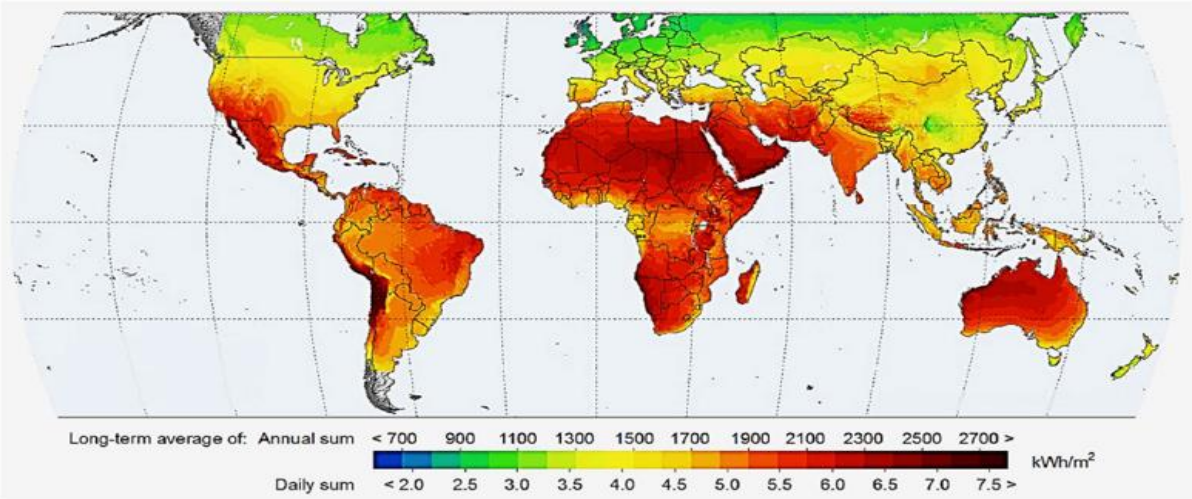

Fig.2.2. Maps of global horizontal irradiation [5].

2.3. Solar Radiation and Sunlight

Solar energy refers to the radiation emitted in all directions by the sun towards Earth.

- Irradiance: (or illumination) represents the power of solar radiation incident that occurred on a unit. It is denoted by (E) and measured in [W/m²].

- Irradiation: measures the total energy of solar radiation incident over a time period (e.g., one hour or one day) over a surface of 1 [m²]. It is symbolized by (G) and measured in [Wh/m²] or [kWh/m²].

When the Earth's surface is perpendicular to the sun, the average amount of electricity it receives from solar radiation is 1.4 [kW/m²]. Earth-Sun direction. This solar flux is reduced as it passes through the atmosphere due to absorption or scattering, and it varies with weather conditions and the latitude of the location. At ground level, the remaining power is around 1 [kW/m²] at our latitudes. The usable energy ranges between 800 and 7 [kWh/m²] depending on the location.

2.4. Types of Solar Radiation at the Ground

Three types of after traveling through the atmosphere, three types of solar radiation—direct, diffuse, and reflected—arrive at the ground.

- Direct Radiation: refers to sunlight that reaches a specific surface from a solid angle centered on the solar disc.

- Diffuse Radiation: is released from all directions by obstructions like buildings, the ground, and clouds.

- Reflected Radiation: also known as albedo, results from the interaction of incident radiation, whether diffuse or direct, with surfaces such as the ground or clouds.

The sum of these three types constitutes the fourth type of radiation referred to as global radiation. Fig.2.3. on the following page illustrates these types of radiation.

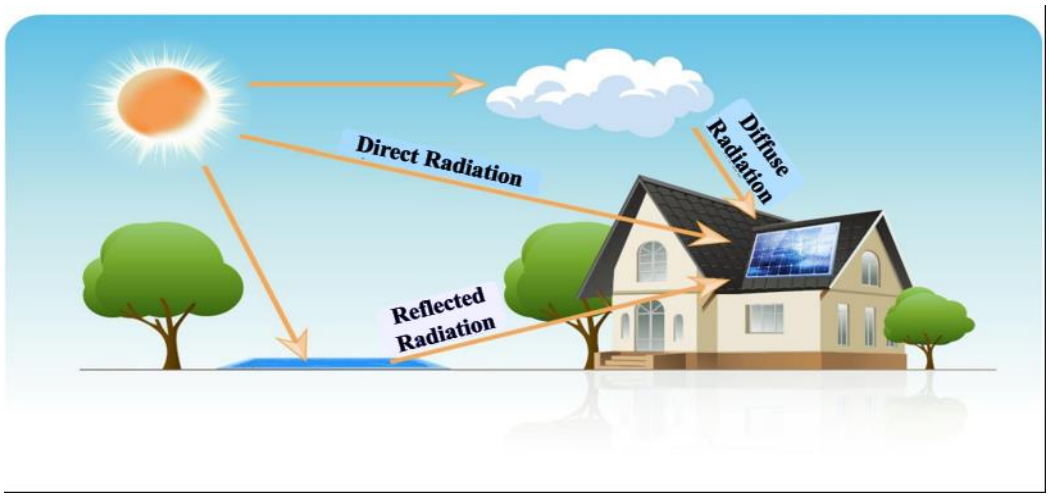

Fig.2.3. Types of solar radiation.

3. General structure of the studied system

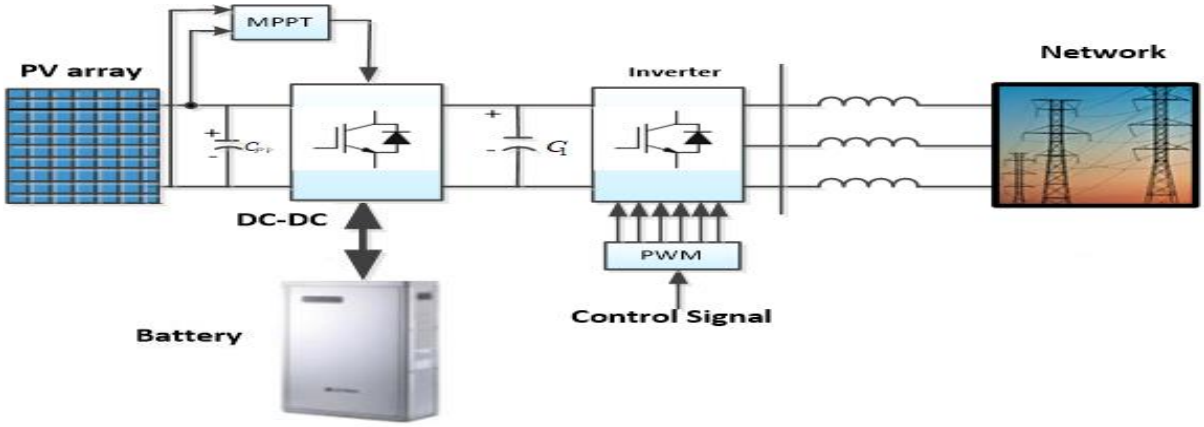

Fig.2.4. structure of the studied system.

3.1. photovoltaic panel

One essential tool for converting photon energy into electrical power is a solar cell. A solar module is produced by connecting these cells in parallel and series arrangements. These modules are joined in parallel and series to create solar arrays. configurations, producing clean and renewable energy. Fig2.5. illustrates the process of constructing the photovoltaic array from the cell.

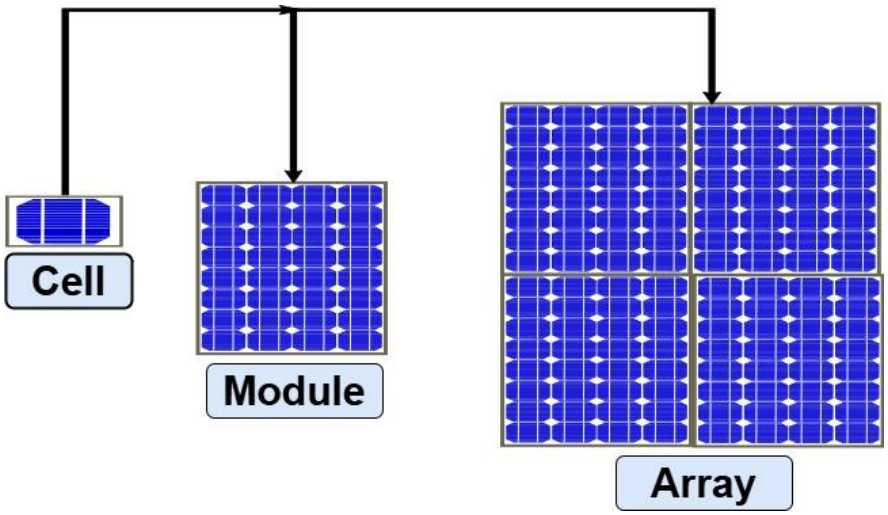

Fig.2.5. Construction of a solar photovoltaic system [6].

Table.2.1. Model type of Panel [7].

Model Type	Complexity	Accuracy	Used For
Single-Diode	Medium	High	General PV performance modeling
Double-Diode	High	Very High	Research, detailed simulations
Empirical (PVWatts)	Low	Moderate	System design, energy estimates
Equivalent Circuit	Medium	High	Circuit-level simulation
Data-Driven	High	Variable	Predictive analytics, AI modeling

3.2. power converter:

Power converters are generally employed to regulate the input voltage in accordance with the application's needs. For ages, power converters have been integral to power distribution systems and drives. The solar systems' output power is changeable and contingent upon climatic circumstances. They cannot be simply connected to an AC inverter; instead, they must first connect to a DC-DC converter to optimize power before being converted to AC via inverters. The system employs a two-step conversion process: the initial stage is DC-DC, followed by a DC-AC stage [8].

3.2.1. DC-DC converters:

Numerous DC-DC converters are currently employed to regulate the input voltage based on application specifications. DC-DC converters are categorized into two primary types: isolated converters, which include Push-Pull, Flyback, Forward, and Multiport, and non-isolated converters, comprising standard DC-DC, interleaved DC-DC, and Multi Device/port [9]. The DC-DC converter ensures that renewable sources operate at their maximum power point (MPP). In this study, we utilized Boost in conjunction with a photovoltaic array. The DC-DC converters, comprising the Buck Boost and Boost topologies, are represented via a state space modeling approach. Initially, state-space modeling is predominantly, where the system matrix is denoted as, the state variable as, the derivative of the state variable as, the input as, and the output as [10].

$$\begin{cases} x' = Ax + Bu \\ y = Cx + Du \end{cases} \quad \text{(II.1)}$$

3.2.1.1. Buck Converter:

A DC-DC converter designed especially for step-down conversion of the applied DC input signal is called a Buck Converter. The fixed DC input signal is converted into a lower-value DC output signal in buck converters. This suggests that it is designed to provide an output signal of direct current that is smaller in magnitude than the applied input. It is sometimes called a Buck Regulator, Step-down Chopper, or Step-down DC to DC Converter.

Operating Principle of Buck Converter

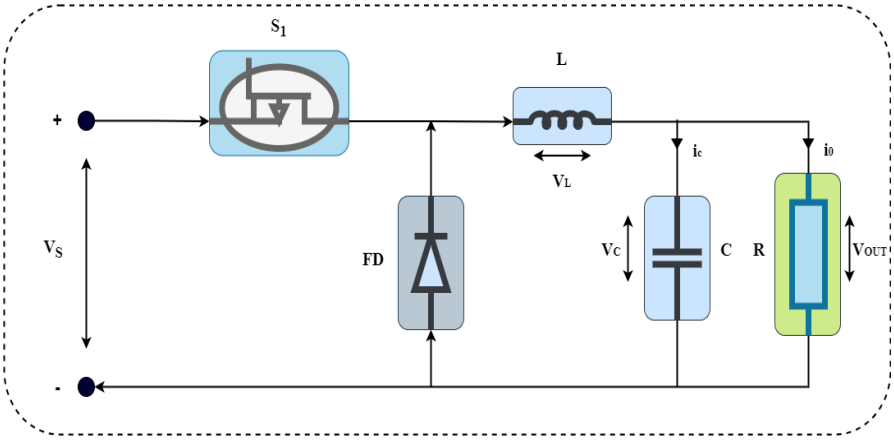

Fig.2.6. The Circuit Representation of Buck Converter

The accompanying diagram makes it very evident that there is another switch in the circuit, a freewheeling diode, in addition to the solid-state power electronics device acting as a switch. By combining these two switches, a low-pass LC filter is connected to reduce voltage or current variations. This makes it easier to produce controlled DC output. The circuit's load is a pure resistor that is connected throughout the entire setup.

3.2.1.2. Boost Converter:

Step-up DC-DC converters, another name for boost converters, are chopper circuits that produce an output voltage higher than the input voltage. DC-DC conversion takes place in boost converters in order for the circuit to produce an output voltage that is larger than the input supply voltage. 'Boost' is the term used because the output voltage is higher than the input voltage.

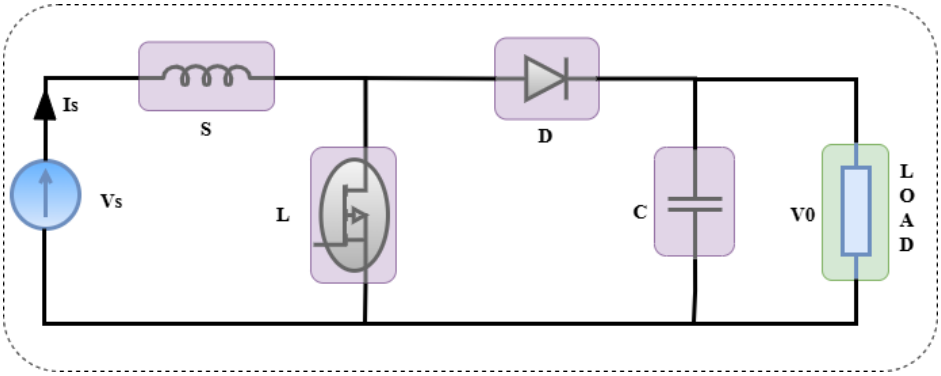

Fig.2.7. The Circuit Representation of Boost Converter

3.2.1.3. Buck-Boost Converter:

A DC-to-DC converter known as a buck-boost converter generates an output voltage magnitude that may be greater than or less than the input voltage magnitude. Like a transformer in AC circuits, it is used to increase the DC voltage. Using a single inductor instead of a transformer is comparable to a fly-back converter. Buck-boost converters come in two different varieties. Often referred to as choppers, DC-DC converters include the versatile Buck-Boost converter. Depending on its duty cycle, shown by DA, this converter can function as a step-up or step-down converter. An example of a typical Buck-Boost converter circuit is shown below:

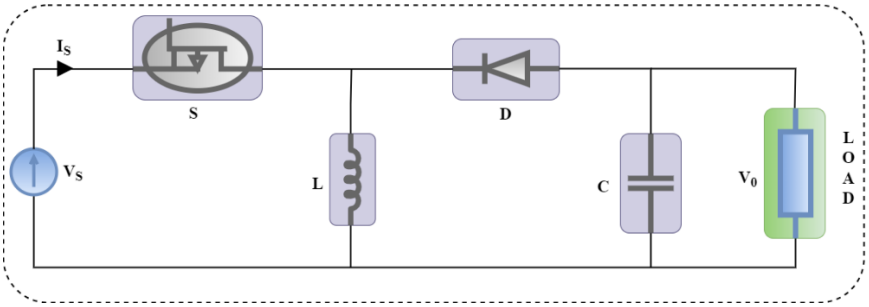

Fig.2.8. The Circuit Representation of Buck-Boost Converter

A solid-state device is coupled to a voltage source. The diode is used as the secondary switch. As seen in the above image, the diode is connected in reverse to the direction of power flow from the source to a capacitor and the load, which are both connected in parallel. Pulse Width Modulation (PWM) is used by the converter's-controlled switch to activate and deactivate. PWM can operate on either a time or frequency basis, though the time-based method

is more commonly used. Although flexible, frequency-based modulation requires a wide range of frequencies to precisely control the switch and get the desired output voltage. The majority of time-based modulation is used in DC-DC converters. It is simple to use and put together. This form maintains the frequency continuously The majority of time-based modulation is used in DC-DC converters. It is simple to use and put together. This type of PWM modulation maintains the frequency consistently. There are two modes of operation for the Buck Boost converter. When the switch is turned on and carrying electricity, it is in the initial mode.

3.2.2. DC-AC inverters topology:

Electricity is generated via renewable energy sources., which is transmitted to the distribution station. Nevertheless, the direct current produced at the (RS) cannot be immediately integrated into the electrical system. Consequently, power electronic converters and electrical components help make it easier to include renewable energy sources into the grid [11]. Utility-scale renewable energy systems generally consist of four components: 1. DC-DC converter with tracking of maximum power points 2. DC-AC inverter, 3. inverter-side output filter, and 4. grid. DC-AC devices called inverters change direct current into alternating current in order to provide electrical power to the grid. Essentially, the voltage source inverter is categorized into two types: 2-level voltage source inverters and multi-level inverters. Refer to Fig.2.9. [12].

Fig.2.9. Block diagram of the voltage inverter.

Voltage Source Inverter (VSI). Generally, VSI denotes an inverter that utilizes the input voltage to generate a regulated output voltage. The utilization of VSI is increasingly obtaining widespread acceptance. The high efficiency of these inverters is the primary restriction and essential criteria for their efficient deployment [11]. The 2-Level VSI is utilized in various

standard industrial machinery. Multi-level voltage source inverters (MLVSI) are more modern and well-known in the field because of their benefits, especially their ability to produce multilayer stepped waveforms with less harmonic distortion, enhanced voltage operation, and greater flexibility [13].

3.2.2.1. Voltage source inverter:

The polarity of the input voltage stays constant since the DC voltage source is placed at the Voltage Source Inverter's (VSI) input. The average power flow through the inverter is determined by the polarity of the incoming DC current.[14].

A variable-width, constant-amplitude the output can generate a waveform of AC voltage. This section describes and highlights the characteristics of many VSI topologies that are frequently used in renewable energy sources. The study looks at both two-level and multi-level voltage source inverter topologies. Three types of MLVSI topologies are distinguished: diode-clamped, flying capacitor, and cascaded H-bridge (CHB).

3.2.2.2. Classification of inverters

Voltage inverters are of many structures and this is due to their applications and controls. Voltage inverters can be categorized using the following standards:

- •Number of phases.
- •Nature of the input source.
- •Nature of the switches.
- •Number of output voltage levels.

a. Classification according to the number of phases

a.1. Single-phase inverters

To generate an alternating voltage from a direct voltage using two switches, there are several possible configurations depending on the location of the midpoint. These configurations include:

•the single-phase inverter with a midpoint output transformer called a push-pull inverter Fig.2.10

• the single-phase inverter with a capacitive divider at the input called a half-bridge inverter Fig.2.11

• If we want to vary the relative width of the slots forming the alternations of the output voltage, four switches are required; this is the single-phase bridge inverter Fig.2.12.

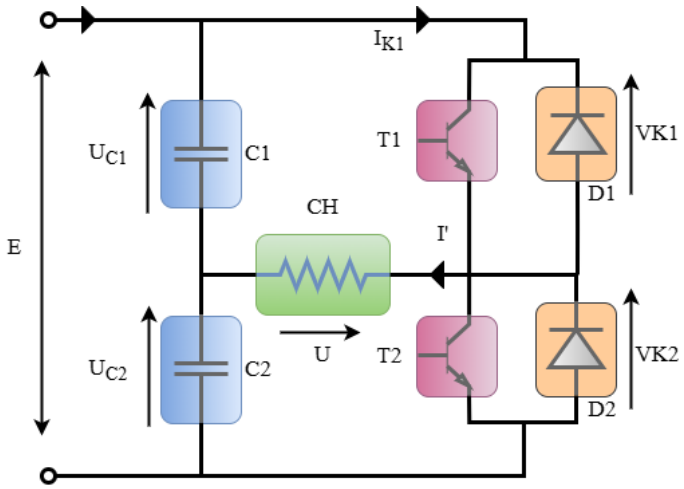

Fig.2.10. Single-phase inverter with capacitive divider.

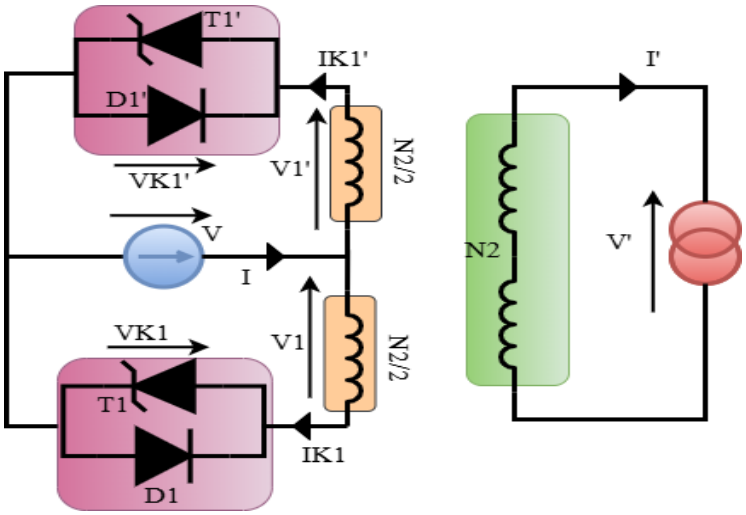

Fig.2.11. Single-phase inverter with mid-tapped output transformer.

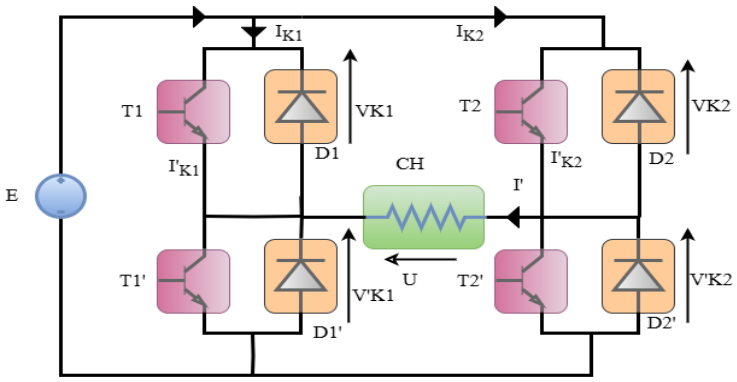

Fig.2.12. Single-phase bridge inverter.

a.2. Three-phase inverters

The simplified diagram of a two-level three-phase inverter is shown in Fig.2.13

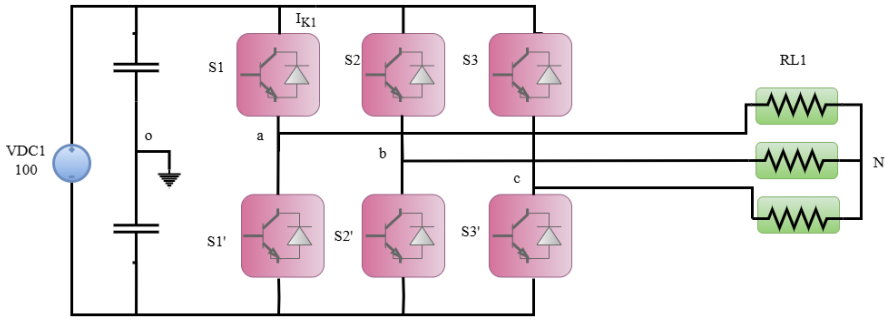

Fig.2.13. Structure of a three-phase voltage inverter.

b. Classification according to Number of output voltage levels.

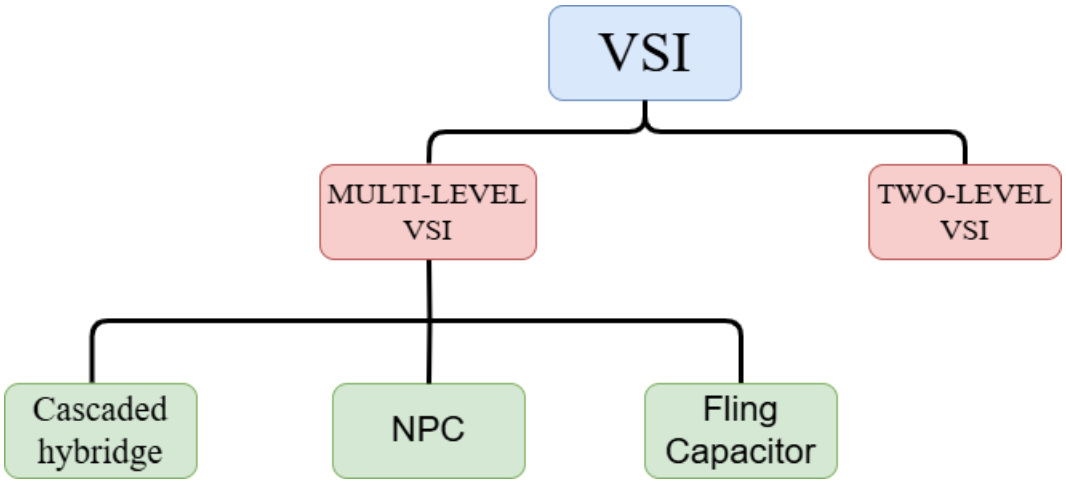

Fig.2.14. Voltage source classifications.

b.1 Tow-level Voltage source inverter:

Two-level converters are frequently employed in the grid integration of renewable energy sources for low-power applications. Nevertheless, credible sources are sometimes associated with medium voltage for high power applications, complicating the utilization of two-level inverters due to the elevated voltages that the switching devices can withstand [15]. This inverter comprises a two-level voltage source inverter (VSI) featuring six switches, each accompanied by a parallel free-wheeling diode [16]. The implementation of multilayer inverters addresses the limitations of two-level voltage source inverters (VSI). The primary characteristic of these converters is their compact size and multiple voltage levels, which enhance power performance, diminish overall harmonic distortion, and lower switching device losses [17].

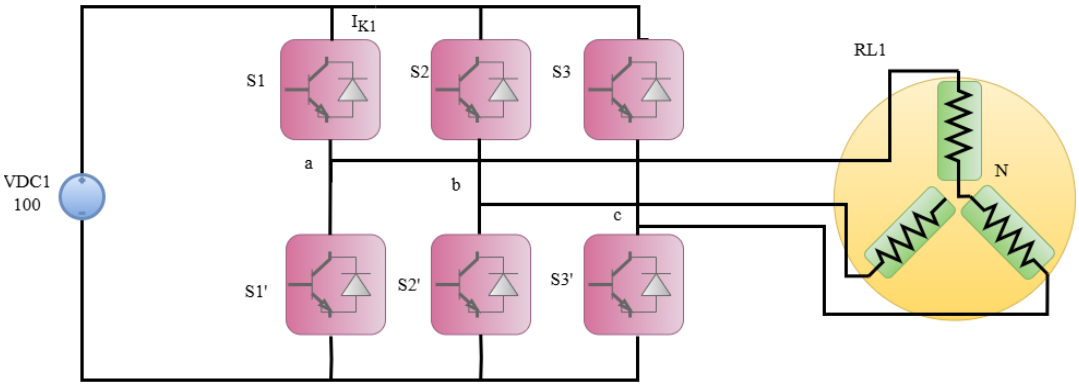

Fig.2.15. Structure of a three-phase two-level voltage inverter.

b.2 Multi-level voltage source Inverter (MlVSI):

b.2.1. Natural point champed inverter:

The diode-clamped multilevel inverter produces multi-level AC voltage waveforms using clamping diodes and cascaded DC capacitors. This inverter features a three-level or higher structure known as Natural Point Clamped, and is predominantly utilized for medium voltage power applications [15]. Moreover, the primary advantages are categorized as follows [18].

- Good dynamic response
- Simple design
- Low const and compact in 3-level structure
- No floating capacitors
- Low THD in AC voltage side, also reduces the dv/dt stresses.

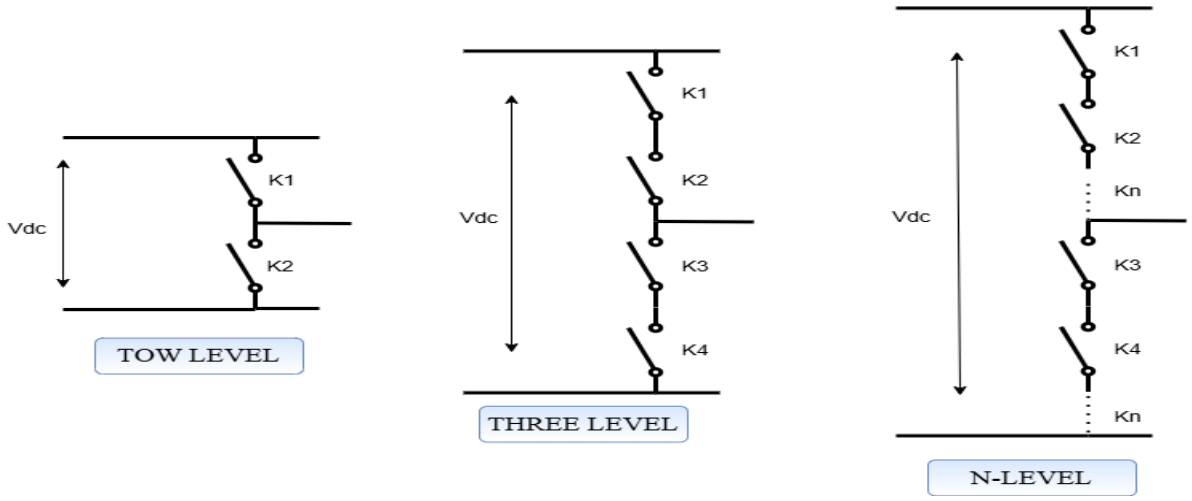

Fig.2.16. Structure of a three-phase multi-level voltage inverter.

3.3. Battery Energy Storage System

It is possible for solar power generation to either outpace or fall behind load demand. The erratic nature of photovoltaic (PV) power necessitates energy storage systems (ESS) to retain surplus energy, provide power during deficiencies, and provide grid stability amid oscillations caused by variable weather conditions, such as shadows cast by clouds on the PV array. A bank of lithium-ion batteries and a bidirectional DC–DC buck–boost converter make up the storage module. Lithium-ion batteries have a long lifespan, a high energy capacity, and little maintenance needs. The control is set up in bus monitoring (BM) mode because the bidirectional buck-boost converter's management controls the Battery Energy Storage System's (BESS) charging and discharging based on the DC bus voltage [19].

4. Modeling the studied system

4.1. The photovoltaic cell

A PV cell is an electronic sensor of sunlight based on semiconductor materials.

It is the elementary element of the PV system whose role is to generate a direct current voltage under exposure to solar radiation (photons), it is the phenomenon of the PV effect which is at the origin of producing electricity [5, 7].

An electrical circuit element can be used to symbolize a single solar cell. It consists of two resistors, a photocurrent generator that generates current from light, and a p-n junction known as a diode. Solar cell characteristics are nonlinear and affected by temperature and irradiation. The single diode, two-diode, and three-diode models are the three different varieties of solar cell models [7]. Solar cells are grouped in parallel or series to form the PV panel, which is part of the photovoltaic (PV) module. These solar cells' configuration is commonly referred to as the SDM (single diode model).[6, 20]. The model employed in our study is the single diode model, the subsequent image illustrates the electrical model of the photovoltaic cell.

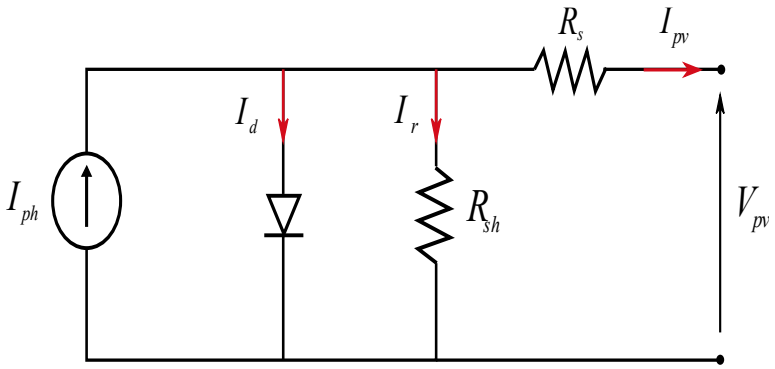

Fig.2.17. equivalent single diode model of solar cell.

The output current (Ipv) may be represented as follows using the circuit mentioned in Fig.2.17:

$$I_{pv} = I_{ph} - I_d - I_{sh} \tag{II.2}$$

$$I_{pv} = I_{ph} - I_{sd}\left[\exp\left(\frac{q(V_{pv} - I_{pv}R_s)}{nkT}\right) - 1\right] - \frac{V_{pv} + I_{PV}R_s}{R_{sh}} \tag{II.3}$$

Where : I_{pv}: the output current of the cell.

I_{ph}: the photocurrent of the cell.

I_{sd}: the reverse saturation current of the diode.

q: the electronic charge its equal to $1.6 \times 10^{-19}C$

V_{pv}/c : the output voltage of cell.

n: the ideality factor of diode.

k: the Boltzmann factor, its equal to $1.38 \times 10^{-23}j/k$

T: the temperature.

R_s: the sears resistance of the cell.

R_{sh}: the parallel resistance of the cell.

4.2. PV module:

The configuration of a photovoltaic cell module is crucial for examining output characteristics; it necessitates arranging the cells in series and parallel due to the low power generated by the individual cells [21].

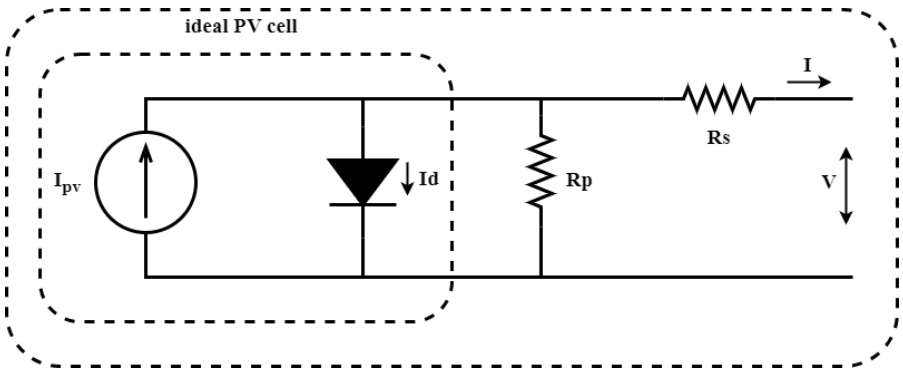

Fig.2.18. An equivalent solar cell circuit.

The ideal PV module current-voltage characteristic can be expressed mathematically using the following formulas, which are thoroughly examined and explained in[16]:

$$I_{pv} = N_p I_{ph} - N_p I_{sd}\left(\exp\left(\frac{N_s V_{pv} + \left(N_s / N_p\right) R_s I_{pv}}{n N_s K T}\right) - 1\right) - \left(\frac{N_s V_{pv} + \left(N_s / N_p\right) R_s I_{pv}}{(N_s / N_P) R_{sh}}\right) \quad \text{(II.4)}$$

Where:

I_{PV}: represent the PV module current

V_{PV}: the pv module voltage

N_S: number of series cells connected.

N_P: number of parallel cells connected.

4.3. Power converter

4.3.1. Boost Converter

Operating Principles of Boost Converter

The boost converter's circuit representation is shown in the image below:

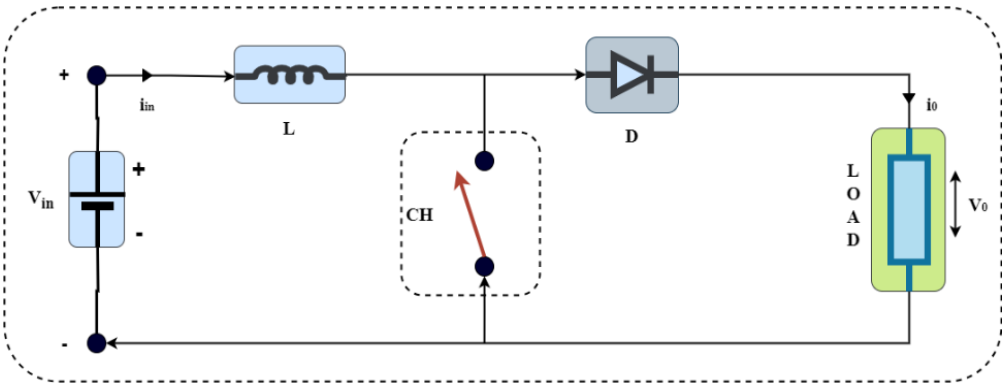

Fig.2.19. Elementary Circuit of Boost Converter.

The circuit shown is a simple step-up DC-DC converter setup that requires a large inductor L connected in series with the voltage source. The goal of the entire circuit design is to maintain a controlled DC signal at the output. Let's examine how the circuit works to improve the direct current signal at the load. The supply DC input current starts flow down the closed-circuit channel and passes through the inductor when the chopper CH is in the on state, as shown in the figure below.

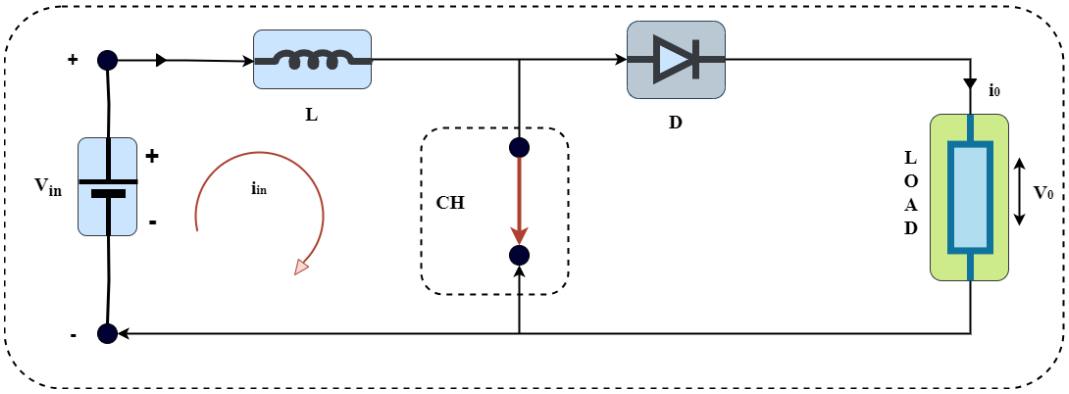

Fig.2.20. The Chopper CH is in on State.

The polarity of the inductor will correspond to the direction of the current flow. In this instance, the diode is in a reverse-biased state, thereby preventing current from flowing through that segment of the circuit during the operational phase of the DC-DC converter. Consequently, the voltage across the DC-DC converter will manifest across the load.

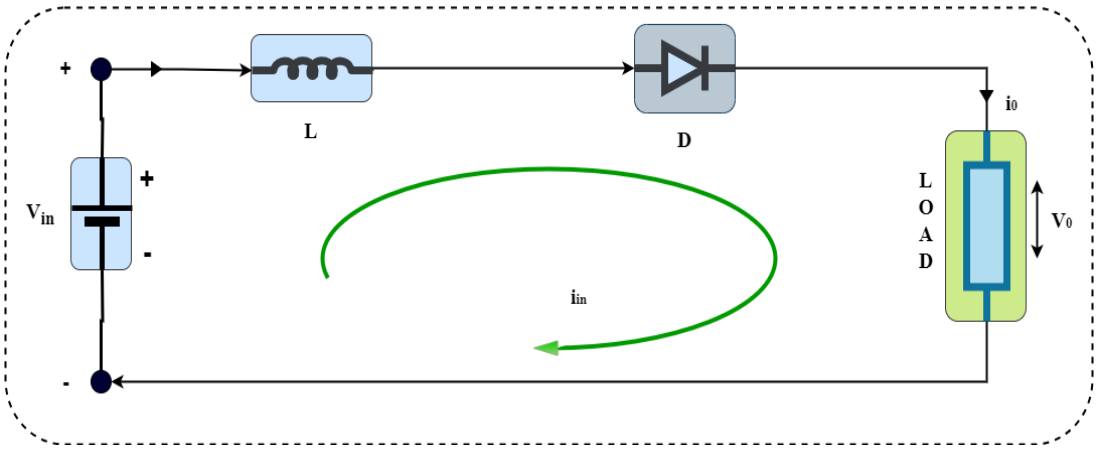

Fig.2.21. The Chopper CH is in Off State

Furthermore, the section of the circuit that previously conducted current will not be functional in this situation while CH is in the off state. Nevertheless, the current passing through the inductor will not instantly stop when it builds up energy in the form of a magnetic field. Lenz's law states that a reverse current opposing the original source will be induced. As a result, the induced current will cause the polarity of the inductor to reverse. The circuit's diode is biassed by the inductor's reverse polarity forward. This shows the current path via the diode that flows through the load when is in the off state, or Toff. Recognizing that the current flowing through the inductor is decreasing and will eventually stop after This shows the current path via the diode that flows through the load when the helicopter is in the off state, or Toff. It is crucial to recognize that the current flowing through the inductor is decreasing and will eventually stop after a specific amount of time.

Consequently, the overall voltage across the load will be displayed as follows:

$$V_{out} = V_{in} + V_L \qquad \textbf{(II.5)}$$

This indicates that the applied input voltage is less than the output voltage. As a result, it performs step-up conversion when the inductor's stored energy from the Ton phase is released

during the Toff phase.

The voltage across the inductor throughout the Ton period will be as follows:

$$V_L = L\frac{di}{dt} \quad \textbf{(II.6)}$$

Let's examine the step-up chopper's waveform representation, which is displayed below:

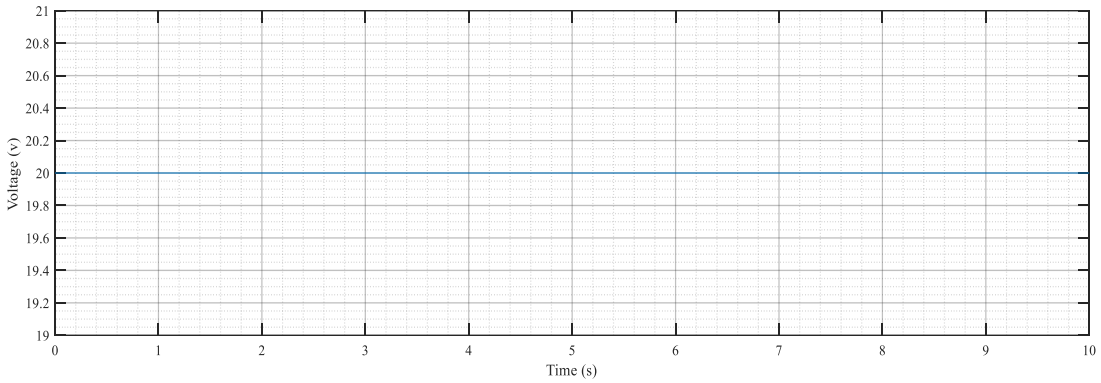

Input Voltage (V_[1]) Profile

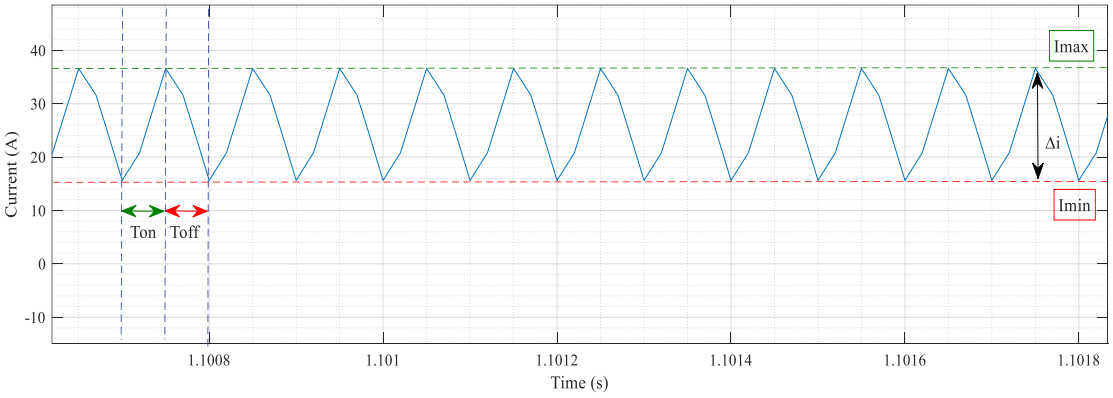

Current of inductor

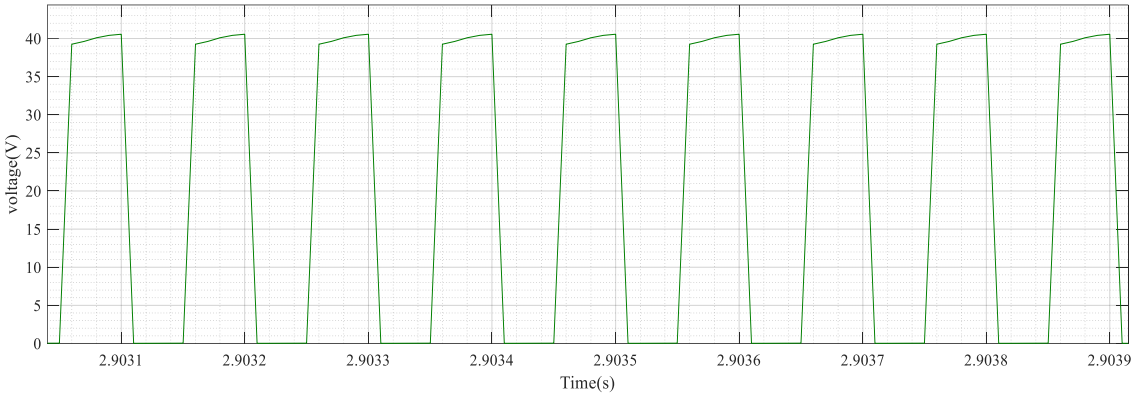

Voltage of MOSFT

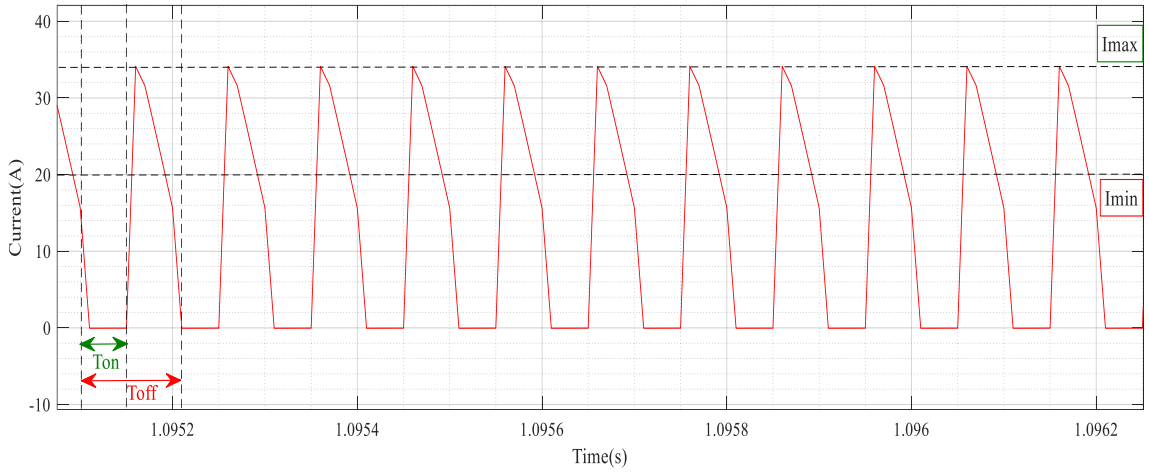

Output current

Fig.2.22. Waveform Representation.

Throughout As shown above, the current passing through the inductor will change from i1 to i2 throughout the Ton period. The inductor current will change from i2 to i1 during the Toff interval. The voltage across the inductor will match the supply input voltage during the turn-on phase. But when CH is disengaged, using Kirchhoff's Voltage Law to the aforementioned figure yields,

$$V_L - V_0 + V_{in} = 0 \quad \textbf{(II}.7\textbf{)}$$

This means,

$$V_L = V_0 - V_{in} \quad \textbf{(II}.8\textbf{)}$$

When CH is on, the energy input from the source to the inductor is as follows, taking into account that the output current varies linearly:

W_{on} = (voltage across the inductor) (average current through the inductor)

$$T_{on}W_{on} = V_{in}(i_{1+}\frac{i_2}{2})T_{on} \quad \textbf{(II}.9\textbf{)}$$

Additionally, while CH is off, the energy released to the load by the inductor is as follows:

W_{off} = (voltage across the inductor) (average current through the inductor) ***T***off

$$W_{off} = V_{out} - V_{in}(i_{1+}\frac{i_2}{2})T_{off} \quad \textbf{(II}.10\textbf{)}$$

When comparing the two energies for a lossless system, we will have,

$Vin\ (i1 + i2/2)Ton\ = Vout\ - Vin\ (i1 + i2/2)Toff$ (**II**.11)

On simplifying,

$V_{in}T_{on} = V_{out}T_{off} - V_{in}T_{off}$ (**II**.12)

$Vout\ Toff\ = Vin\ Ton\ + Vin\ Toff$ (**II**.13)

$Vout\ Toff\ = Vin\ (Ton\ + Toff\ )$ (**II**.14)

Since we know, $T\ =\ Ton\ +\ Toff$, therefore,

$Vout\ Toff\ = Vin\ T$ (**II**.15)

$Vout\ = Vin\ .T/Toff$

$Vout\ = Vin.T/T - Ton$ (**II**.16)

$Vout\ = Vin.1/(T/T - Ton\ /T)$ (**II**.17)

Since, we know, duty cycle i.e., $\alpha\ =\ Ton/\ T$

$V0ut = Vin\ 1(1 - \alpha)$ (**II**.18)

We can therefore draw the conclusion that a change in duty cycle can increase the average load voltage.

4.4. Modeling of Three-Phase Voltage Inverter

Each arm of the three-phase, two-level voltage inverter includes two switches. These are unique in that they can be opened and closed in both directions and are completely controlled. For low power and extremely high frequencies, they can be MOSFETs; for high power and high frequencies, they can be IGBTs; or for very high power and low frequencies, they need GTOs. The switch must be positioned in antiparallel with a diode to guarantee current flow in both directions. A two-level voltage inverter's general layout is displayed in Fig.2.23.

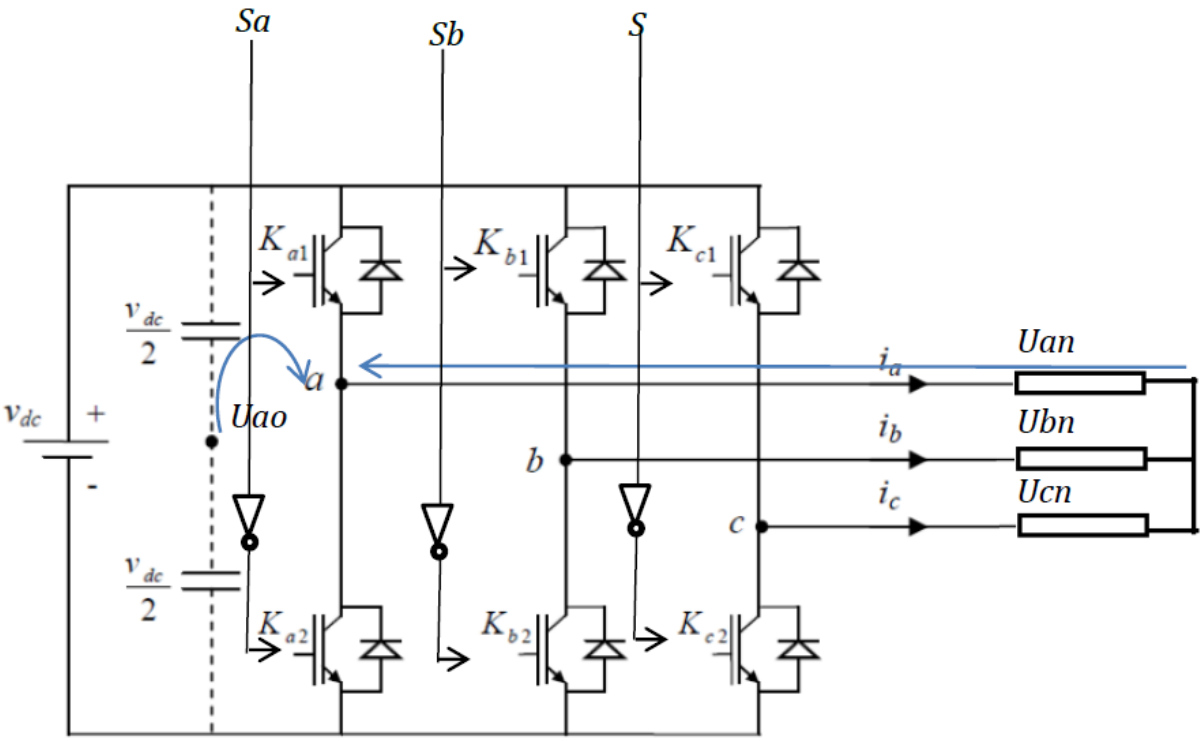

Fig.2.23. Schematic diagram of the three-phase voltage inverter.

In controllable mode, the arm is a two-way switch that allows two voltage levels to be obtained at the output. An arm of the inverter is represented by Fig.2.24.

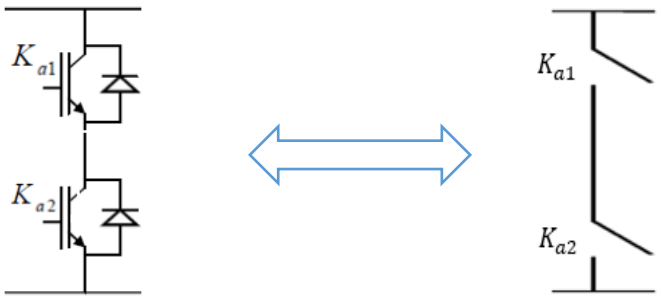

Fig.2.24. Representation of a GTO.

The reference voltages are the desired single voltages Uan; Ubn; Ucn referenced to the neutral point.

Three Boolean control quantities Si (i = a, b, c) can be used to specify the switches' state, assuming that it is perfect:

-If = 1 indicates that the bottom switch is open and the top switch is closed.

-If = 0 indicates that the bottom switch is closed and the top switch is open.

The phase voltages Uao, Ubo, and Uco can be expressed as a function of the control signals Si in these circumstances:

$$U_{a0} = \begin{cases} \frac{V_{dc}}{2}, S_a = 1 \\ -\frac{V_{dc}}{2}, S_a = 0 \end{cases} \rightarrow U_{a0} = K_a * \frac{V_{dc}}{2} \quad \text{(II.19)}$$

$$U_{b0} = \begin{cases} \frac{V_{dc}}{2}, S_a = 1 \\ -\frac{V_{dc}}{2}, S_a = 0 \end{cases} \rightarrow U_{b0} = K_b * \frac{V_{dc}}{2} \quad \text{(II.20)}$$

$$U_{c0} = \begin{cases} \frac{V_{dc}}{2}, S_a = 1 \\ -\frac{V_{dc}}{2}, S_a = 0 \end{cases} \rightarrow U_{c0} = K_c * \frac{V_{dc}}{2} \quad \text{(II.21)}$$

We have Ka, Kb, and Kc show the case where 1 or -1 depends on Si, as defined by the equations Uao, Ubo, and Uco.

When the load is deemed balanced, the following happens:

$$U = \frac{2}{3}(U_{an} + aU_{bn} + a^2U_{cn}) \quad \text{(II.22)}$$

$$U_{an} + U_{bn} + U_{cn} = 0 \quad \text{(II.23)}$$

$$\begin{cases} U_{a0} + U_{On} = U_{an} \\ U_{b0} + U_{On} = U_{bn} \\ U_{c0} + U_{On} = U_{cn} \end{cases} \quad \text{(II.24)}$$

From the sum of equations (II.23), we have

$$(U_{aO} + U_{bO} + U_{cO}) + 3.U_{on} = U_{an} + U_{bn} + U_{cn} \quad \text{(II.25)}$$

Substituting (II.22) into (II.24) gives us:

$$U_{on} = -\frac{1}{3}\left(U_{ao} + U_{bo} + U_{co}\right) \quad \text{(II. 26)}$$

Replacing (II.25) in (II.23) we obtain:

$$\begin{cases} U_{an} = \frac{2}{3}U_{ao} - \frac{1}{3}U_{bo} - \frac{1}{3}U_{co} \\ U_{bn} = \frac{1}{3}U_{ao} + \frac{2}{3}U_{bo} - \frac{1}{3}U_{co} \\ U_{cn} = -\frac{1}{3}U_{ao} - \frac{1}{3}U_{bo} + \frac{2}{3}U_{co} \end{cases} \quad \text{(II.27)}$$

Replacing (II.19), (II.20) and (II.21) in (II.26) we obtain:

$$\begin{cases} U_{an} = \frac{2}{3}K_a * \frac{V_{dc}}{2} - \frac{1}{3}K_b * \frac{V_{dc}}{2} - \frac{1}{3}K_c * \frac{V_{dc}}{2} \\ U_{bn} = -\frac{1}{3}K_a * \frac{V_{dc}}{2} + \frac{2}{3}K_b * \frac{V_{dc}}{2} - \frac{1}{3}K_c * \frac{V_{dc}}{2} \\ U_{cn} = -\frac{1}{3}K_a * \frac{V_{dc}}{2} - \frac{1}{3}K_b * \frac{V_{dc}}{2} + \frac{2}{3}K_c * \frac{V_{dc}}{2} \end{cases} \quad \text{(II.28)}$$

Eight voltage vectors can be created using the various combinations of the three values (Ka, Kb, and Kc), two of which match the zero vector. Considering the basic voltages in relation to the control quantities:

$$\begin{bmatrix} U_{an} \\ U_{bn} \\ U_{cn} \end{bmatrix} = \frac{V_{dc}}{2}\begin{bmatrix} \frac{2}{3} & -\frac{1}{3} & -\frac{1}{3} \\ -\frac{1}{3} & \frac{2}{3} & -\frac{1}{3} \\ -\frac{1}{3} & -\frac{1}{3} & \frac{2}{3} \end{bmatrix}\begin{bmatrix} K_a \\ K_b \\ K_c \end{bmatrix} \quad \text{(II.29)}$$

Table.2.2. Establishment of expressions for simple and compound tensions:($Vdc = E$).

K_{a1}	K_{b1}	K_{c1}	U_{AO}	U_{BO}	U_{CO}	U_A	U_B	U_C	U_{AB}	U_{BC}	U_{CA}
0	0	0	E/2	E/2	E/2	0	0	0	0	0	0
0	1	0	E/2	-E/2	E/2	E/3	-2E/3	E/3	E	-E	0
0	0	1	E/2	E/2	-E/2	E/3	-E/3	-2E/3	0	E	-E
0	1	1	E/2	-E/2	-E/2	2E/3	-E/3	-E/3	E	0	-E
1	0	0	-E/2	E/2	E/2	-2E/3	E/3	E/3	-E	0	E
1	1	0	-E/2	-E/2	E/2	-E/3	-E/3	2E/3	0	-E	E
1	0	1	-E/2	E/2	-E/2	E/3	2E/3	-E/3	-E	E	0
1	1	1	-E/2	-E/2	-E/2	0	0	0	0	0	0

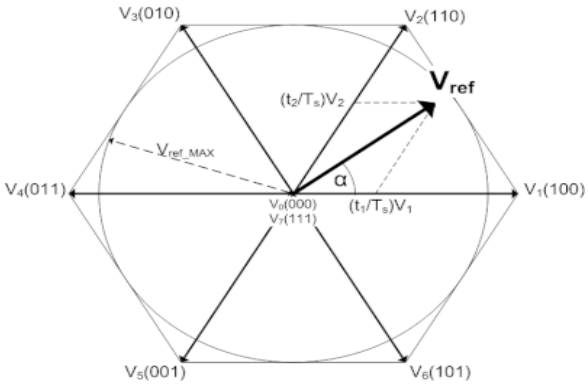

Fig.2.25. Tension vectors in the complex plane

4.5. Modeling of battery

The battery model depicted in Fig.2.26. can be represented using a broad dynamic model characterized by the equations [22]:

$$V_{batt} = E_g - i_{batt}R_{batt} \quad \text{(II.30)}$$

$$E_g = E_{go} - K\frac{Q}{Q-\int i_{batt}dt} + Ae^{\beta}\int i_{batt}dt \quad \text{(II.31)}$$

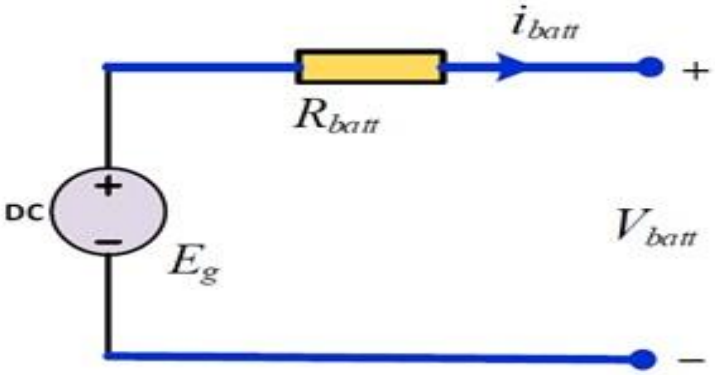

Fig.2.26. Equivalent circuit of battery.

By providing a duty cycle to the converter, the local control unit for storage controls battery current to manage battery charging and discharging, as shown in Fig.2.27. Consequently, the DC bus voltage remains steady.

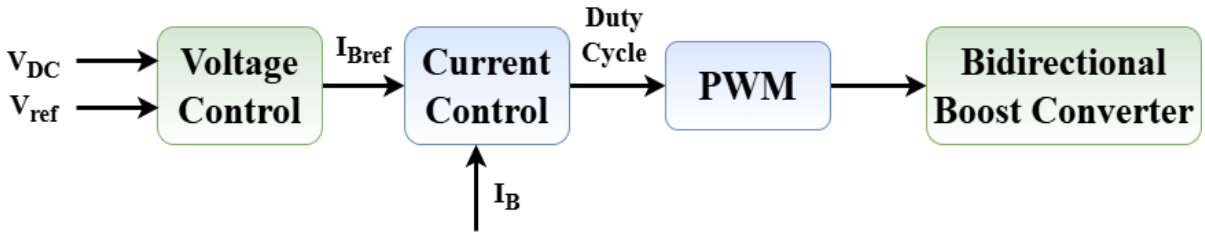

Fig.2.27. Battery local control.

Where:

Eg = no-load voltage (V)

Ego = battery constant voltage (V)

K = polarization voltage (V)

QR = maximum battery capacity (Ah)

$ibattdt$ = actual battery charge (Ah)

A = Exponentiel zone amplitude (V)

B = Exponential zone time constant inverse (Ah)

$Vbatt$ = battery output voltage (V)

$Rbatt$ = internal resistance (resistance that the battery opposes to the flow of energy) (W)

$ibatt$ = battery current (A)

5. Conclusion:

This chapter aims to provide an overview of the grid-connected photovoltaic system model components that will be used in the control system and simulation chapters to follow. First, the P-V and I-V characteristic curves of photovoltaic models (cell, module) have been outlined. The power converters used in the suggested grid-connected system were then demonstrated, including a DC-DC converter that effectively illustrated their power circuits and modeling. Additionally, a DC-AC inverter was characterized, encompassing a a battery energy storage system, a two-level inverter, a three-level natural pointed champ inverter, and a voltage source inverter.

DC-DC converters are essential in contemporary electronics, enabling effective power management through the conversion of one voltage level to another. Including other varieties such as buck, boost, and buck-boost. They provide adaptability in addressing the varied voltage

specifications of distinct electronic systems.

These converters have extensive uses in sectors including automotive, renewable energy, telecommunications, and consumer electronics. DC-DC converters are essential for powering small electronic devices and regulating energy flow in solar power systems. Maximum Power Point Tracking (MPPT) is an essential technique, especially in renewable energy systems like solar power. It facilitates the optimal extraction of maximum power from solar panels by modifying the electrical operating point. In the subsequent chapter, we will explore MPPT, its significance, and its diverse implementation techniques.

Chapter II: Modeling of photovoltaic System and power converter

Reference

[1] C.-H. Li, X.-J. Zhu, G.-Y. Cao, S. Sui, and M.-R. Hu, "Dynamic modeling and sizing optimization of stand-alone photovoltaic power systems using hybrid energy storage technology," *Renewable energy,* vol. 34, no. 3, pp. 815–826, 2009.

[2] M. A. Green, "Photovoltaic physics and devices," in *Solar Energy*: Routledge, 2013, pp. 291–355.

[3] B. Mohammed, "Modélisation d'un système de captage photovoltaïque autonome," *Mémoire de Magister Centre Universitaire de Bechar, Institut des Sciences Exactes,* p. 24, 2008.

[4] M. A. Abdelkareem, M. E. H. Assad, E. T. Sayed, and B. Soudan, "Recent progress in the use of renewable energy sources to power water desalination plants," *Desalination,* vol. 435, pp. 97–113, 2018.

[5] M. H. Mohamed Hariri, M. K. Mat Desa, S. Masri, and M. A. A. Mohd Zainuri, "grid-connected PV generation system—Components and challenges: A review," *Energies,* vol. 13, no. 17, p. 4279, 2020.

[6] S. M. Ebrahimi, E. Salahshour, M. Malekzadeh, and F. Gordillo, "Parameters identification of PV solar cells and modules using flexible particle swarm optimization algorithm," *Energy,* vol. 179, pp. 358–372, 2019.

[7] R. Kumar and S. Singh, "Solar photovoltaic modeling and simulation: As a renewable energy solution," *Energy Reports,* vol. 4, pp. 701–712, 2018.

[8] S. Singh, "Selection of non-isolated DC-DC converters for solar photovoltaic system," *Renewable and Sustainable Energy Reviews,* vol. 76, pp. 1230–1247, 2017.

[9] A. Gopi and R. Saravanakumar, "High step-up isolated efficient single switch DC-DC converter for renewable energy source," *Ain shams engineering journal,* vol. 5, no. 4, pp. 1115–1127, 2014.

[10] J. D. Navamani, K. Vijayakumar, and R. Jegatheesan, "Non-isolated high gain DC-DC converter by quadratic boost converter and voltage multiplier cell," *Ain Shams Engineering Journal,* vol. 9, no. 4, pp. 1397–1406, 2018.

[11] P. Koski *et al.*, "Development of reformed ethanol fuel cell system for backup and off-grid applications—system design and integration," in *2016 IEEE International Telecommunications Energy Conference (INTELEC)*, 2016: IEEE, pp. 1–8.

[12] R. Rai, R. Bhatia, and P. Nijhawan, "Z-Source Inverter based DC-DC converter using SPWM technique for fuel cell application," in *2016 IEEE 1st International Conference on Power Electronics, Intelligent Control and Energy Systems (ICPEICES)*, 2016: IEEE, pp. 1–4.

[13] F. A. Silva, "Advanced DC\/AC inverters: applications in renewable energy (Luo, FL and Ye, H.; 2013)[book news]," *IEEE Industrial Electronics Magazine,* vol. 7, no. 4, pp. 68–69, 2013.

[14] J. T. Hawke, H. S. Krishnamoorthy, and P. N. Enjeti, "A family of new multiport power-sharing converter topologies for large grid-connected fuel cells," *IEEE Journal of Emerging and Selected Topics in Power Electronics,* vol. 2, no. 4, pp. 962–971, 2014.

[15] A. Zorig, M. Belkheiri, S. Barkat, and A. Rabhi, "Control of three-level NPC inverter based grid connected PV system," in *2015 3rd International Conference on Control, Engineering & Information Technology (CEIT)*, 2015: IEEE, pp. 1–6.

[16] M. H. Rashid, *Power electronics handbook*. Butterworth-heinemann, 2017.

[17] M. Inci and Ö. Türksoy, "Review of fuel cells to grid interface: Configurations, technical challenges and trends," *journal of cleaner Production,* vol. 213, pp. 1353–1370, 2019.

[18] A. Poorfakhraei, M. Narimani, and A. Emadi, "A review of multilevel inverter topologies in electric vehicles: Current status and future trends," *IEEE Open Journal of Power Electronics,* vol. 2, pp. 155–170, 2021.

[19] C. Jin, P. Wang, J. Xiao, Y. Tang, and F. H. Choo, "Implementation of hierarchical control in DC microgrids," *IEEE transactions on industrial electronics,* vol. 61, no. 8, pp. 4032–4042, 2013.

[20] A. A. Z. Diab, H. M. Sultan, R. Aljendy, A. S. Al-Sumaiti, M. Shoyama, and Z. M. Ali, "Tree growth based optimization algorithm for parameter extraction of different models of photovoltaic

cells and modules," *IEEE Access,* vol. 8, pp. 119668–119687, 2020.
[21] B. Yang *et al.*, "Comprehensive overview of meta-heuristic algorithm applications on PV cell parameter identification," *Energy conversion and management,* vol. 208, p. 112595, 2020.
[22] O. Tremblay, L.-A. Dessaint, and A.-I. Dekkiche, "A generic battery model for the dynamic simulation of hybrid electric vehicles," in *2007 IEEE vehicle power and propulsion conference*, 2007: Ieee, pp. 284–289.
[23] S. Sepasi, C. Talichet, and A. S. Pramanik, "Power quality in microgrids: A critical review of fundamentals, standards, and case studies," *IEEe Access,* vol. 11, pp. 108493–108531, 2023.

Chapter III: Photovoltaic system management using MPPT and SVPWM controls within microgrid

1. Introduction

To address the performance issues of solar panels and get optimal efficiency, it is essential to refine the design of all components of the photovoltaic system. Furthermore, it is imperative to optimize the DC/DC converters serving as the input interface for the photovoltaic generator and the load to ensure continuous maximum power extraction, thereby enabling the photovoltaic system to function at its maximum power point (MPP) without energy transfer loss, utilizing a maximum power point tracking (MPPT) controller.

Thus, optimal power is achieved under diverse loads and environmental variables (illumination and temperature). Since the 1970, numerous MPPT control approaches have been developed, beginning with basic methods utilizing voltage and current feedback and advancing to more sophisticated controllers employing algorithms to determine the PV system's MPP.

An overview of the most common control schemes for grid-connected solar systems is given in this chapter.

Initially, discuss the most prevalent strategies, including the Incremental Conductance (INC) method and the Perturb and Observe (P&O) method [1]. Subsequently, we will attempt to demonstrate a strategy for identifying the optimal point indicative of enhanced performance in the INC technique through the application of fuzzy logic [the hybrid approach]. We will also discuss inverter strategies in photovoltaic systems represented by controlling the SVPWM method.

2. Maximum Power Point trucking strategies

A few years ago, researchers commenced the development of ways to maximize power extraction from renewable energy sources, particularly photovoltaic arrays. The photovoltaic array experiences issues related to efficiency, weather dependence, and intermittency in the generated electric power [2, 3]. Additionally, there exists a distinct point on the nonlinear P.V curve of the solar array known as the Maximum Power Point (MPP), where the entire photovoltaic system functions at optimal efficiency [4, 5].

Consequently, it is imperative to develop a controller that enables photovoltaic systems to consistently track and rapidly extract maximum power. This method is referred to as the Maximum Power Point Tracking (MPPT) controller, which is essential for predicting and tracking the Maximum Power Point (MPP) under all conditions, thereby ensuring the photovoltaic (PV) system operates at that MPP. Their application is in the DC-DC converter (in the initial stage); this section presents and compares the most frequently utilized MPPT algorithms. This overview encompasses numerous MPPT approaches for photovoltaic arrays.

These MPPT systems utilize iterative search algorithms to identify the optimal operating point of the solar module, ensuring maximal power generation without disrupting system functionality. They are based on the ongoing optimization of the power produced by the photovoltaic modules. The power derived from the module is determined by the product of its current and voltage measurements. These measures are employed by several techniques that seek the true maximum power point (MPP). Various types of MPPT controls exist, including the concepts of numerous ways such as the constant voltage method, The method of constant current, the incremental conductance algorithm, and the perturbation and observation method.

Fig.3.1. illustrates three (03) categories of disturbances. Depending on the disturbance's nature, the operating point shifts from the maximum power point MPP1 to a new operating point P1, which may be quite away from the optimal position. To attain a fluctuation in sunlight (instance a), it is essential to adjust the duty cycle value to correspond with the revised MPP2. In the occurrence of a load fluctuation (case b), a change in the operating point may transpire, perhaps resulting in a new ideal position due to command intervention. The ultimate occurrence of operating point variation may result from alterations in the operating temperature of the solar module (case c). Although we must function at the command level, it does not encounter the same temporal limitations as the prior two instances.

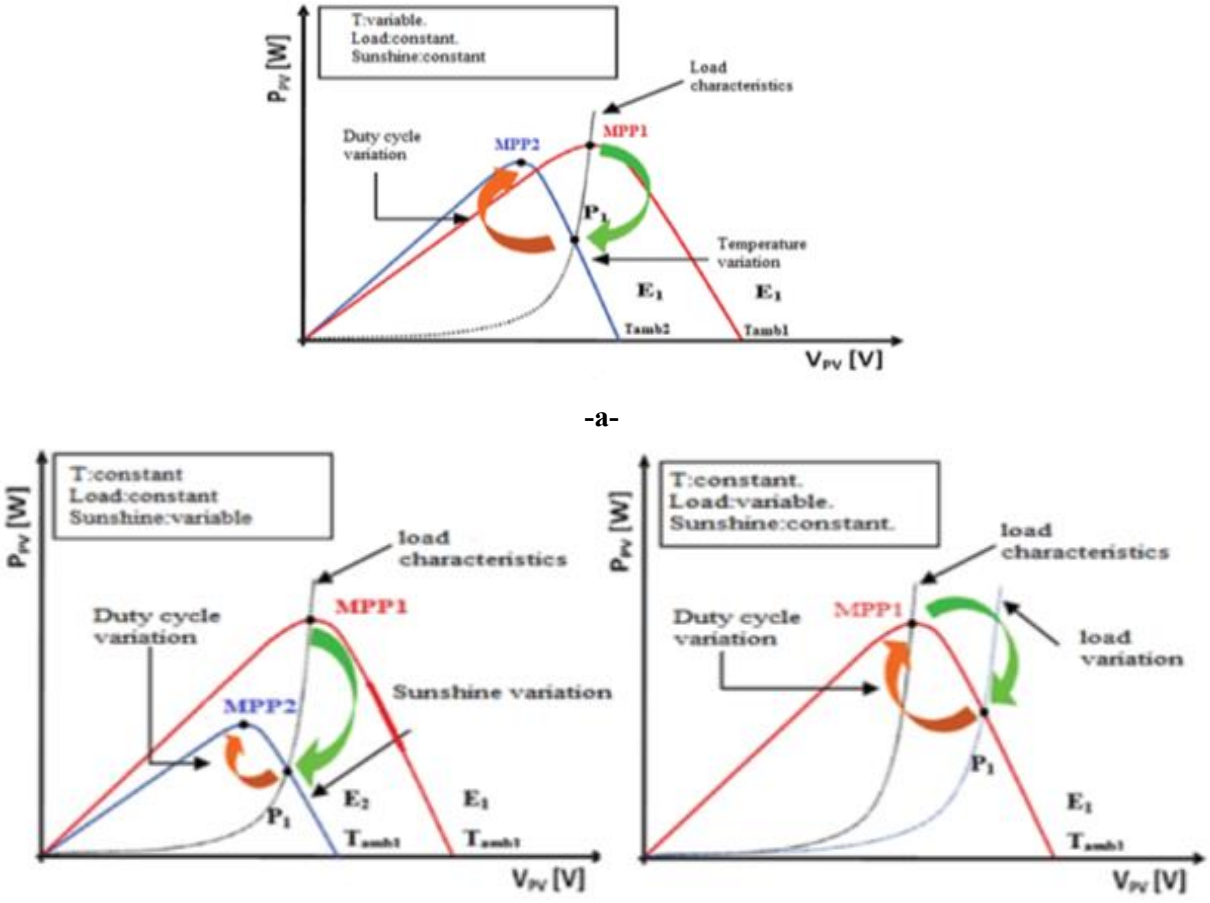

Fig.3.1. Search and Recovery Of MPP.

3. MPPT modeling

The photovoltaic output power is influenced by temperature and irradiance. Over the course of a day, the atmospheric conditions change. As a result, the MPP is displaced in reaction to changes in temperature and radiation. When the operating point deviates from the Maximum Power Point (MPP), significant power losses take place. To guarantee the best possible power extraction from the photovoltaic panel, it is crucial to always watch the Maximum Power Point (MPP).

The temperature and irradiance have an impact on solar systems' output power. Within a single day, the atmospheric conditions vary. Temperature and radiation conditions cause the MPP to

be displaced as a result. There are large power losses when the working point differs from the MPP, or maximum power point. To ensure the best possible power extraction from the photovoltaic panel, it is imperative to constantly check the Maximum Power Point (MPP).

$$PPV\ (t)\ =\ F\ (VPV\ (t), IPV\ (t), \gamma\ (t)) \tag{III.1}$$

where the power curve at time t is defined by γ, which stands for all variables outside of current and voltage. The outcome is dependent on the climate and photovoltaic settings. In reaction to variations in input factors, such as temperature and irradiance, an MPP tracking technique involves modifying the photovoltaic system's output voltage to optimize the extraction of available power. The Maximum Power Point (MPP) is where In relation to output voltage, the derivative of output power is zero; it is positive to the left of the MPP and negative to the right. This is the basis upon which the MPPT operates. **Fig.3.1.**

It is essential to observe that the curves defined by Eq. (III.1) possess the following characteristic:

$$\begin{cases} \frac{dp_{pv}}{dV_{pv}} = 0 \quad when \quad V_{pv} = V_{MPP} \\ \frac{dp_{pv}}{dV_{pv}} > 0 \quad when \quad V_{pv} < V_{MPP} \\ \frac{dp_{pv}}{dV_{pv}} < 0 \quad when \quad V_{pv} > V_{MPP} \end{cases} \tag{III.2}$$

The tracking technique for the attributes of the curves delineated by Eqs. (III.1) and (III.2) adheres to the subsequent principle:

$$\frac{dp_{pv}}{dV_{pv}} . \frac{dp_{pv}}{dV_{pv}} > 0 \tag{III.3}$$

Calculating the output power in relation to the output voltage results in:

$$\frac{dp_{pv}}{dV_{pv}} = \frac{d(V_{pv}.I_{pv})}{dV_{pv}} = I_{pv} + V_{pv}\frac{dI_{pv}}{dV_{pv}} \tag{III.4}$$

Since the power derivative with respect to voltage is zero at MPP :

$$\frac{dp_{pv}}{dV_{pv}} = 0 \rightarrow \frac{V_{pv}}{I_{pv}} = -\frac{V_{pv}}{I_{pv}} \tag{III.5}$$

The following is an expression for the error between the instantaneous and derivative values:

$$\varepsilon = \frac{V_{pv}}{I_{pv}} + \frac{dV_{pv}}{dI_{pv}} \tag{III.6}$$

Combining Eqs (III. 2) and (III.6), the MPP can be tracked by comparing

$$\frac{V_{pv}}{I_{pv}} \; to \; \frac{dV_{pv}}{dI_{pv}} \tag{III.7}$$

$$\varepsilon = 0 \longleftrightarrow \frac{V_{pv}}{I_{pv}} = -\frac{dV_{pv}}{dI_{pv}} \; at \; the \; MPP \varepsilon > 0 \longleftrightarrow \frac{V_{pv}}{I_{pv}} \tag{III.8}$$

$$-\frac{dV_{pv}}{dI_{pv}} \; left \; to \; the \; MPP \varepsilon < 0 \longleftrightarrow \frac{V_{pv}}{I_{pv}} < -\frac{dV_{pv}}{dI_{pv}} \; right \; to \; the \; MPP$$

Equation (III.7) is illustrated in Fig.3.4. The intersection of the dPPV/dVPV curves with the current axis and the intersection of VPV/IPV with the dVPV/dIPV curves mark the Maximum Power Point (MPP), which is located at the top of the power graph where IPV = IMPP. The dVPV/dIPV and VPV/IPV curves intersect at the Maximum Power Point (MPP), which aligns with VMPP on the voltage axis Fig.3.3. The ideal current IMPP is located at the intersection of the current curve and VMPP.

4. MPPT selection criteria

Although numerous tracking strategies exist for solar systems, identifying the most effective one is not simple. When selecting MPP approaches, the following criteria must be evaluated.

4.1. Implementation

The simplicity of execution is a crucial consideration in selecting an MPPT technique. Certain approaches can be readily executed without requiring on-site calibration or modification. Other methods are more complex, and their calibration differs based on geographical location and climate circumstances.

4.2. Sensors

The decision-making process is also impacted by the quantity of sensors needed to carry out MPPTs. In order to monitor the maximum power, it is

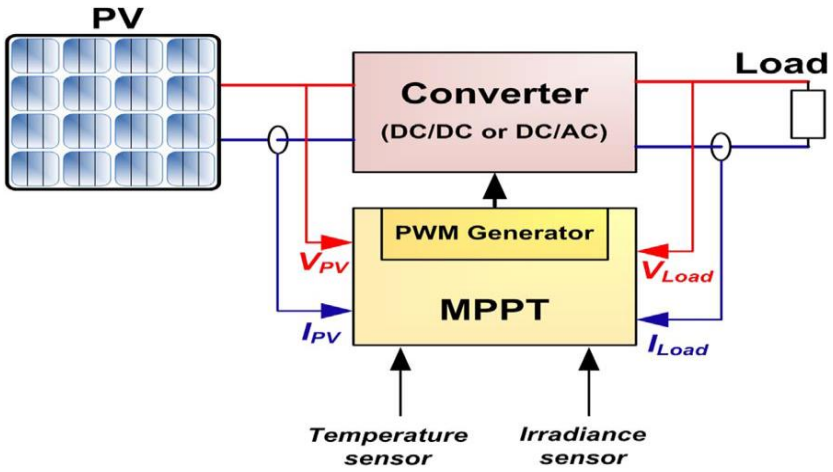

Fig.3.2. General scheme of a PV with an MPPT system.

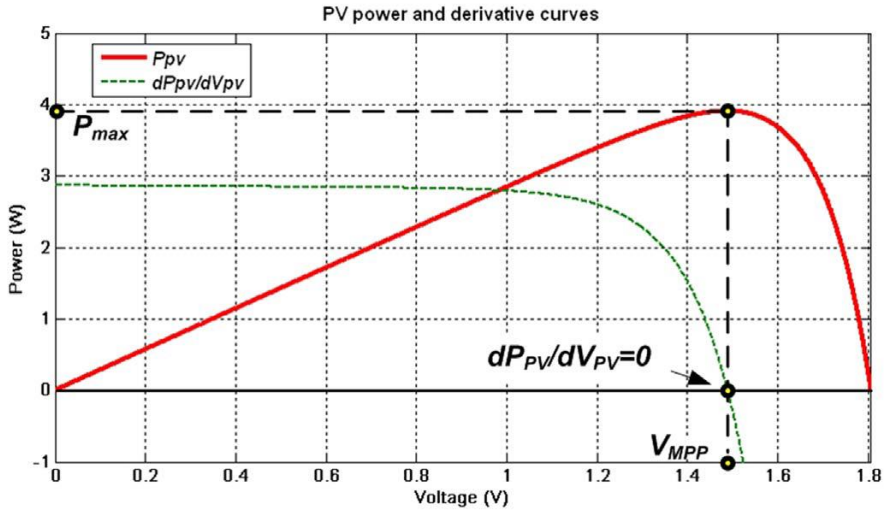

Fig.3.3. Power curve and its derivative with respect to VPV.

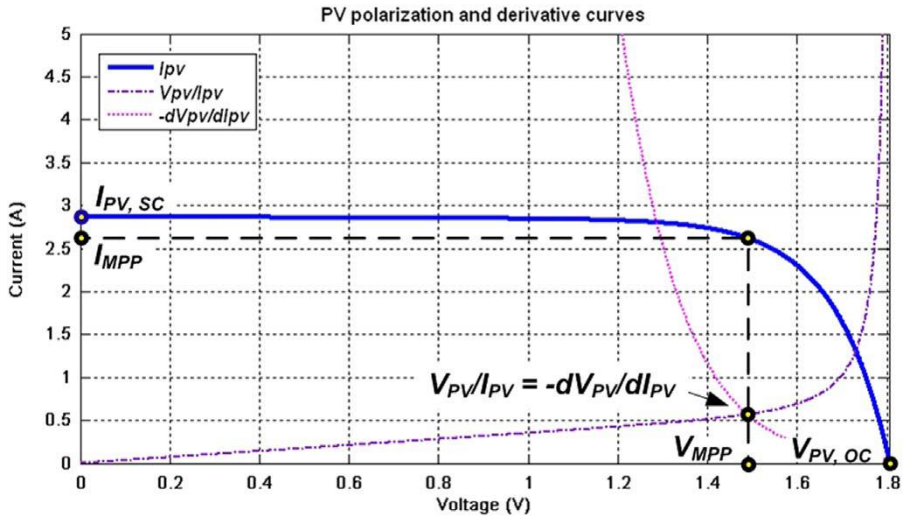

Fig.3.4. Intersection of dVPV /dIPV and the VPV /IPV at MPP.

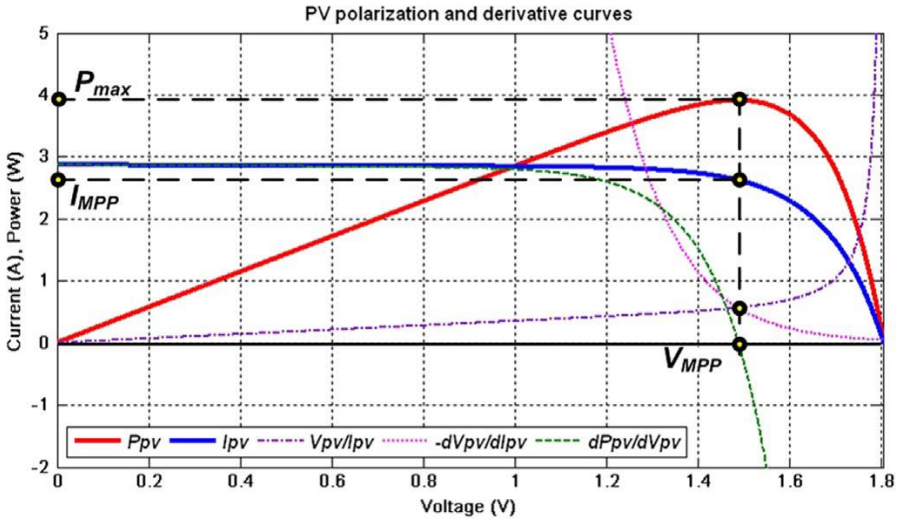

Fig.3.5. Polarization curves and derivatives show the location of the MPP, VMPP, and IMPP.

vital for the tracker to identify the photovoltaic outputs (voltage and current) and inputs (temperature and irradiance). Four sensors are therefore needed.

However, some MPPT lower the number of sensors by using updated approaches. All that is needed to measure the maximum power using the Open-Circuit method is a voltage sensor.

4.3. Efficiency

The efficacy of the tracker is correlated with the accuracy of identifying the Maximum Power Point in a limited timeframe. Some MPPT approaches demonstrate oscillations around the MPP due to their trial procedures for identifying maximum power, hence reducing the overall efficiency of the PV system.

4.4. Cost

The cost of a tracking device depends on the system's functionality, hardware expenses, software complexity, and the number of sensors. Generally, the cost of analog systems is inferior to that of digital systems, including those dependent on microprocessors or FPGAs.

4.5. Application

In evaluating tracking methodologies, focus is occasionally restricted to tracking control, overlooking the influence of power maximization on the environmental hardware linked to the photovoltaic system. A solar system generally includes batteries, requiring meticulous attention

to essential charging and discharging parameters. Consequently, the choice of the MPPT method must consider the battery type, charging techniques, and cycles.

5. MPPT method classification

Since the emergence of photovoltaics as both independent and grid-connected systems, researchers have sought to develop methods to enhance the power absorption of PV panels. A significant array of MPPT algorithms and designs has been documented in the literature to far. Each methodology has specific prerequisites, constraints, and utilizations.

No evaluation study classifies techniques, as each may be suitable for one application but not for another. This section classifies tracking methods according to their methodology, divided into five categories Table.3.1:

• Tracking methodologies with constant parameters: These techniques employ established fixed variables that delineate the MPP.

• Monitoring approaches encompassing measurement and comparison: This method depends on identifying external variables (PV voltage, current, irradiance, or temperature) and comparing them with a specified Maximum Power Point (MPP).

• Tracking strategies utilizing trial and error: These techniques entail performing calculations and analyzing the ensuing outcomes, which guide the directional parameters for following endeavors to attain the MPP.

• Mathematical calculation-based tracking techniques: These approaches determine the location of the MPP by mathematical computations based on available data and equations.

• Sophisticated predictive tracking methodologies: These systems utilize an advanced learning framework that facilitates the forecasting of the MPP's position.

Table.3.1. List of MPPT methods.[1]

Tracking techniques	#	Tracking methods
Tracking techniques with constant parameters	1	Constant voltage method
	2	Open-circuit voltage method
	3	Short-circuit current method
	4	Open-circuit voltage pilot PV cell method
	5	Temperature Gradient (TG) Algorithm
	6	Temperature Parametric (TP) Method
	7	Feedback voltage or current method
	8	P-N junction drops voltage tracking technique
Tracking techniques with measurement and comparison	9	Look-up table method
	10	Load current or load voltage maximization
	11	Linear current control method
Tracking techniques with trial and error	12	The only-current photovoltaic method
	13	PV Output Senseless (POS) control method
	14	Perturb and Observe (P&O) method
	15	Modified P & O with fixed perturbation step
	16	Conventional P&O with adaptive perturbation
	17	Modified P & O with adaptive perturbation
	18	Three-point weight comparison method
	19	On-Line MPP search algorithm
	20	DC-Link capacitor droop control
	21	Array Reconfiguration Method
	22	MPPT with a variable inductor
	23	State-based MPPT method
	24	Linear reoriented coordinates method
	25	Curve-fitting method
	26	Differentiation method
	27	Slide control method
	28	Current sweep method

Tracking techniques with mathematical calculation	29	dP/dV or dP/dI feedback control
	30	Incremental Conductance method
	31	Variable step incremental conductance method
	32	Variable step-size incremental-resistance method
	33	Parasitic capacitance (PC) method
	34	ß method
	35	IMPP and VMPP computation method
	36	Methods by modulation
	37	Ripple correlation control
Tracking techniques with intelligent prediction	38	Fuzzy logic control 38
	39	Neural network
	40	Biological swarm chasing algorithm

6. Investigated MPPT Methodologies

A key method for increasing photovoltaic (PV) systems' efficiency is Tracking Maximum Power Point (MPPT). The point on the current-voltage (I-V) curve where the photovoltaic (PV) system generates the most power is known as the Maximum Power Point (MPP). The MPP is influenced by several factors, such as temperature, shadow, and sun exposure. To optimize power extraction, adjust the solar system's operating point and determine the Maximum Power Point (MPP) in reaction to shifting environmental conditions are the goals of MPPT procedures [6, 7].

6.1. The Perturbation and Observation (P&O)

Because of how easy it is to use, the Perturbation and Observation technique is widespread. By varying the output voltage of the solar panels either upward or downward, the P&O algorithm will force the photovoltaic system to converge on the maximum power point Fig.3.6 illustrates the control flow diagram of the P&O algorithm.

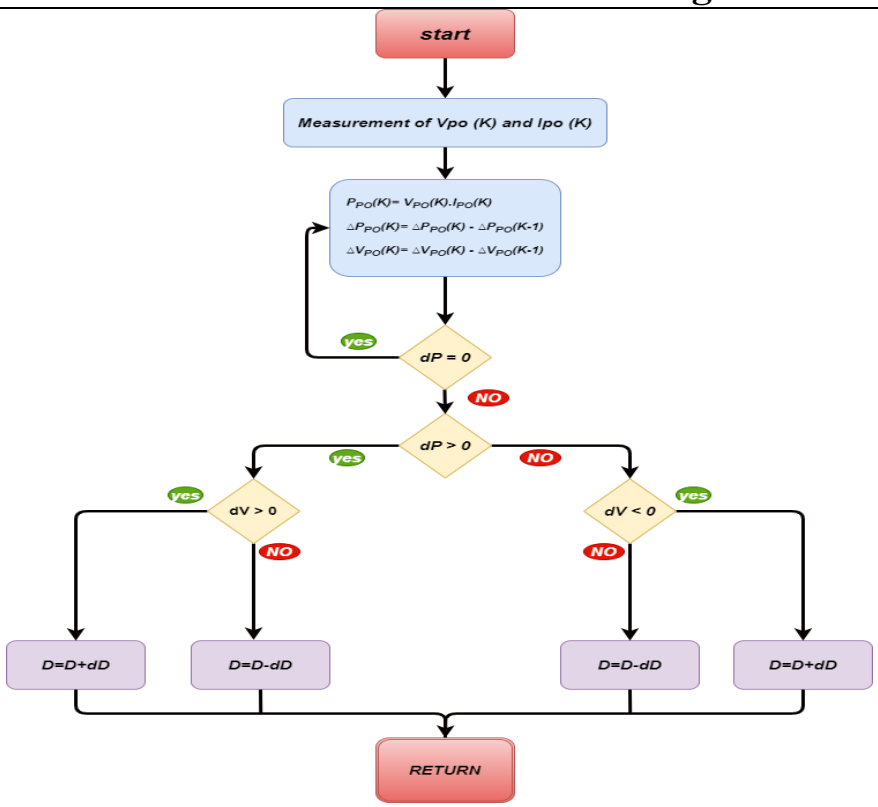

Fig.3.6. Flowchart of the P&O algorithm

The P&O method modifies the PV panel's operating voltage to identify the best direction for power maximization; if power rises, the voltage is further modified in the same direction, and if power falls, the perturbation direction is reversed. Until the MPP is reached, this process is carried out periodically.[8]. After then, there was oscillation in the system around the Maximum Power Point (MPP). The following link can be used to calculate the duty cycle variation at time (t+1) [1]:

$$d(t+1) = d(t) + (2sign - 1)D \quad \text{(III.9)}$$

Where sign is given by:

$$sign = ([P(t) - p(t-1)] > 0) + ([V(t) - V(t-1)] > 0) \quad \text{(III.10)}$$

The voltage and power taken from the photovoltaic panel are shown by the symbols P(t) and V(t), respectively. While reducing the perturbation step-size D helps reduce the oscillation around the Maximum Power Point (MPP), a lower perturbation step-size has a negative impact on dynamic performance Fig.3.6 Because of this trade-off, the duty cycle perturbation step size must be carefully adjusted.

6.2. The Incremental Conductance method (INC)

The foundation of the Incremental Conductance (Inc Cond) technique is the idea that the power versus voltage curve of a photovoltaic panel should slope zero at the Maximum Power Point (MPP), positive to the left, and negative to the right of the MPP. The following is an expression for the relationship between incremental conductance dI/dV and instantaneous conductance I/V:

$$\begin{cases} \frac{\Delta I}{\Delta V} + \frac{I}{V} = 0 & at\ MPP \\ \frac{\Delta I}{\Delta V} + \frac{I}{V} > 0 & left\ of\ MPP \\ \frac{\Delta I}{\Delta V} + \frac{I}{V} < 0 & right\ of\ MPP \end{cases} \quad \text{(III.11)}$$

Due to noise, measurement errors, and quantification, the condition $dI\ dV\ +\ I\ V\ =\ 0$ is rarely fulfilled, hence, in a steady state, the system oscillates about the Maximum Power Point (MPP). To address this limitation, we propose a new parameter ε, defined as:

$$\left\| \frac{\Delta I}{\Delta V} + \frac{I}{V} \right\| \leq\ \varepsilon \quad \text{(III.12)}$$

The INC method is illustrated in the flowchart depicted in Fig.3.7 [2].

The amplitude of the oscillations around the MPP is governed by the value of ε. It diminishes as ε increases Fig.3.7.

Nonetheless, with a somewhat large value of ε, the operating point deviates from the genuine Maximum Power Point (MPP). Therefore, the ε parameter must be selected judiciously to enhance the performance of the MPPT system [3].

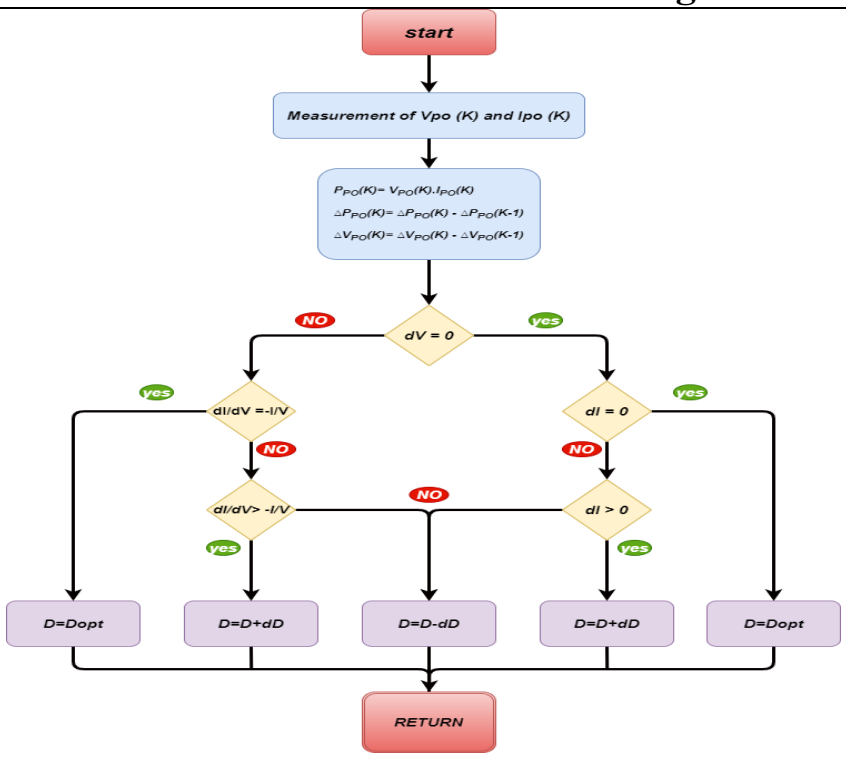

Fig.3.7. The INC algorithm flowchart.

7. Modulation techniques Inverter

Increasing the number of output levels can enhance the quality of the multilevel inverter's output voltage and power.[9]. The harmonic content decreases and the dv/dt stress on the switches is evened out as the output level rises. Choosing the right modulation technique can also improve the inverter's output power quality. Much work is being done to increase converter efficiency while reducing the percentage of THD in the output voltage waveforms under a variety of loading scenarios. These can be accomplished by controlling MLI using appropriate modulation techniques. The modulation strategy's primary goals are:

• The capacity to function with a broad modulation index range.
• To reduce switching losses and increase the converter's overall efficiency.
• To have a lower output voltage THD percentage.
• To achieve a high fundamental frequency component output value.
• It should be simple to put the control method into practice.
• It ought to be less complicated and time-consuming. The modulation techniques are categorized according on the switching frequency as indicated in Fig.3.14 [10, 11].

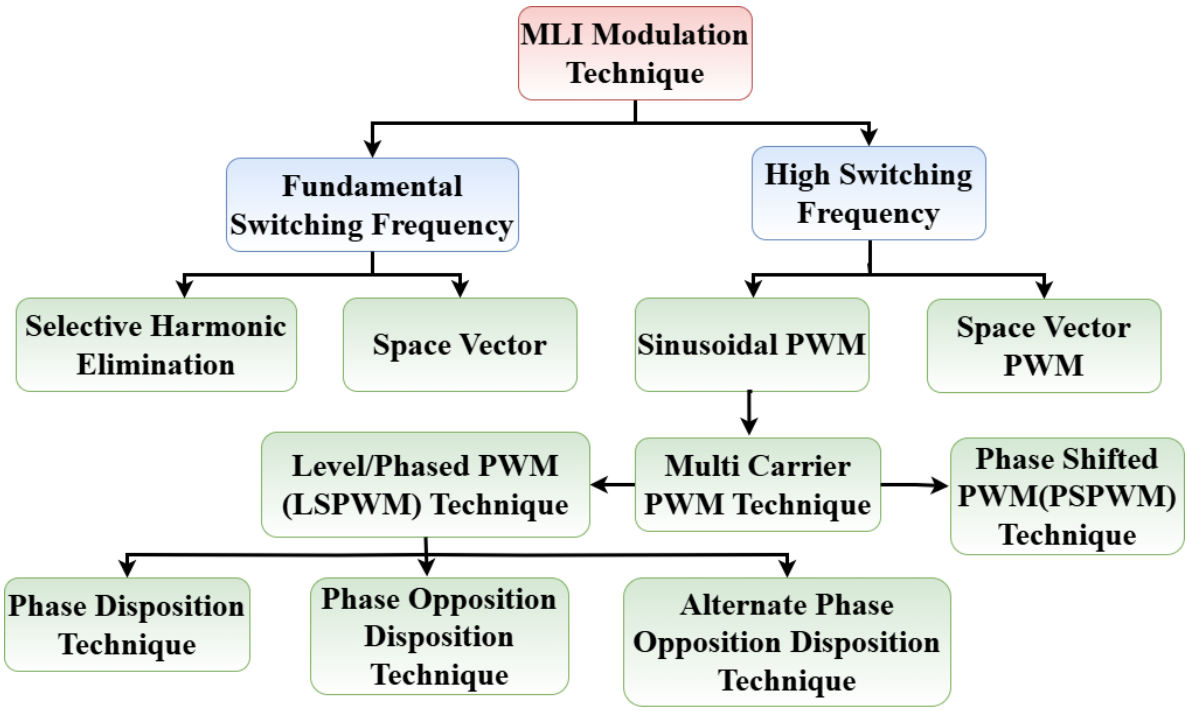

Fig.3.14. Classification of modulation technique

7.1. Space Vector PWM (SVPWM) Technique

In the "SVPWM" technique, the switching state is a mixture of phase voltage levels. The Space vector theorem states that every switching state is an instantaneous voltage vector composed of three-phase voltage levels. All of the switching states form a voltage hexagon lattice when shown graphically. Each node on the lattice represents a producible voltage vector; only a few nodes have more than one redundant switching state. The controller assigns the time-averaged voltage vector produced by these nodes. The voltage vector is related to a stationary stator reference frame using the artesian αβ coordinate system. Selecting such switching states that come into contact with the reference is the modulator's task. This method's benefit is that the entire lattice-enclosed region can be utilized without taking modulation indices into account.[12].

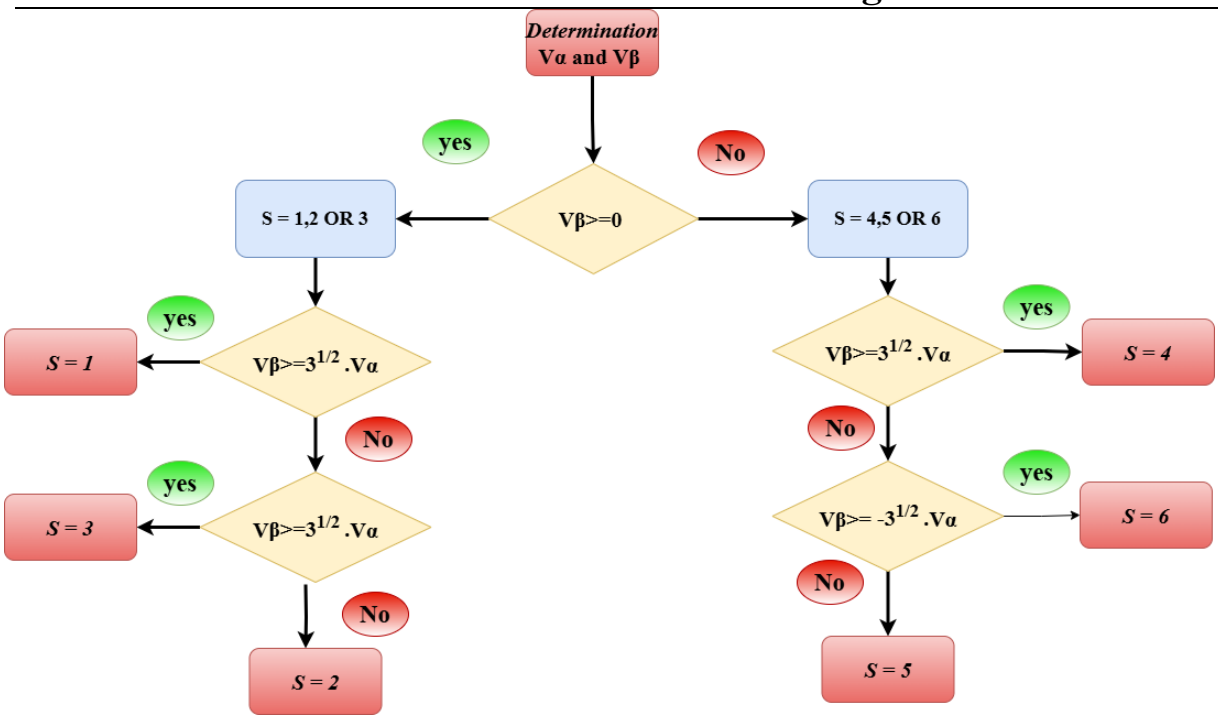

Fig.3.15. flowchart Sector calculation.

The structure of the two-level voltage inverter is shown in the figure

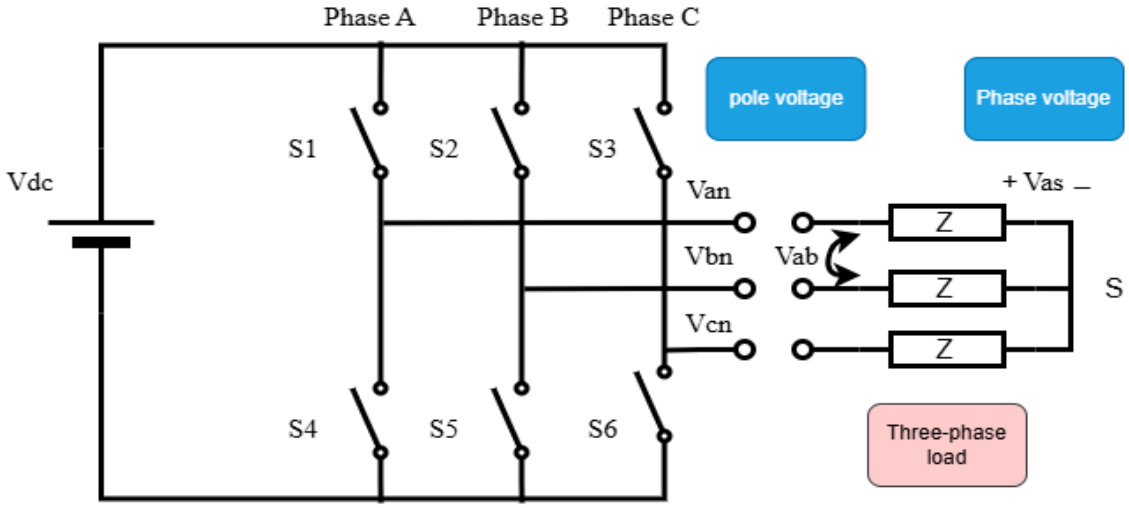

Fig.3.16. Structure of a three-phase two-level voltage inverter

Table.3.2 represents the different states of the inverter (000, 100,110, 010, 011, 001, 101,111) and the coordinates of the output voltage vector vi (vα, vβ) corresponding to each switching state.

Any column has state 0 or1

1 mean the upper switch is on and lower switch is off

0 mean lower switch is on and the upper switch is off

Tabel.3.2. probabilities of inverter

Space vector	S1	S2	S3
V0	0	0	0
V1	1	0	0
V2	1	1	0
V3	0	1	0
V4	0	1	1
V5	0	0	1
V6	1	0	1
V7	1	1	1

The following equations describe how phase voltages can be determined by applying the voltage divider rule in the context of a symmetric three-phase inverter system. The voltage divider rule allows us to calculate the voltage drop across an impedance in a series network. These equations aim to model the relationship between applied DC voltage (Vdc) and the resulting line-to-neutral phase voltages (Vas, Vbs, etc.).

For a general voltage divider involving impedances Z_1 and Z_2,the voltage across Z_1 is given by:

$$V_{z1} = \frac{Z_1}{Z_1 + Z_2} V_{dc} \quad \text{(III.13)}$$

This principle is applied repeatedly in the given expressions.

A. Phase Voltage Vas

Given:

$$V_{as} = \frac{Z}{Z + \frac{Z.Z}{Z+Z}} V_{dc} \quad \text{(III.14)}$$

This expression represents the voltage across impedance Z, where it is in series with a parallel combination of two other impedances Z. Simplifying the denominator:

So, the total impedance becomes:

$$Z + \frac{Z}{2} = \frac{3Z}{2} \quad \text{(III.15)}$$

Thus, the voltage becomes:

$$V_{as} = \frac{2}{3} V_{dc} \quad \text{(III.16)}$$

This corresponds to the standard phase voltage for a two-level inverter where the output is $\frac{2}{3} V_{dc}$.

B. Phase Voltage Vbs

Given:

$$V_{bs} = \frac{-\frac{1}{2}Z}{Z + \frac{1}{2}Z} V_{dc} \quad \text{(III.17)}$$

Thus:

$$V_{bs} = \frac{-\frac{1}{2}Z}{\frac{3}{2}Z} V_{dc} = -\frac{1}{3} V_{dc} \quad \text{(III.18)}$$

C. Phase Voltage Vcs

This represents the negative phase voltage component, again consistent with a balanced three-phase system where the sum of phase voltages is zero.

From the simplifications above, the phase voltages derived from a balanced DC bus voltage Vdc are as follows:

$$V_{as} = \frac{2}{3} V_{dc}\ , V_{bs} = -\frac{1}{3} V_{dc}\ , V_{cs} = -\frac{1}{3} V_{dc} \quad \text{(III.19)}$$

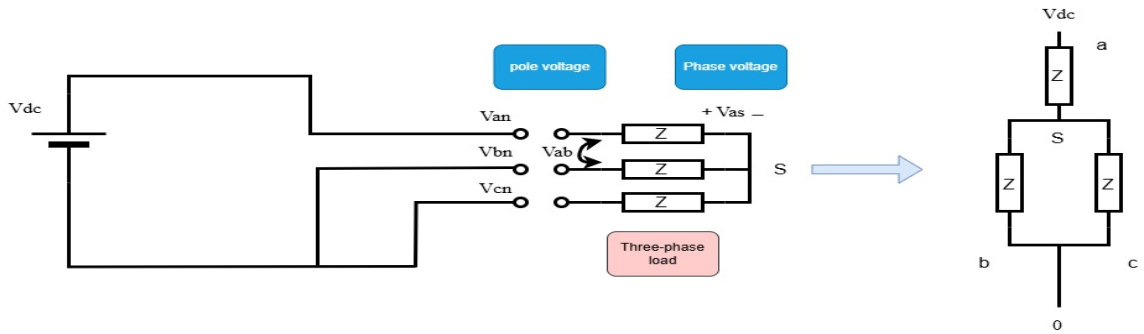

Fig.3.17. Equivalent load configurations for different switching states.

Space vectors and phase voltages

Table.3.3. Establishment of expressions for simple tensions

Space vector	Vas	Vbs	Vcs
V0 (000)	0	0	0
V1(100)	$\frac{2}{3}V_{dc}$	$-\frac{1}{3}V_{dc}$	$-\frac{1}{3}V_{dc}$
V2(110)	$\frac{1}{3}V_{dc}$	$\frac{1}{3}V_{dc}$	$-\frac{2}{3}V_{dc}$
V3(010)	$-\frac{1}{3}V_{dc}$	$\frac{2}{3}V_{dc}$	$-\frac{1}{3}V_{dc}$
V4(011)	$-\frac{2}{3}V_{dc}$	$\frac{1}{3}V_{dc}$	$\frac{1}{3}V_{dc}$
V5(001)	$-\frac{1}{3}V_{dc}$	$-\frac{1}{3}V_{dc}$	$\frac{2}{3}V_{dc}$
V6(101)	$\frac{1}{3}V_{dc}$	$-\frac{2}{3}V_{dc}$	$\frac{1}{3}V_{dc}$
V7(111)	0	0	0

1. Clarke Transformation Matrix

The Clarke Transformation is a mathematical technique used to convert three-phase quantities (in the **abc** frame) into two orthogonal components in the stationary reference frame (denoted as **α-β**). This transformation is widely used in vector control of AC machines and in space vector modulation to simplify the control algorithms.

The transformation is given by the matrix:

$$\begin{bmatrix} V_\alpha \\ V_\beta \end{bmatrix} = \begin{bmatrix} 1 & -\frac{1}{2} & -\frac{1}{2} \\ - & \frac{\sqrt{3}}{2} & \frac{-\sqrt{3}}{2} \\ 0 & & \end{bmatrix} \begin{bmatrix} V_a \\ V_b \\ V_c \end{bmatrix} \quad \text{(III.20)}$$

Va, Vb,Vc are the instantaneous voltages of the three-phase system.

Vα, Vβ, are the two orthogonal components in the 2D stationary frame.

This transformation assumes a balanced three-phase system where Va+Vb+Vc=0

After applying the Clarke transformation, the space vector's magnitude and angle in the α-β plane are calculated as:

$$V_r = \sqrt{V_\alpha^2 + V_\beta^2} \quad , \quad \alpha = \tan^{-1}\left(\frac{V_\beta}{V_\alpha}\right) \tag{III.21}$$

These equations define the length (magnitude) and direction (angle) of the resulting voltage vector in the stationary reference frame.

Apply for space vector 2

In space vector modulation, the vector representation of the output voltage is placed within a hexagonal structure divided into 6 sectors. When the system operates in Sector 2, the space vector is synthesized using a combination of adjacent vectors that bound that sector.

Given:

$$V_\alpha = 0.500.V_{dc} \quad , \quad V_\beta = 0.8661.V_{dc} \tag{III.22}$$

Magnitude Calculation:

$$V_r = \sqrt{(0.5\,V_{dc})^2 + (0.8661\,V_{dc})^2} = \sqrt{1}\,V_{dc} \tag{III.23}$$

Angle Calculation:

$$\alpha = \tan^{-1}\left(\frac{0.8661}{0.5}\right) \simeq 60 \tag{III.24}$$

So:

$$V_{resultan} = V_{dc} \quad , \quad \alpha = 60 \tag{III.25}$$

This confirms that the space vector lies in Sector 2 of the SVM hexagon (each sector spans 60°), and the synthesized vector points in the direction of α=60◦ with a magnitude equal to the full DC link voltage Vdc.

Table.3.4. États du réflecteur et coordonnées vectorielles vr aux angles α

Space vector	Vas	Vbs	Vcs	Vr	α
V0 (000)	0	0	0	0	0
V1(100)	$\frac{2}{3}V_{dc}$	$-\frac{1}{3}V_{dc}$	$-\frac{1}{3}V_{dc}$	V_{dc}	0
V2(110)	$\frac{1}{3}V_{dc}$	$\frac{1}{3}V_{dc}$	$-\frac{2}{3}V_{dc}$	V_{dc}	60
V3(010)	$-\frac{1}{3}V_{dc}$	$\frac{2}{3}V_{dc}$	$-\frac{1}{3}V_{dc}$	V_{dc}	120
V4(011)	$-\frac{2}{3}V_{dc}$	$\frac{1}{3}V_{dc}$	$\frac{1}{3}V_{dc}$	V_{dc}	180
V5(001)	$-\frac{1}{3}V_{dc}$	$-\frac{1}{3}V_{dc}$	$\frac{2}{3}V_{dc}$	V_{dc}	240
V6(101)	$\frac{1}{3}V_{dc}$	$-\frac{2}{3}V_{dc}$	$\frac{1}{3}V_{dc}$	V_{dc}	360
V7(111)	0	0	0	0	0

The inverter voltage vectors' representation in the complex α, β plane is displayed in Fig.3.18. These vectors form The two-level inverter's vector diagram, commonly referred to as the switching hexagon.

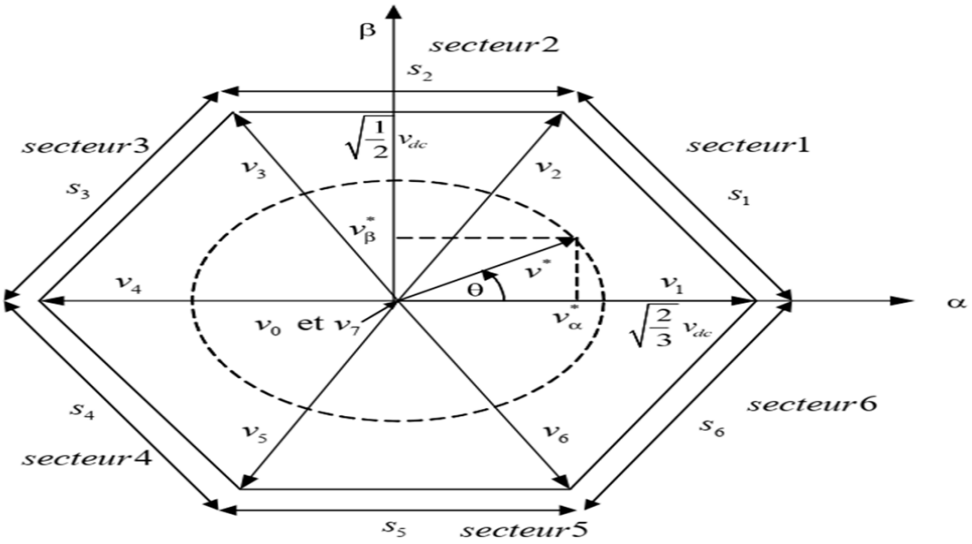

Fig.3.18Vector diagram of the two-level inverter (switching hexagon).

Define linear relation between vectors time of activation and voltage

$$\begin{cases} V_a = \dfrac{T_a}{T_{period}} V_{dc} \quad to \quad T_a = \dfrac{T_{period}}{V_{dc}} V_a \\ V_b = \dfrac{T_b}{T_{period}} V_{dc} \qquad to \qquad T_b = \dfrac{T_{period}}{V_{dc}} V_b \end{cases} \tag{III.26}$$

Apply sine rule to the tringle

$$\frac{V_r}{\sin\frac{2\pi}{3}} = \frac{V_a}{\sin\frac{\pi}{3} - \alpha} = \frac{V_b}{\sin\alpha} \tag{III.27}$$

Solve for Va and Vb component

$$\begin{cases} V_a = V_r \frac{\sin\frac{\pi}{3} - \alpha}{\sin\frac{2\pi}{3}} \quad to \quad V_a = \frac{2}{\sqrt{3}} V_r \ \sin\frac{\pi}{3} - \alpha \\ V_b = V_r \frac{\sin\alpha}{\sin\frac{2\pi}{3}} \qquad to \qquad V_b = \frac{2}{\sqrt{3}} V_r \ \sin\alpha \end{cases} \qquad \text{For } \alpha < \frac{\pi}{3} \tag{III.28}$$

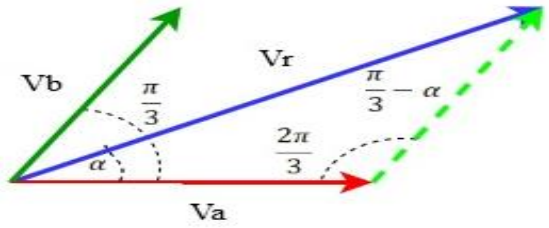

Fig.3.19. Limitation of the reference vector Vr

Generalization of the Formula for any angle

$$\begin{cases} T_a = \dfrac{2.T_{period}}{\sqrt{3}\,V_{dc}} V_r \sin\left(\dfrac{\pi}{3} - \alpha\right) \\ T_b = \dfrac{2.T_{period}}{\sqrt{3}\,V_{dc}} V_r \sin(\alpha) \\ T_0 = T_{period} - T_a - T_b \end{cases} \qquad \text{For } \alpha < \frac{\pi}{3} \tag{III.29}$$

For any angle K: sector Number

$$\begin{cases} T_a = \dfrac{2.T_{period}}{\sqrt{3}\,V_{dc}} V_r \sin\left(\dfrac{K * \pi}{3} - \alpha\right) \\ T_b = \dfrac{2.T_{period}}{\sqrt{3}\,V_{dc}} V_r \sin\left(\alpha - \dfrac{(K-1) * \pi}{3}\right) \\ T_0 = T_{period} - T_a - T_b \end{cases} \tag{III.30}$$

Performance Analysis of SVPWM

Assume that at the center of the sector the time is divide between Va & Vb only

$$\alpha = \frac{\pi}{6} \qquad \frac{T_a+T_b}{T_{period}} = 1 \tag{III.31}$$

$$\frac{2\,V_r}{\sqrt{3}\,V_{dc}}\sin\left(\frac{\pi}{3}-\alpha\right)+\frac{V_r}{\sqrt{3}\,V_{dc}}\sin(\alpha)=1 \tag{III.32}$$

$$\frac{V_r}{\sqrt{3}\,V_{dc}}+\frac{V_r}{\sqrt{3}\,V_{dc}}=1 \text{ to } \frac{2\,V_r}{\sqrt{3}\,V_{dc}}=1 \tag{III.33}$$

$$V_r=\frac{\sqrt{3}}{2}\,V_{dc} \;\; to \;\; V_r=0.866\,V_{dc} \tag{III.34}$$

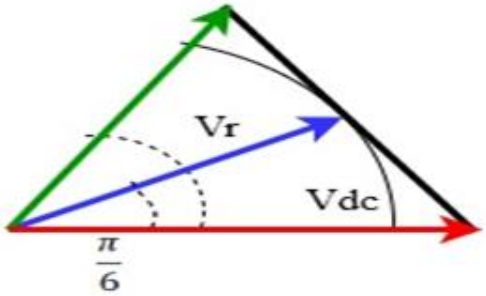

Fig.3.20. Limitation of the maximum reference Vr.max

If we connect between the top of space 1&2 and calculate the projection of the space vector on the reference vector

$$V_{rmax} = V_{dc}\cos\left(\frac{\pi}{6}\right)=\frac{\sqrt{3}}{2}\,V_{dc} \tag{III.35}$$

The phase voltages' peak is two-thirds the space vector's amplitude.

$$V_{r\,phase\,max}=\frac{2}{3}\frac{\sqrt{3}}{2}\,V_{dc}=\frac{1}{\sqrt{3}}\,V_{dc}=0.577\,V_{dc} \tag{III.36}$$

Symmetrical SVPWM algorithm

Tabel.3.5. Switch closing time in state 1.

Switch	Timer compares value	Reduced formula
S1	$\frac{T_0}{2} + T_1 + T_2$	$T_{period} - \frac{T_0}{2}$
S2	$\frac{T_0}{2} + T_2$	$\frac{T_0}{2} + T_2$
S3	$\frac{T_0}{2}$	$\frac{T_0}{2}$

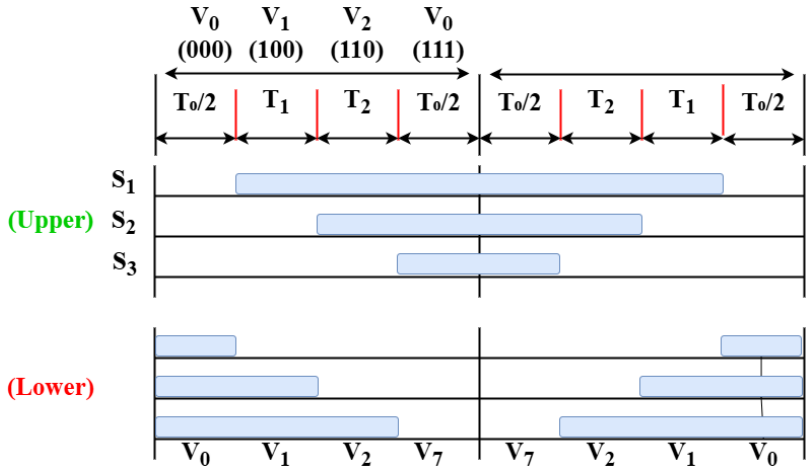

Fig.3.21. Principle of generating control pulses by vector PWM for state 1.

Tabel.3.6. Switch closing time in state 2.

Switch	Timer compares value	Reduced formula
S1	$\frac{T_0}{2} + T_1$	$\frac{T_0}{2} + T_1$
S2	$\frac{T_0}{2} + T_1 + T_2$	$T_{period} - \frac{T_0}{2}$
S3	$\frac{T_0}{2}$	$\frac{T_0}{2}$

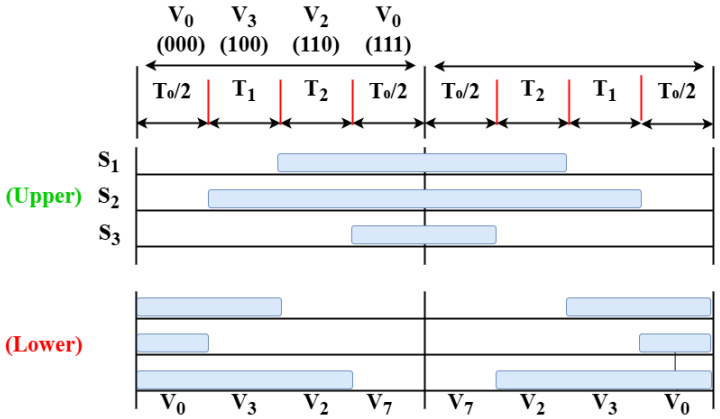

Fig.3.22. Principle of generating control pulses by vector PWM for state 2.

Tabel.3.7. Switch closing time in state 3.

Switch	Timer compares value	Reduced formula
S1	$\frac{T_0}{2}$	$\frac{T_0}{2}$
S2	$\frac{T_0}{2} + T_1 + T_2$	$T_{period} - \frac{T_0}{2}$
S3	$\frac{T_0}{2} + T_2$	$\frac{T_0}{2} + T_2$

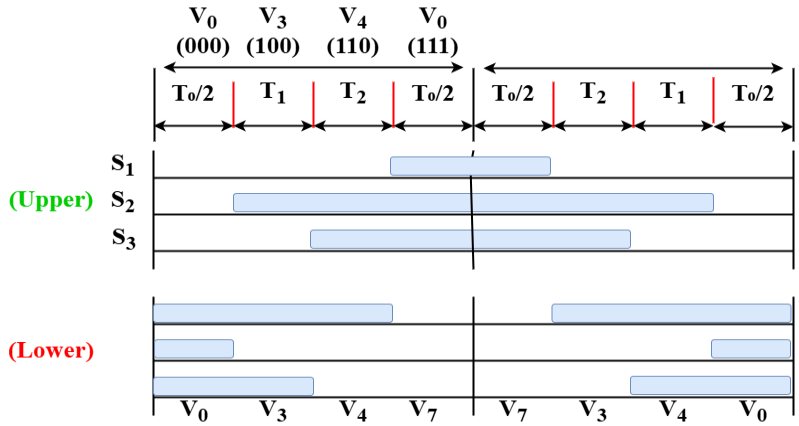

Fig.3.23. Principle of generating control pulses by vector PWM for state 3.

Tabel.3.8. Switch closing time in state 4.

Switch	Timer compares value	Reduced formula
S1	$\frac{T_0}{2}$	$\frac{T_0}{2}$
S2	$\frac{T_0}{2} + T_1$	$\frac{T_0}{2} + T_1$
S3	$\frac{T_0}{2} + T_1 + T_2$	$T_{period} - \frac{T_0}{2}$

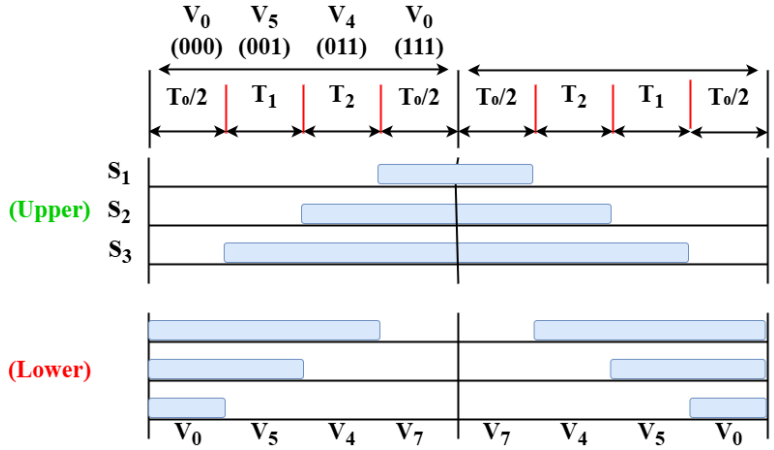

Fig.3.24. Principle of generating control pulses by vector PWM for state 4.

Tabel.3.9. Switch closing time in state 5.

Switch	Timer compares value	Reduced formula
S1	$\frac{T_0}{2}+T_2$	$\frac{T_0}{2}+T_2$
S2	$\frac{T_0}{2}$	$\frac{T_0}{2}$
S3	$\frac{T_0}{2}+T_1+T_2$	$T_{period}-\frac{T_0}{2}$

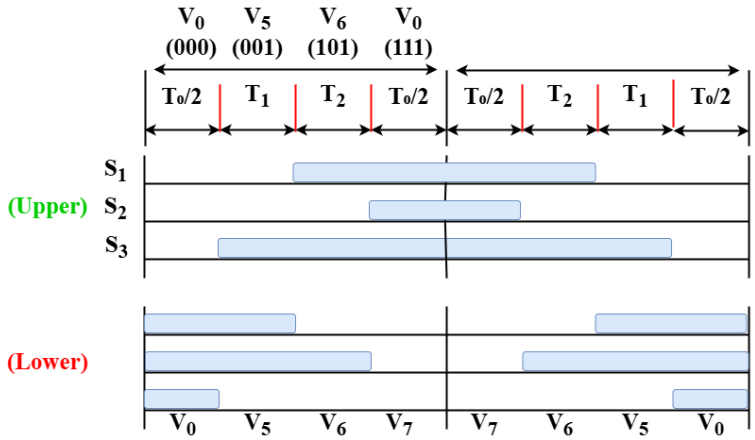

Fig.3.25 Principle of generating control pulses by vector PWM for state 5.

Tabel.3.10 Switch closing time in state 6.

Switch	Timer compares value	Reduced formula
S1	$\frac{T_0}{2}+T_1+T_2$	$T_{period}-\frac{T_0}{2}$
S2	$\frac{T_0}{2}$	$\frac{T_0}{2}$
S3	$\frac{T_0}{2}+T_1$	$\frac{T_0}{2}+T_1$

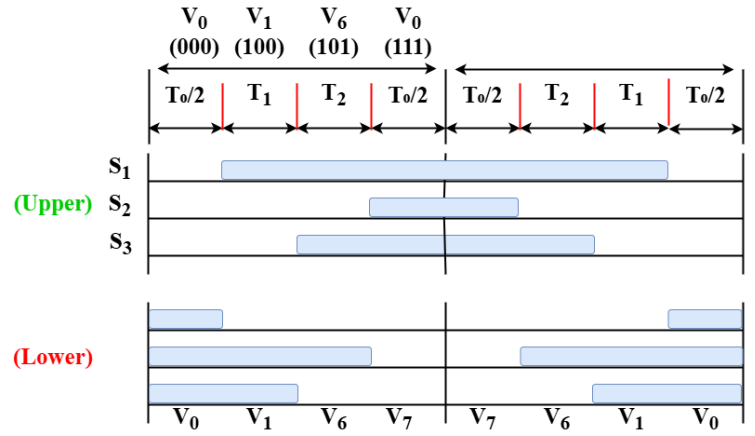

Fig.3.26. Principle of generating control pulses by vector PWM for state 6.

Tabel.3.11 Section closing time in each states .

Section	T_{s1}	T_{s2}	T_{s3}
Section 1	$T_{period} - \frac{T_0}{2}$	$\frac{T_0}{2} + T_2$	$\frac{T_0}{2}$
Section 2	$\frac{T_0}{2} + T_1$	$T_{period} - \frac{T_0}{2}$	$\frac{T_0}{2}$
Section 3	$\frac{T_0}{2}$	$T_{period} - \frac{T_0}{2}$	$\frac{T_0}{2} + T_2$
Section 4	$\frac{T_0}{2}$	$\frac{T_0}{2} + T_1$	$T_{period} - \frac{T_0}{2}$
Section 5	$\frac{T_0}{2} + T_2$	$\frac{T_0}{2}$	$T_{period} - \frac{T_0}{2}$
Section 6	$T_{period} - \frac{T_0}{2}$	$\frac{T_0}{2}$	$\frac{T_0}{2} + T_1$

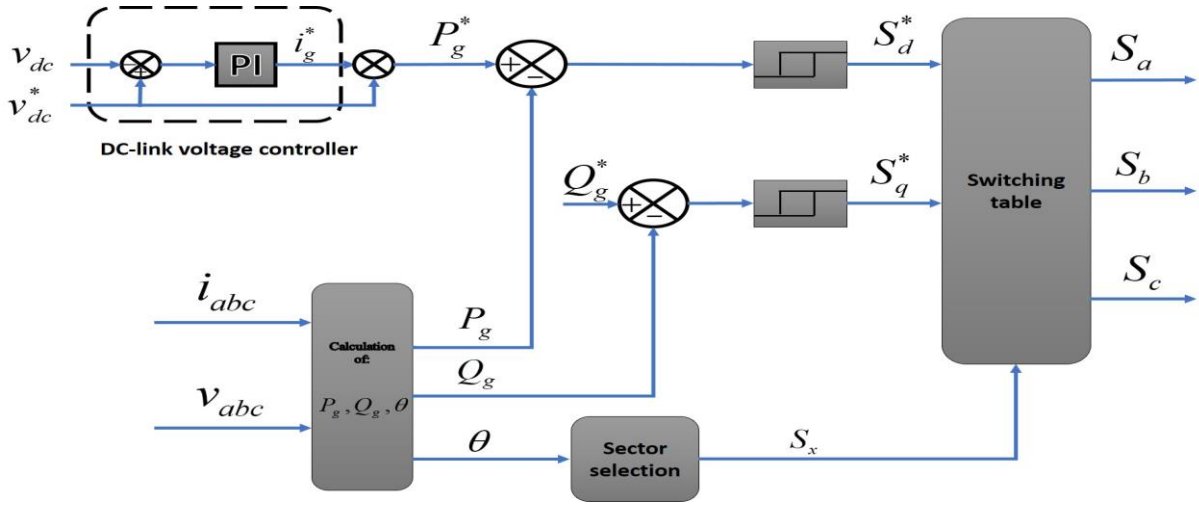

Fig.3.27.DPC (direct power control) scheme.

7.1.1. The advantages of SVPWM are [13]:

• A higher basic output voltage.

•A decrease in the percentage of THD due to enhanced harmonic performance.

• Digital Signal Processor (DSP) direct hardware implementation is straightforward.

7.1.2. The disadvantages of SVPWM are [14]:

• As the number of levels rises, the complexity of choosing switching states and duplicated switching states increases significantly.

• Low order harmonics cannot be entirely eliminated.

• Only three-phase MLI is suitable.

8. Parameters of System Simulation

The subsequent properties of the panel and the parameters of the boost converter utilized in our system simulation are presented in the tables below:

8.1. PV panel

Tabel.3.12. The solar panel's user-defined settings at STC

Maximum rating for power	178.068 W
Voltage open-circuit (Voc)	42.1 V
Current on short circuit (Isc)	5.423 A
Maximum voltage for power (Vmp)	35.5 V
Maximum current power (Imp)	5.016 A
Quantity of cells	60
typical cell temperature for operation	25

8.2. The Boost Converter

Tabel.3.16. Boost the design parameter of a DC-DC converter

Inductor	110 µH
Input capacitor	200 µF
Output capacitor	420 µF
Switching frequency	20 Hz

8.3. The NPC Inverter

Tabel.3.17. NPC Inverter the design parameter of a DC-AC converter

DC Link Voltage	600 – 1000 V
Number of levels	3
Output frequency	50/60 Hz
Switching frequency	2 - 20 Hz
Output power	10 kw – 1 MW
THD	< 3 %

8.4. load of system

Tabel.3.18. Load the design parameter

Type of load	Y
Resistance	10 Ohm
Inductance	0,01 H

9. Simulation results (panel with boost converter by conventional methods)

We conducted a simulation using fifteen solar panels arranged in series.

9.1. Characteristics of PV System (I.V, PV curve) for one panel

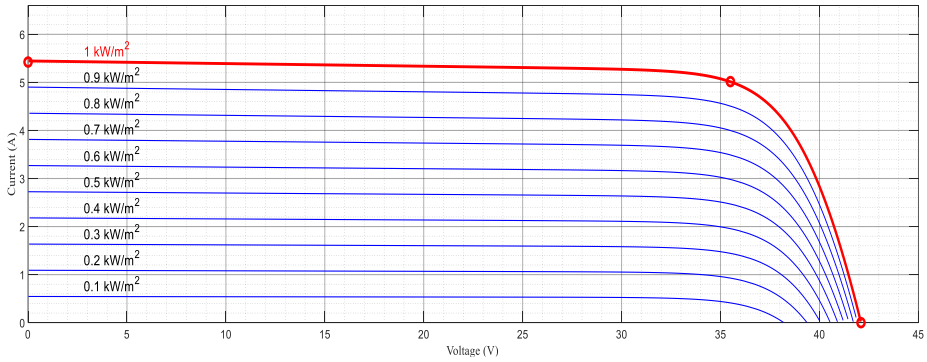

Fig.3.28. the PV panel's current output and voltage for the specified irradiations and temperatures (1000, 900, 800, 700, 600, 500, 400, 300, 200, 100, W/m² under 25°c of temperature)

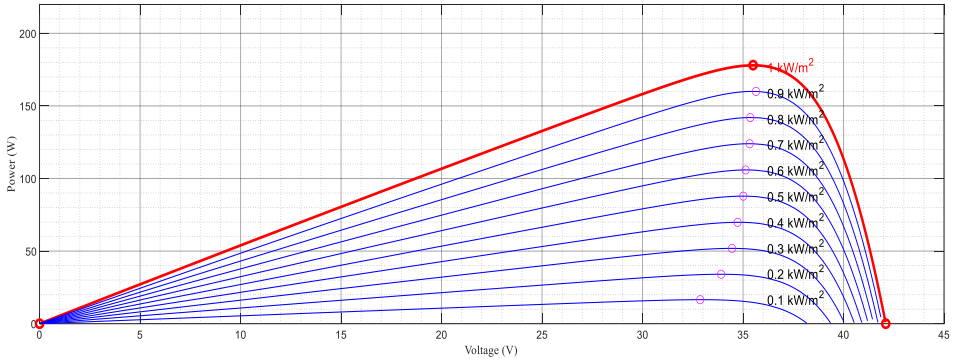

Fig.3.29. the PV panel's power output and voltage for the specified irradiations and temperatures (1000, 900, 800, 700, 600, 500, 400, 300, 200, 100, W/m² under 25°c of temperature)

9.2. Irradiance curve (for a constant value of deltaD=0.0012)

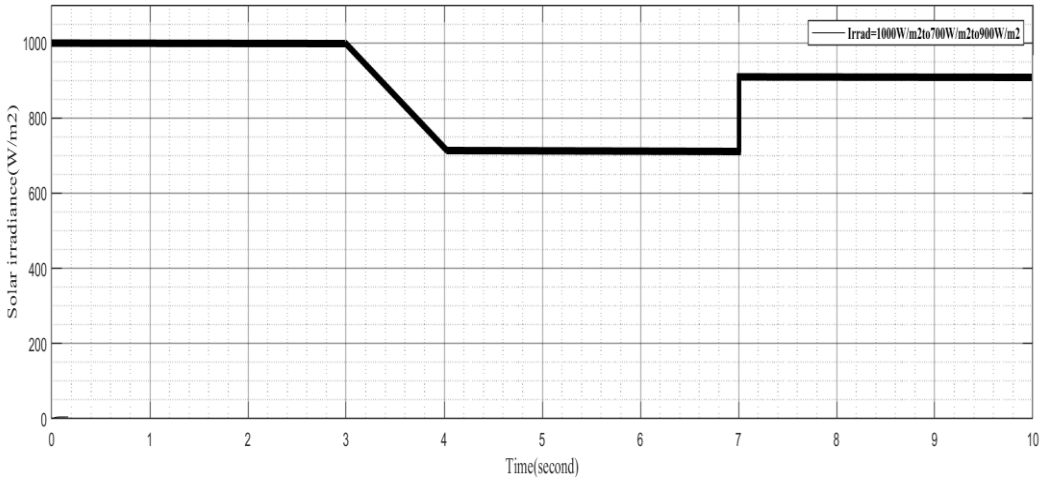

Fig.3.30. Change in solar irradiance (1000, 700 ,900 W/m²)

9.3. Results of INC method

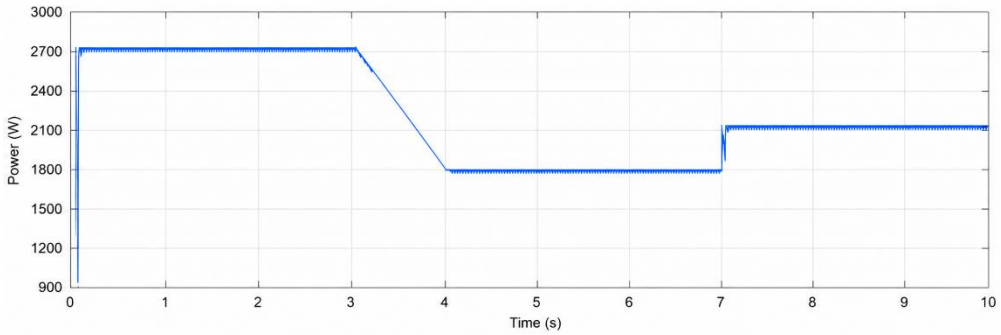

Fig.3.31. Output power for INC method Change in solar irradiance (1000, 700 ,900 W/m^2)

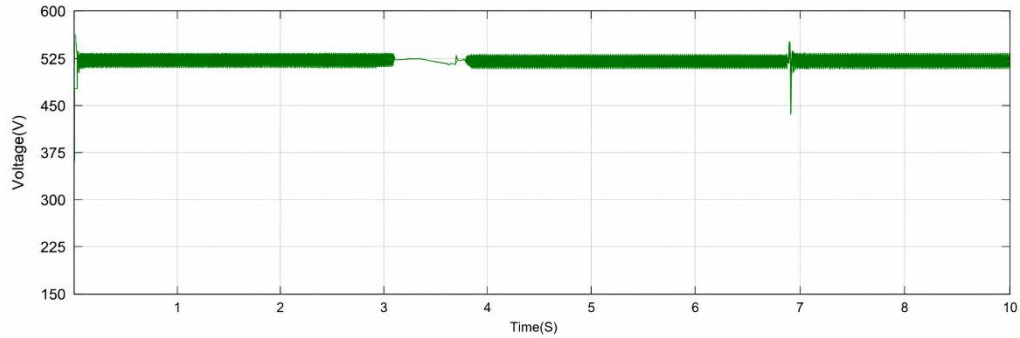

Fig.3.32. Output voltage for INC method Change in solar irradiance (1000, 700 ,900 W/m^2)

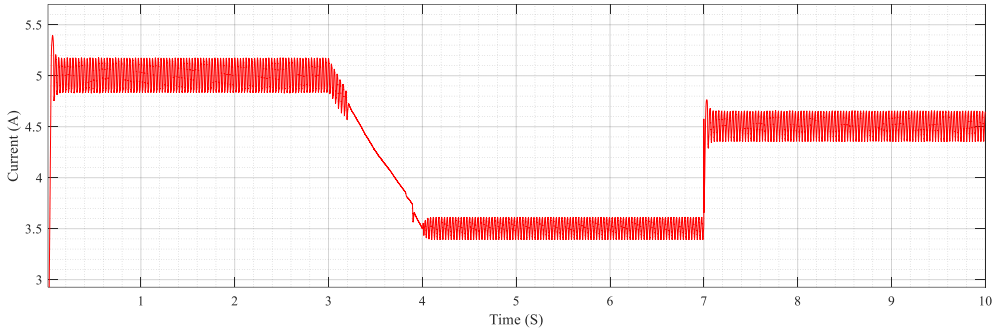

Fig.3.33. Output current for INC method Change in solar irradiance (1000, 700 ,900 W/m^2)

9.4. Results of P&O method

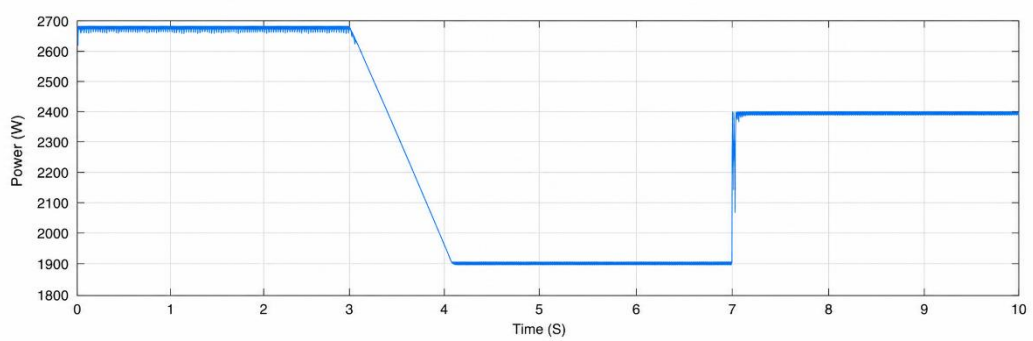

Fig.3.34. Output power for P&O method Change in solar irradiance (1000, 700 ,900 W/m^2)

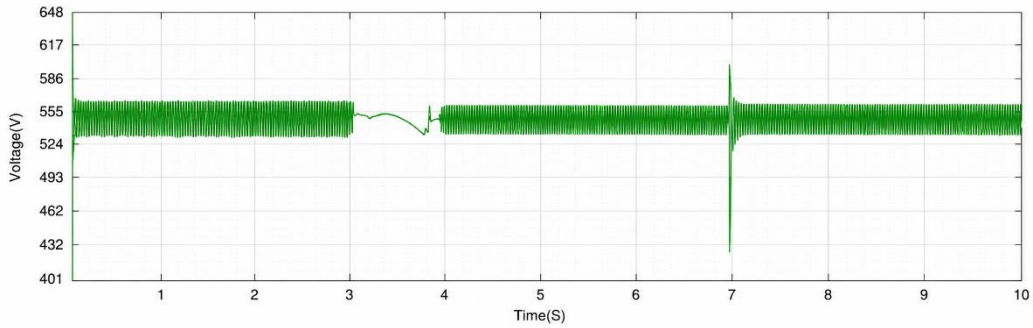

Fig.3.35 Output voltage for P&O method Change in solar irradiance (1000, 700 ,900 W/m^2)

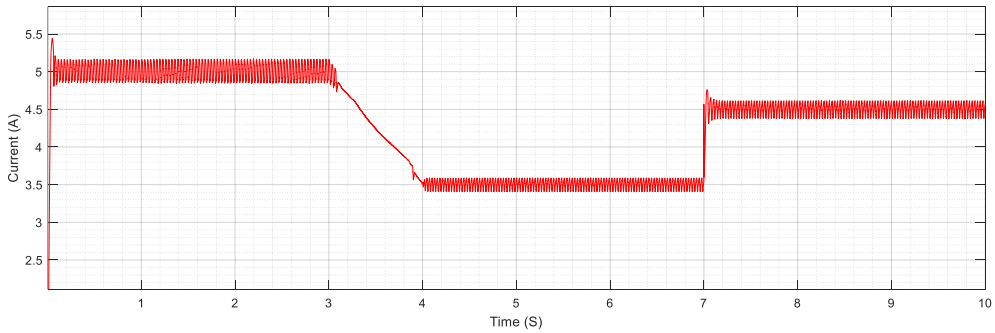

Fig.3.36 Output current for P&O method Change in solar irradiance (1000, 700 ,900 W/m^2)

10. Simulation and Results (NPC inverter with grid):

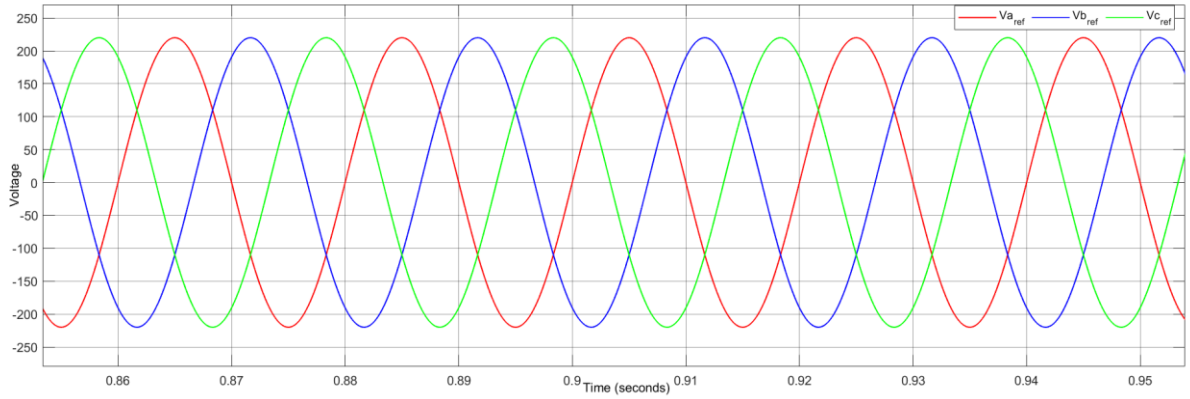

Fig.3.37. Source voltage 3 identical phases and a phase shift of 120 degrees

When simulating two-level voltage inverters with three identical phases and a 120-degree phase shift, with a maximum voltage (Vmax) of 220V, several results can be obtained and interpreted. Here are some key points to consider when analyzing the results:

Voltage waveform: One of the most important aspects of a voltage inverter is the quality of the output voltage. You can examine the voltage waveform generated by the inverter for each phase. In the case of a two-level inverter, the voltage waveform is typically a sine wave with abrupt transitions between voltage levels.

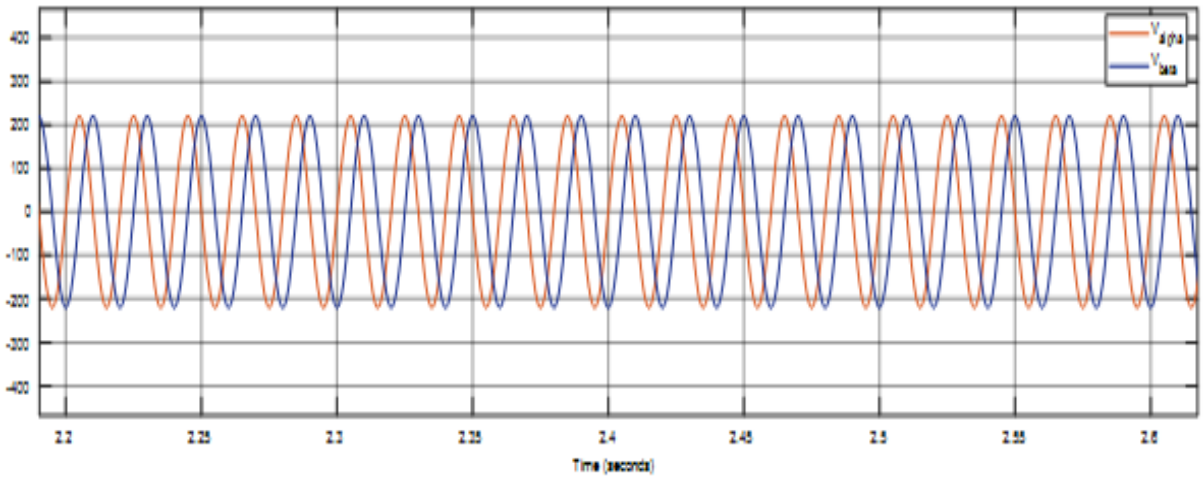

Fig.3.38. Clarke transformation (α, β)

Once the reference voltage is transformed into (α, β) coordinates, a comparison is made with carrier signals (a triangular wave) to generate the appropriate control signals for the inverter switches.

The simulation results involving (α, β) coordinators depend on the specific simulation objectives. You can analyze the (α, β) coordinate values to understand output voltage variations, inverter switch switching levels, switching losses, and so on. This information can be used to evaluate inverter performance and optimize pulse width modulation parameters.

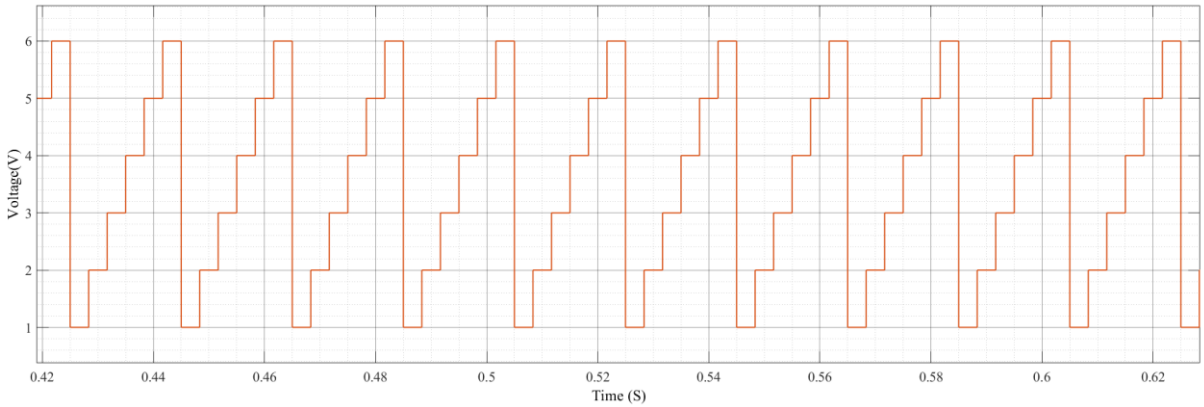

Fig.3.39. Mains switches of a three-phase inverter

Each sector defines which switches are turned on and which are turned off to generate the desired output voltage. Switching between sectors occurs at specific times during the modulation period, usually determined by comparing the reference voltage with the carrier waveform.

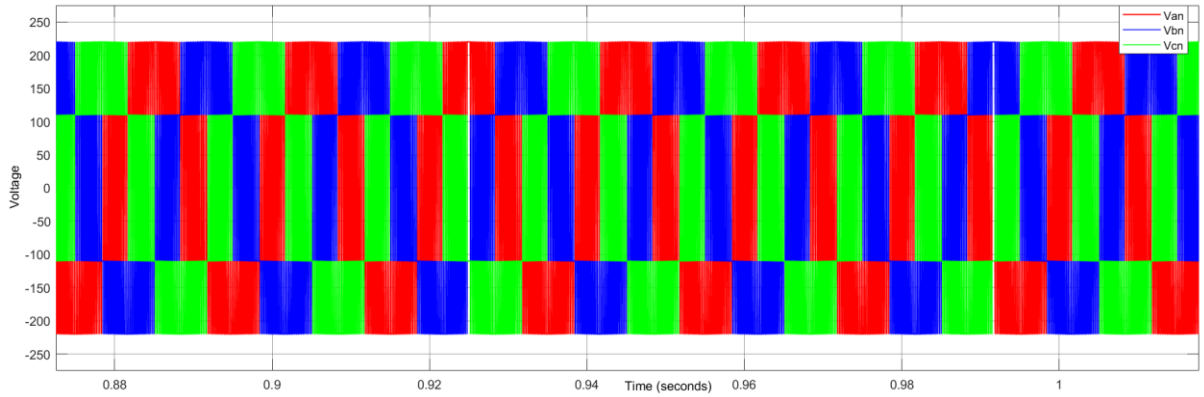

Fig.3.40. The simple voltage of a three-phase inverter

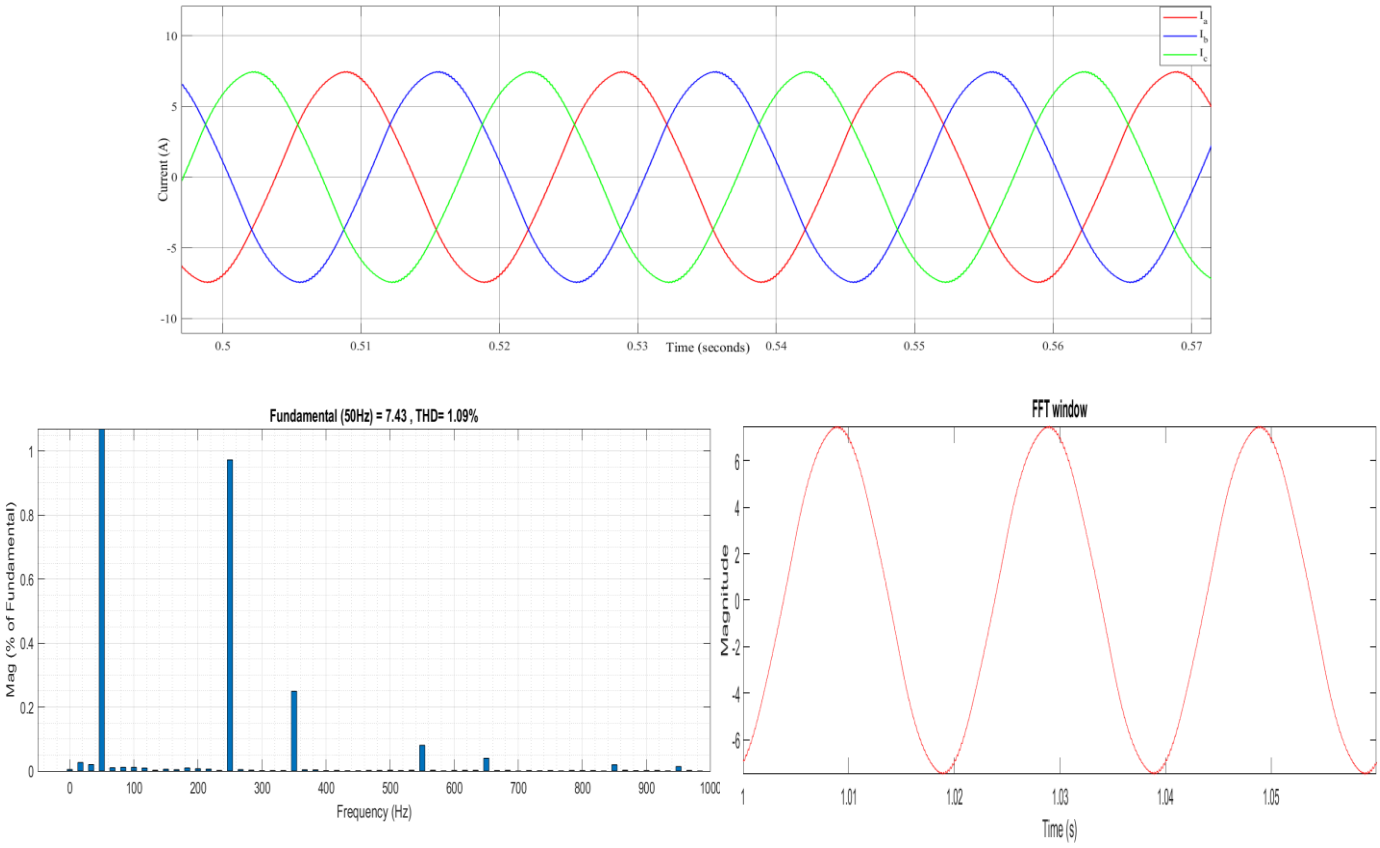

Fig.3.41. The current of a three-phase inverter

Current THD of 1.09%: Such a low THD indicates low harmonic distortion in the measured current. This is generally considered a good result, as low harmonic distortion indicates a current waveform close to a pure sine wave.

Maximum current value (I_{max}) of 7.5A: This indicates the highest peak reached by the current during the simulation.

Minimum current value (I_{min}) of -7.5A: This indicates the lowest peak reached by the current during the simulation.

11. Conclusions

This chapter introduces an implementation strategy for the Maximum Power Point Tracking (MPPT) algorithm utilizing a fixed-step controller, specifically the Perturb and Observe (PO) and Incremental Conductance (INC) methods. Simulation and validation results reveal notable drawbacks, including delayed response times and pronounced steady-state oscillations around the Maximum Power Point (MPP). These issues negatively affect the inverter's DC-to-AC conversion efficiency, leading to degraded output signal quality. Although the Space Vector Modulation (SVPWM) technique was employed for inverter control, the overall results remained suboptimal. To address these limitations, the following chapter proposes an enhanced MPPT technique employing a variable-step-size Fuzzy Logic (FL) controller, termed Modified Incremental Conductance (M-FL-INC). This approach aims to overcome the inherent constraints of conventional fixed-step-size MPPT algorithms by improving dynamic performance and reducing steady-state error.

Chapter III: Photovoltaic system management using MPPT and SVPWM controls within microgrid

Reference

[1] R. Kassem *et al.*, "A techno-economic-environmental feasibility study of residential solar photovoltaic/biomass power generation for rural electrification: A real case study," *Sustainability,* vol. 16, no. 5, p. 2036, 2024.

[2] S. Manna *et al.*, "Design and implementation of a new adaptive MPPT controller for solar PV systems," *Energy Reports,* vol. 9, pp. 1818–1829, 2023.

[3] J.-S. Ko, J.-H. Huh, and J.-C. Kim, "Overview of maximum power point tracking methods for PV system in micro grid," *Electronics,* vol. 9, no. 5, p. 816, 2020.

[4] M. Sarvi and A. Azadian, "A comprehensive review and classified comparison of MPPT algorithms in PV systems," *Energy Systems,* vol. 13, no. 2, pp. 281–320, 2022.

[5] N. F. Ibrahim *et al.*, "A new adaptive MPPT technique using an improved INC algorithm supported by fuzzy self-tuning controller for a grid-linked photovoltaic system," *Plos one,* vol. 18, no. 11, p. e0293613, 2023.

[6] J. Enrique, E. Duran, M. Sidrach-de-Cardona, and J. Andujar, "Theoretical assessment of the maximum power point tracking efficiency of photovoltaic facilities with different converter topologies," *Solar Energy,* vol. 81, no. 1, pp. 31–38, 2007.

[7] Y. Ma, X. Zhou, Z. Gao, and T. Bai, "Summary of the novel MPPT (maximum power point tracking) algorithm based on few intelligent algorithms specialized on tracking the GMPP (global maximum power point) for photovoltaic systems under partially shaded conditions," in *2017 IEEE International Conference on Mechatronics and Automation (ICMA)*, 2017: IEEE, pp. 311–315.

[8] A. K. Sharma *et al.*, "Role of metaheuristic approaches for implementation of integrated MPPT-PV systems: a comprehensive study," *Mathematics,* vol. 11, no. 2, p. 269, 2023.

[9] O. A.-O. SOHAIB, "Implémentation d'une commande trapézoïdale d'un moteur BLDC," faculté des sciences et de la technologie* univ bba, 2024.

[10] S.-a. Hameurlaine, H. Zelilef, and B. E. Makhlouf, "Commande d'un onduleur triphasé par les techniques de modulation de largeurs d'impulsions à élimination sélective d'harmoniques," Université de Jijel, 2018.

[11] B. Chahinez and B. Randa, "Commande de moteur synchrone à aimant permanent par un système photovoltaïque pour application d'un pompage d'eau," Abdelhafid boussouf university Centre mila, 2020.

[12] C. Cabal, "Optimisation énergétique de l'étage d'adaptation électronique dédié à la conversion photovoltaïque," Université Paul Sabatier-Toulouse III, 2008.

[13] D. KERCHA, "Conception d'une chaîne de conversion photovoltaïque monophasé à base de convertisseur multiniveaux," university Ghardaia, 2023.

[14] S. Issaadi, "Commande d'une poursuite du point de puissance maximum (MPPT) par les réseaux de neurones," Alger, Ecole Nationale Polytechnique, 2006.

[15] J. L. Santos, F. Antunes, A. Chehab, and C. Cruz, "A maximum power point tracker for PV systems using a high performance boost converter," *Solar energy,* vol. 80, no. 7, pp. 772–778, 2006.

[16] M. Fannakh, M. L. Elhafyani, and S. Zouggar, "Hardware implementation of the fuzzy logic MPPT in an Arduino card using a Simulink support package for PV application," *IET Renewable Power Generation,* vol. 13, no. 3, pp. 510–518, 2019.

[17] J. Kim and I. Kwon, "Design of a high-efficiency dc-dc boost converter for rf energy harvesting iot sensors," *Sensors,* vol. 22, no. 24, p. 10007, 2022.

[18] B. Hasaneen and A. A. E. Mohammed, "Design and simulation of DC/DC boost converter," in *2008 12th International Middle-East Power System Conference*, 2008: IEEE, pp. 335–340.

[19] R. M. Asif, M. A. B. Siddique, A. U. Rehman, M. T. Sadiq, and A. Asad, "Modified fuzzy logic MPPT for PV system under severe climatic profiles," *Pakistan Journal of Engineering and Technology,* vol. 4, no. 2, pp. 49–55, 2021.

[20] G. Bayrak and D. Ghaderi, "An improved step-up converter with a developed real-time fuzzy-based MPPT controller for PV-based residential applications," *International Transactions on Electrical Energy Systems,* vol. 29, no. 12, p. e12140, 2019.

[21] N. TERKI, B. P. AZOUI, and R. CHENNI, "Thèse Zaghba Layachi 2017."

[22] F. Mnif, "Étude et réalisation des lois de commande par mode de glissement et par approche géométrique: application à un onduleur de tension monophasé," Université du Québec à Trois-Rivières, 1991.
[23] A. Ahmadi, S. Kabiri, and K. Omidfar, "Advances in HbA1c biosensor development based on field effect transistors: a review," *IEEE Sensors Journal,* vol. 20, no. 16, pp. 8912–8921, 2020.
[24] S. Madhusoodhanan *et al.*, "Comparison study of 12kV n-type SiC IGBT with 10kV SiC MOSFET and 6.5 kV Si IGBT based on 3L-NPC VSC applications," in *2012 IEEE Energy Conversion Congress and Exposition (ECCE)*, 2012: IEEE, pp. 310–317.
[25] N. Patil, J. Celaya, D. Das, K. Goebel, and M. Pecht, "Precursor parameter identification for insulated gate bipolar transistor (IGBT) prognostics," *IEEE Transactions on Reliability,* vol. 58, no. 2, pp. 271–276, 2009.
[26] S. OKBA and W. BEDDIAR, "Etude et réalisation d'un onduleur de tension triphasé à MLI," *Magister en électrotechnique, UNIVERSITE MOHAMED BOUDIAF-M'SILA,* 2019.
[27] J. S. Oliver, P. W. David, P. K. Balachandran, and L. Mihet-Popa, "Analysis of grid-interactive PV-fed BLDC pump using optimized MPPT in DC–DC converters," *Sustainability,* vol. 14, no. 12, p. 7205, 2022.
[28] L. Fan and X. Ma, "Maximum power point tracking of PEMFC based on hybrid artificial bee colony algorithm with fuzzy control," *Scientific Reports,* vol. 12, no. 1, p. 4316, 2022.
[29] S. Chakraborty, M. Razzak, M. S. U. Chowdhury, and S. Dey, "Design of a transformer-less grid connected hybrid photovoltaic and wind energy system," in *2014 9th International Forum on Strategic Technology (IFOST)*, 2014: IEEE, pp. 400–403.
[30] S. Saridakis, E. Koutroulis, and F. Blaabjerg, "Optimal design of modern transformerless PV inverter topologies," *IEEE transactions on energy conversion,* vol. 28, no. 2, pp. 394–404, 2013.
[31] A. Zemmit *et al.*, "GWO and WOA variable step MPPT algorithms-based PV system output power optimization," *Scientific Reports,* vol. 15, no. 1, p. 7810, 2025.
[32] B. E. Elnaghi, A. M. Ismaiel, M. M. Ismail, H. A. Zedan, and A. A. Salem, "Experimental validation of an adaptive fuzzy logic controller for MPPT of grid connected PV system," *Scientific Reports,* vol. 15, no. 1, p. 27173, 2025.
[33] N. Shanker, K. S. Rao, and E. Srilakshmi, "PO-InC-APSO: An Improved Hybrid MPPT Technique for Grid-Tied Partially Shaded Condition Photovoltaic Systems," in *E3S Web of Conferences*, 2025, vol. 616: EDP Sciences, p. 01015.
[34] M. B. S. Bechekir[1], M. Brahami[1], H. Bendaho, and A. Brahimi, "Comparative Analysis of MPPT Algorithms: P&O and Inc for Optimizing PV Systems," *Smart Computing and Control Renewable Energy Systems: Advanced Computational Techniques for Wireless Network Optimization,* vol. 1238, p. 60, 2025.
[35] D. Joseph, "MPPT ALGORITHM FOR SOLAR-PV SYSTEM," *Journal of Intelligent System and Telecommunication,* vol. 2, no. 1, pp. 1–20, 2025.
[36] G. Ezhilarasan and C. S. SM, "Advanced SVPWM Technique for Multilevel Inverter Systems," *Engineering, Technology & Applied Science Research,* vol. 15, no. 3, 2025.
[37] M. Madhavan, C. N, and R. C. Bansal, "Segment Reduction-Based SVPWM Applied Three-Level F-Type Inverter for Power Quality Conditioning in an EV Proliferated Distributed System," *International Transactions on Electrical Energy Systems,* vol. 2025, no. 1, p. 5526266, 2025.
[38] X. Xu, Y. Zhang, and J. Huang, "Comparison of Midpoint Voltage Control of T-Type Three-Level Inverter with SVPWM and DPWMA Modulation Methods," in *2025 IEEE 20th Conference on Industrial Electronics and Applications (ICIEA)*, 2025: IEEE, pp. 1–6.
[39] Z. Lin, W. Du, Y. Bai, H. H. C. Iu, T. Fernando, and X. Zhang, "Carrier-Based Implementation of SVPWM for a Three-Level Simplified Neutral Point Clamped Inverter with XOR Logic Gates," *Electronics,* vol. 14, no. 7, p. 1408, 2025.
[40] S. Karvekar and A. Karvekar, "Simulation Modeling for Comparative Analysis of SPWM and SVPWM in Solar PV Inverters," in *2025 4th International Conference on Computational Modelling, Simulation and Optimization (ICCMSO)*, 2025: IEEE, pp. 249–254.

Chapter VI: Photovoltaic system management using MPPT (FL-INC) and Predictive Current controls

1. Introduction

This chapter examines the performance evaluation and comparison of four prominent Maximum Power Point Tracking (MPPT) algorithms: Perturb and Observe (P&O), Incremental Conductance (INC), Fuzzy Logic (FL), and Incremental Conductance with Fuzzy Logic (INC-Fuzzy). These algorithms are essential for maximizing the power output of photovoltaic (PV) systems by continuously altering the operating point to maximize energy extraction from solar panels. By precisely monitoring the highest power point, these algorithms enhance the efficiency and efficacy of photovoltaic systems, which is crucial for optimizing overall performance and energy output. The P&O technique utilizes periodic perturbations and observations to identify the ideal position, while the INC algorithm employs the incremental conductance approach for more precise modifications. The INC-Fuzzy algorithm utilizes artificial intelligence to accurately anticipate and monitor the maximum power point. Our thorough research seeks to elucidate the strengths and drawbacks of each algorithm, offering critical insights into their appropriateness for various operating settings. We will also discuss inverter strategies in photovoltaic systems represented by controlling the Module predictive control (MPC) [1].

2. Fuzzy logic controller method

Fuzzy logic control has been the most important and fruitful application of fuzzy logic theory because to developments in microelectronic technology. A mathematical foundation for converting linguistic control principles represented as (IF-THEN) statements into an automated control approach is provided by fuzzy logic controllers, which are based on fuzzy logic.[2, 3]. According to formula (IV.1), the error E and the associated change of error CE are the two inputs of the FLC.

$$\begin{cases} E(k) = \dfrac{P(k) - P(k-1)}{V(k) - V(k-1)} \\ CE(k) = E(k) - E(k-1) \end{cases} \quad \text{(IV.1)}$$

P(k) and V(k) denote the output power and voltage of the photovoltaic panel at the sampling instant k.

Fuzzification, fuzzy rules and inference engine, and defuzzification are the three functional parts of the fuzzy logic controller.

2.1. Fuzzification

Each variable used to articulate the control rules must be represented using fuzzy set notations with linguistic labels in order to use the fuzzy technique [3]. Fig.4.2 shows the output variable dD(k) and the membership functions of the input variables E(k) and CE(k). Five fuzzy sets—PB (Positive Big), PS (Positive Small), ZE (Zero Equivalent), NS (Negative Small), and NB (Negative Big)—are linked to each membership function.

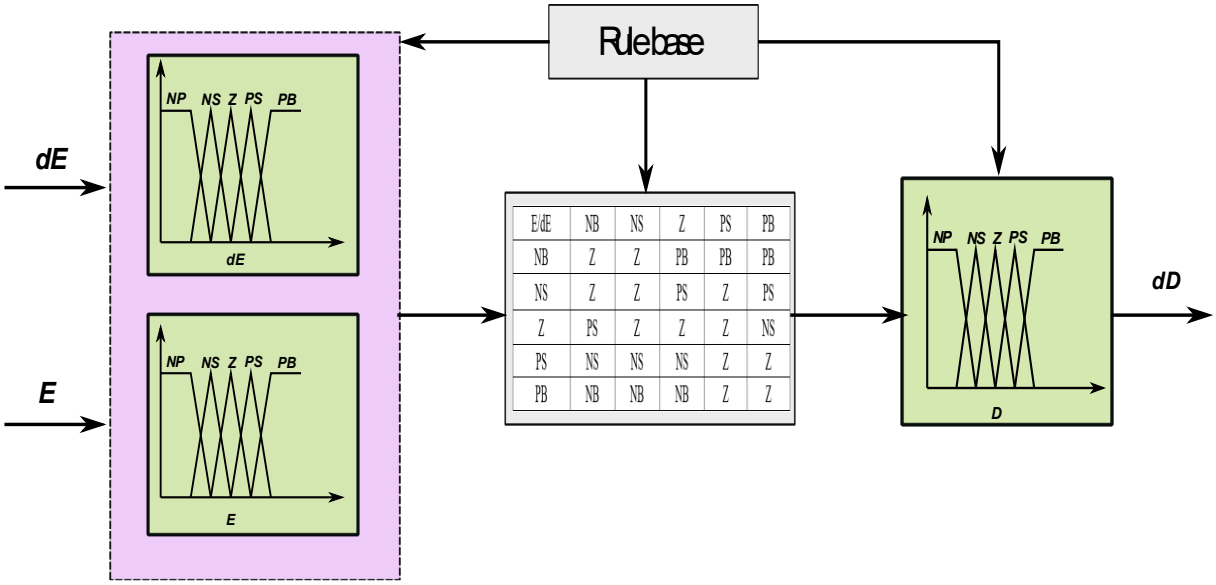

Fig.4.1. Fuzzy logic membership

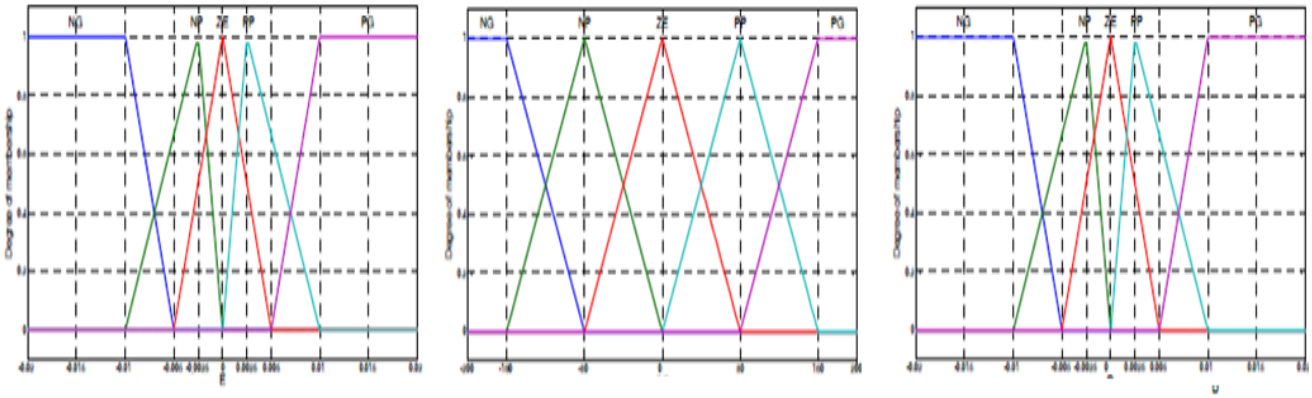

Fig.4.2. Membership function

2.2. Fuzzy rules and inference engine

The fuzzy inference system is the central part of a fuzzy logic controller. The process of using fuzzy logic to determine the link between a given input and an output is known as fuzzy inference. A basis for decision-making is then established by the mapping. The error function E in formula (VI.1) should be minimized to zero using the proposed Mamdani-type inference system. Two situations warrant consideration [4].

• Initial scenario: The operational point is located to the left of the MPP, and E is positive. The operating point gets closer to the maximum power point (MPP) if the change of error (CE) is positive. The opposite happens when CE is negative.

• In the second scenario, the operating point is located to the right of the MPP because E is negative. The working point differs from the MPP if CE is positive; if CE is negative,it approaches the MPP.
We summarize this process reasoning in Table 1 as a collection of fuzzy IF-THEN rules [4].

Table.4.1. A collection of fuzzy IF-THEN rules

		CE				
E = Voltage step / **Δe = S(k)**		NG	NP	ZE	PP	PG
E	NG	ZE	ZE	PG	PG	PG
	NP	ZE	ZE	PP	PP	PP
	ZE	PP	ZE	ZE	ZE	NP
	PP	NP	NP	NP	ZE	ZE
	PG	NG	NG	NG	ZE	ZE

2.3. Defuzzification

Defuzzification establishes the Fuzzy Logic Controller's (FLC) exact output. It describes how a domain of fuzzy logic statements relating to the inferred output is transformed into a non-fuzzy control action. The center of gravity defuzzifier is used in this study, which is the most prevalent method.

2.4. Application of fuzzy logic

Fuzzy logic is extensively used in many different industries because of its ability to handle uncertainty, ambiguity, and imprecise data much like how humans make decisions. In engineering, it's used to control complex systems such as industrial processes, robotics, and smart vehicles, where traditional binary logic is too rigid. In everyday electronics like washing machines, air conditioners, and cameras, fuzzy logic allows for smarter, adaptive responses based on real-world conditions. It plays a vital role in healthcare for medical diagnosis and image analysis, where symptoms and results are often not black and white. Additionally, fuzzy logic is used in renewable energy systems to optimize power output and in artificial intelligence to enhance learning and decision-making. Its human-like reasoning makes it a practical and powerful tool in both scientific and consumer applications.

3. Grid connected using BOOST converter and three level NPC:

3.1. Grid connected PV system:

As depicted in Fig4.3, the analyzed system comprises a photovoltaic (PV) array, a DC-DC converter operating in boost mode, a three-level neutral-point-clamped (NPC) inverter, and an R-L filter connected to the grid. The Photovoltaic arrays produce electrical energy in proportion to the level of solar irradiation. The buck-boost converter is employed to track and maintain the maximum power point (MPP) and its continuous delivery to the DC link. The current sourced from the buck-boost converter is injected into the grid through the three-level NPC inverter.

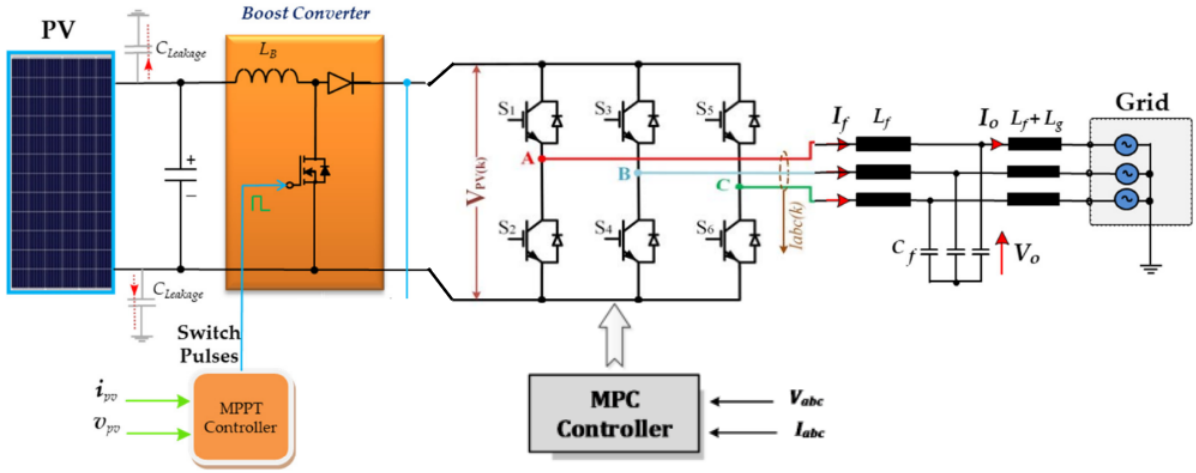

Fig.4.3. Diagram of the MPPT Based on the FL-INC Algorithm for the PV Solar System Inverter Associated with a Boost Converter

3.2. Proposed MPPT Technique (INC and Fuzzy Logic-Based Variable Step Size) (FL-INC)

3.2.1 Proposed MPPT technique

Since the traditional INC technique typically works on fixed step size perturbation, the convergence of rising step size perturbation and the limiting oscillation of PV array output power near MPP are incompatible. When employing the INC approach with a fixed step size, it takes a long time to reach MPP.

This is because the PV system follows a predetermined path to obtain MPP after it reaches a certain operational threshold. To get to the MPP faster, we use a variable step when the operating point is near the MPP and a large step when it is distant from the MPP. This study modified the step size for an INC MPPT algorithm using the FL approach in order to address the shortcomings of the conventional fixed step size INC MPPT. The flowchart for the proposed FL-based variable step size INC MPPT algorithm is displayed inFig.4.4.

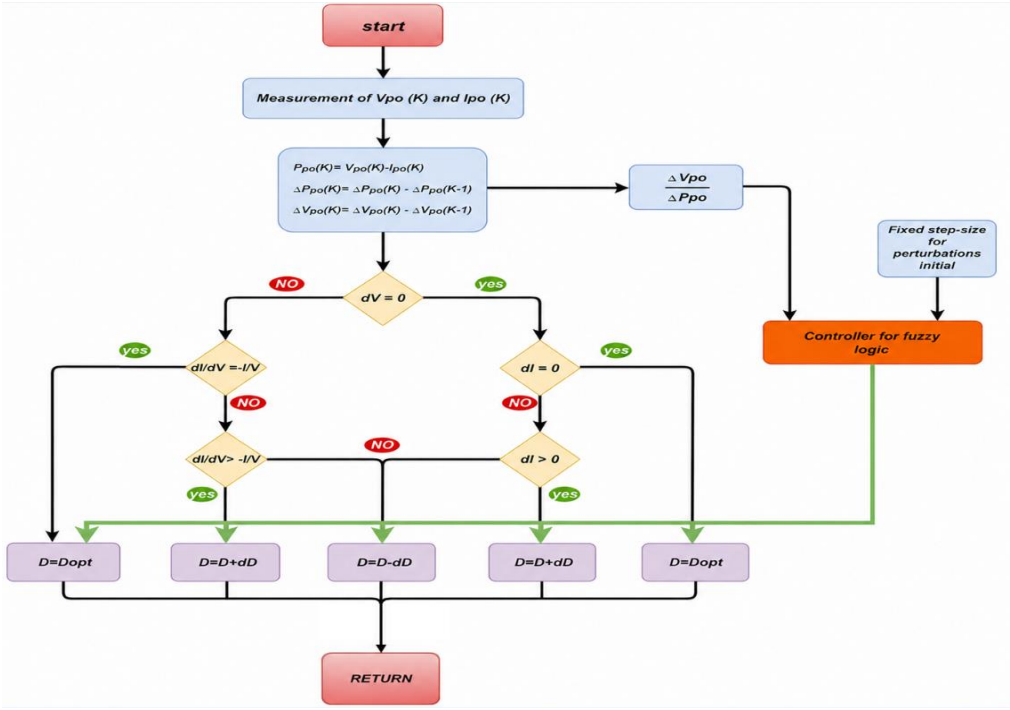

Fig.4.4. Flowchart of FL-based variable step size INC-MPPT algorithm.

By providing a variable step size reference, the FL approach utilized to calculate the variable step size in the suggested variable step size INC-MPPT algorithm may allow for automatic updating of the PV array operating point. A Max-Min operation structure and Mamdani's FL rule-based method were used to determine the variable step size control action. The FL controller is made up of five sections, as shown in Fig. 4.5. The controller was designed using 25 rules with "if" and "then" syntax. Additionally, the fuzzy was categorized as positive

medium (PM), positive small (PS), and positive extremely tiny (PET). These values are shown as positive high (PH) and positive very high (PVH) in Table 4.3.

The suggested variable step size INC MPPT algorithm, which determines the variable step size using a FL technique, may cause the related power converter to automatically adjust the PV array's operating point. This is achieved by giving the corresponding power converter a variable step size reference voltage, or Vpv. The variable step size control action was found using Mamdani's FL rule-based approach and a Max-Min operation structure. Five parts make up the FL controller, as illustrated inFig.4.6. The controller was developed using the operators "if" and "then" along with twenty-five restrictions. Furthermore, positive average (PA), positive low (PL), and positive very low (PVL) are displayed in Table 4.2.

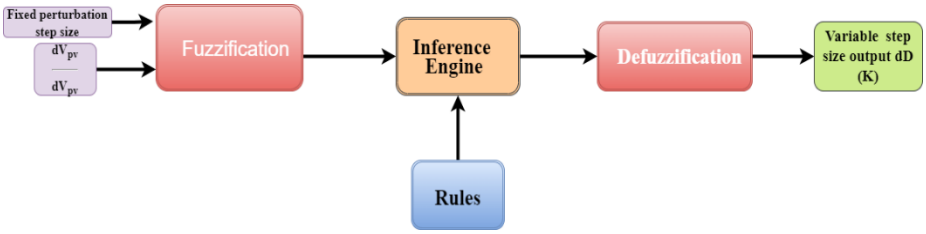

Fig.4.5. Block schematic of a FL controller

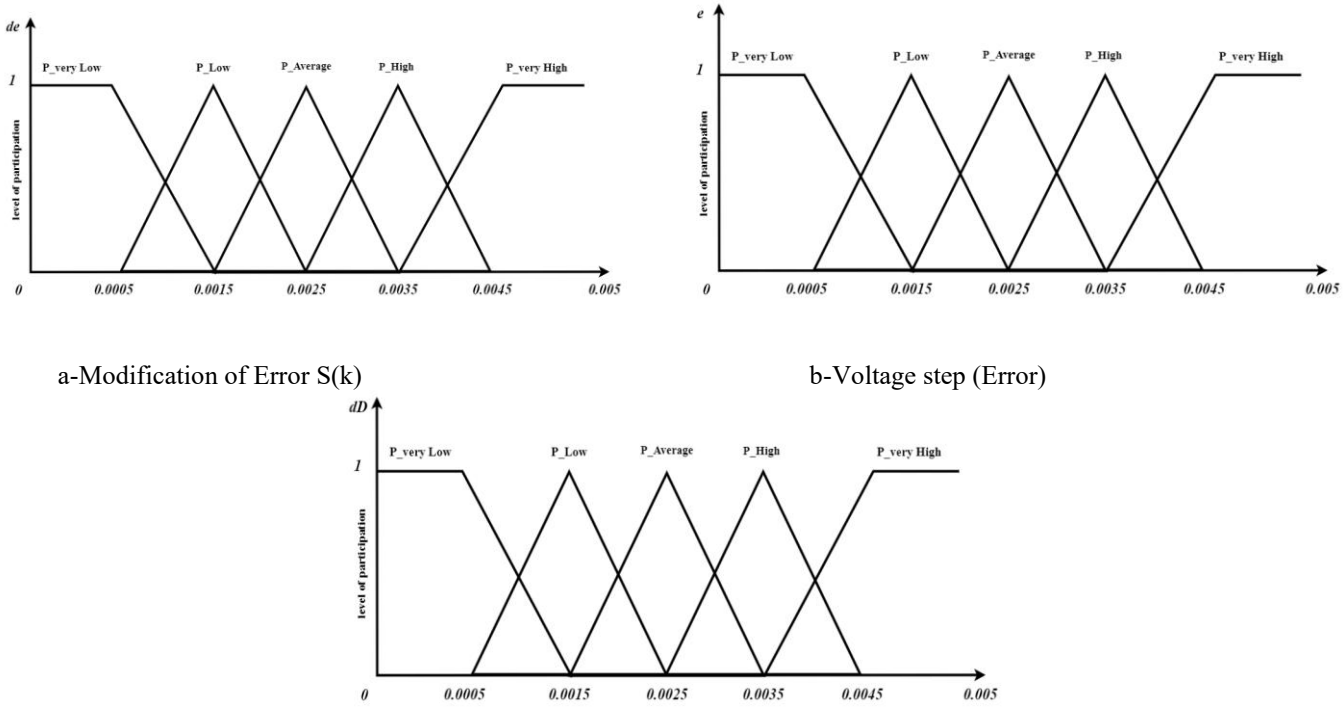

a-Modification of Error S(k)

b-Voltage step (Error)

c-variable step size variation.

Fig.4.6.The membership function of the proposed FL controller for the variable step size MPPT algorithm.

Table.4.2.FL rules for the proposed MPPT technique

Δe = S(k) \ E = Voltage step	PVL	PL	PA	PH	PVH
PVL	PVH	PVL	PVL	PL	PL
PL	PVH	PVL	PVL	PL	PL
PA	PL	PL	PL	PVH	PVH
PH	PL	PVH	PL	PVL	PVH
PVH	PVL	PVL	PVH	PH	PVH

The needed outcome of each of the 25 FL controller rules is the output variable step size, represented as ΔD(k). A surface known as the control viewer displays the input-output mapping of a FL controller with two inputs and one output.Fig.4.7.

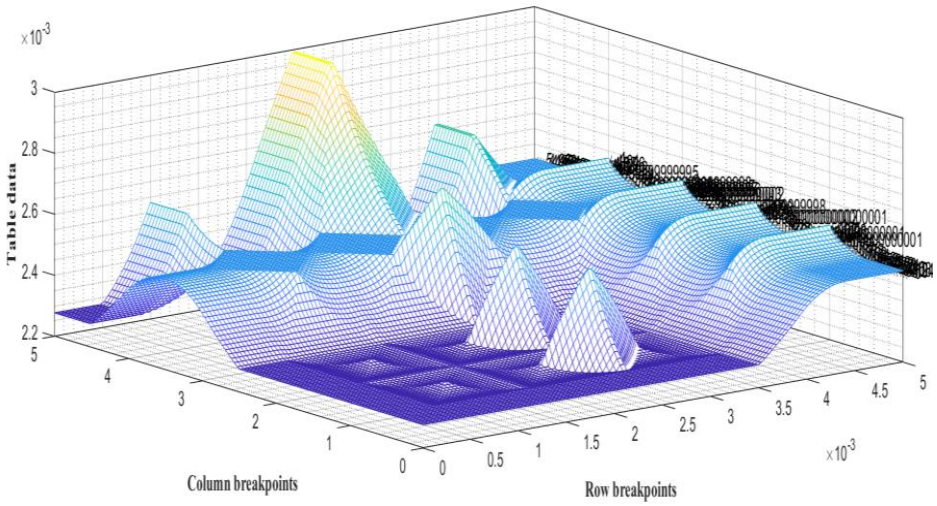

Fig.4.7. The relationship between the output variable step ΔDpv(k), the fixed perturbation voltage step size, and the measured PV curve slope S(k) is shown by an input-output mesh plot

3.3 Predictive Current Control

The idea behind the suggested predictive control method is that a static power converter can only produce a small number of switching states. Furthermore, it is feasible to predict how variables will behave for every switching state by using system models. A selection criterion is needed to identify the best switching state. A cost function that assesses the anticipated values of the controllable variables is part of this criterion. Following the computation of projections for the future values of these variables for every potential switching state, the state that minimizes the cost function is selected [5]

The following stages can be used to summarize this control strategy:

Establish a cost function g.

Create a model of the converter that includes all of its potential switching states.

Develop a model of the load in order to make predictions.

In order to predict how the factors assessed by the cost function more especially, the load currents—will behave, a discrete-time model of the load is required.

3.3.1 Cost Function

The main objective of the current control strategy remains unchanged, which is to minimize the deviation between the measured currents and the desired values. This objective can be formulated as a cost function, representing the difference in orthogonal coordinates, which evaluates the deviation between the desired currents and the predicted values.

$$g = \left|i_{\alpha}^{*}(k+1) - i_{\alpha}^{p}(k+1)\right| + \left|i_{\beta}^{*}(k+1) - i_{\beta}^{p}(k+1)\right| \quad \text{(IV.2)}$$

3.3.2 Converter Model

The three-phase inverter's power circuit is used to convert electrical energy from direct current (DC) to alternating current (AC)., using the electrical configuration shown in Fig.16. To prevent any potential short circuits, the two switches of each inverter phase operate in a complementary manner, ensuring the proper functioning of the system. [6]

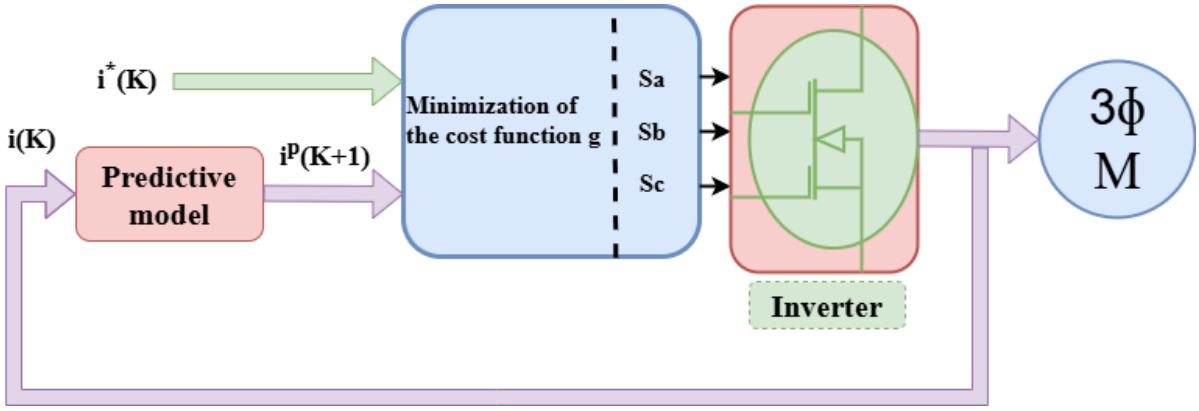

Fig.4.8. Functional Diagram of Predictive Current Control

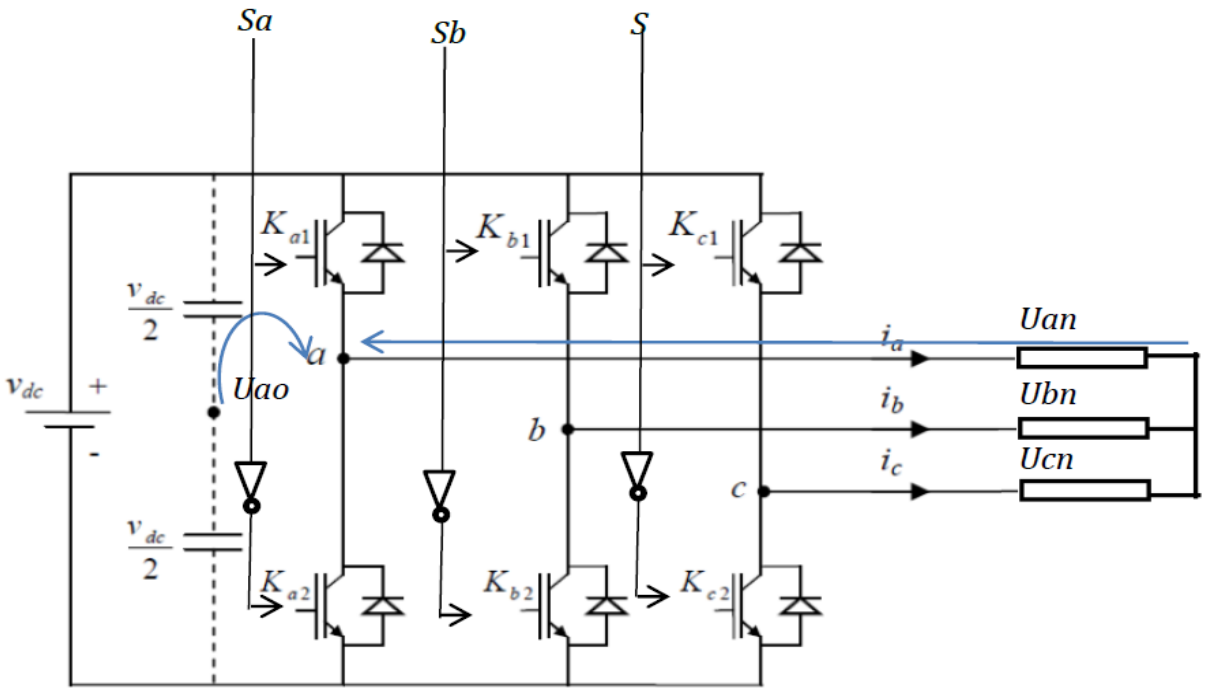

Fig.4.9. Inverter with grid.

N	Table 4.3. Predictive Current Control Algorithm.
1	The reference current i(k) is obtained (from an external control loop) and the load current i(k) is measured.
2	The system model is used to predict the load current value in the next sampling interval i(k+ 1) for each of the different voltage vectors.
3	The cost function g evaluates the error between the reference and predicted currents at the next sampling interval for each voltage vector.
4	The voltage that minimizes the current error is selected and the corresponding switching state signals are generated.

3.3.3 Load Model

Given the definitions of the circuit variables illustrated in Fig.4.9, the expressions describing the dynamics of the load current for each phase can be formulated as follows.

$$U_{an} = L\frac{di_a}{dt} + Ri_a + e_a + U_{nN} \quad \text{(IV.3)}$$

$$U_{bn} = L\frac{di_b}{dt} + Ri_b + e_b + U_{nN} \quad \text{(IV.4)}$$

$$U_{cn} = L\frac{di_c}{dt} + Ri_c + e_c + U_{nN} \quad \text{(IV.5)}$$

Where R is the load resistance and L is the load inductance.

A vector equation for the load current dynamics can be obtained by substituting equations (IV.3) to (IV.5) into equation (II.22).

$$V = L\frac{d}{dt}[\frac{2}{3}(i_a + ai_b + a^2 i_c)] + R(\frac{2}{3}(i_a + ai_b + a^2 i_c) + \frac{2}{3}(e_a + ae_b + a^2 e_c) + \frac{2}{3}(U_{nN} + aU_{nN} + a^2 U_{nN}) \quad \text{(IV.6)}$$

Taking into account the definition of the space vector given in equation (II.22) for the inverter voltage, as well as the subsequent interpretations of the load current vectors and the background space vectors.

$$i = \frac{2}{3}(i_a + ai_b + a^2 i_c) \quad \text{(IV.7)}$$

$$e = \frac{2}{3}(e_a + ae_b + a^2 e_c) \quad \text{(IV.8)}$$

and assuming that the last term of equation (II.21) and (IV.6) is equal to zero.

$$\frac{2}{3}(U_{nN} + aU_{nN} + a^2 U_{nN}) = U_{nN}\frac{2}{3}(1 + a + a^2) = 0 \quad \text{(IV.9)}$$

then the load current dynamics can be described by the vector differential equation.

$$V = Ri + L\frac{di}{dt} + e \quad \text{(IV.10)}$$

Where v is the voltage vector generated by the inverter, i is the load current vector, and e is the load back-emf vector.[7]

Please be aware that the back electromotive force (emf) of the load is expected to follow a sinusoidal waveform with constant amplitude and frequency for simulation and testing findings.

Discrete-time prediction model

The discretization of the load current equation (IV.10) for a sample time Ts is explained in this section. Based on the measured voltages and currents at sampling moment k, the discrete-time model will be used to forecast the load current's future value. A suitable discrete-time model for prediction computations can be obtained using a variety of discretization techniques. A straightforward derivative approximation can be used to develop the discrete-time model since the load can be represented as a first-order system. Nevertheless, this approximation might generate mistakes for more complicated systems.[5]

The derivative of the load current di/dt is substituted using the direct Euler approximation. The derivative is estimated in this approximation as follows:

$$\frac{di}{dt} \approx \frac{i(k+1) - i(k)}{T_s} \quad \text{(IV.11)}$$

The substitution made in equation (IV.10) allows obtaining an expression to predict the future load current at time k+1 for each of the voltage vector v(k)'s seven potential values produced by the inverter. This phrase is

$$i^{p}(k+1) = \left(1 - \frac{RT_S}{L}\right) i(k) + \frac{T_S}{L}(V(k) - \hat{e}(k)) \quad \text{(IV.12)}$$

The symbol e^(k) represents the estimated back electromotive force (back-emf), where the superscript p indicates predicted variables. The expression provided in equation (IV.10) can be used to calculate the back-emf by utilizing the measurements of the load voltage and current as follows:

$$\hat{e}(k-1) = V(k-1) - \frac{L}{T_S} i(k) - \left(R - \frac{L}{T_S}\right) i(k-1) \quad \text{(IV.13)}$$

Where e^(k−1) is the estimated value at time k−1. The back-emf at time k, required in (IV.12) (IV.13), can be estimated by extrapolating past values of the estimated back-emf. Alternatively, since the frequency of the back-emf is much lower than the sampling frequency, it is assumed that it does not change significantly within one sampling interval, and thus we set:

$$\hat{e}(k) = \hat{e}(k-1) \quad \text{(IV.14)}$$

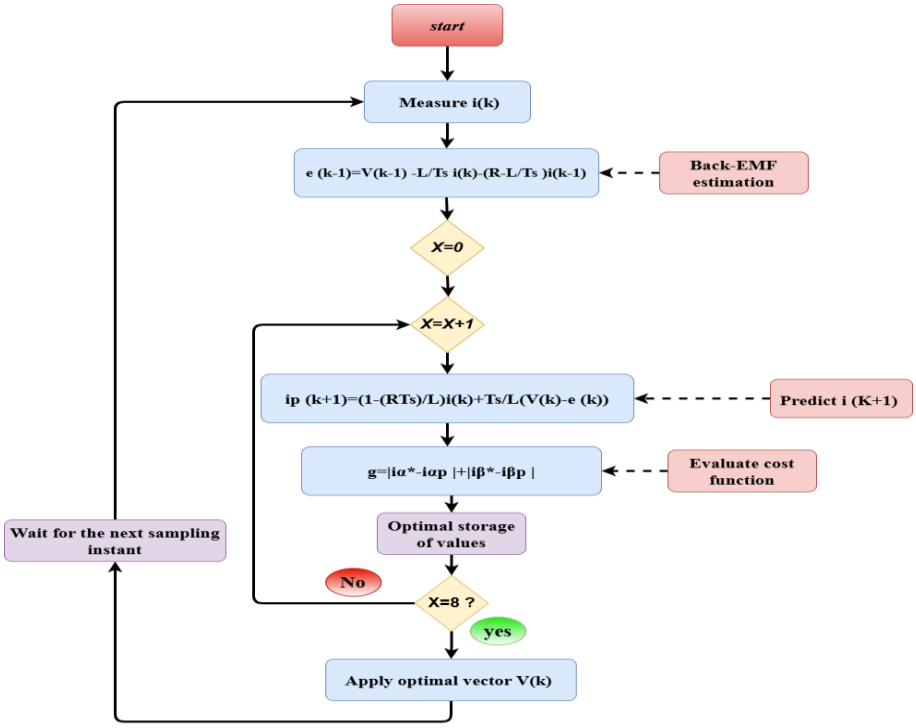

Fig.4.10. Flowchart of Predictive Current Control

4. Simulation results

4.1. panel with boost converter by proposed method (FL-INC)

MATLAB Two different MPPT strategies a fixed step size INC MPPT and a variable step size INC MPPT using a proposed FL controller are simulated and contrasted using Simulink. Fig.4.8 shows the system under investigation. To demonstrate the effectiveness of the suggested method, this system is evaluated under varying sun irradiation (1000, 700, and 900 W/m2), as shown in Fig.4.9. When comparing the proposed modified INC based on FL and variable step size to the conventional INC with fixed step size voltage consumption, there is a moderate efficiency difference favoring the conventional INC with fixed step size voltage in steady state. Fig.4.10 demonstrates the effectiveness of the suggested approach in increasing the output power in terms of settling time, rising time, and under/overshoot by comparing the two MPPT strategies that were studied. The output voltage Fig.4.11 and output current Fig.4.12 demonstrate the precision, dependability, and efficacy of the suggested approach. Table 4 illustrates the function of the proposed method by comparing it with three previously published methodologies.

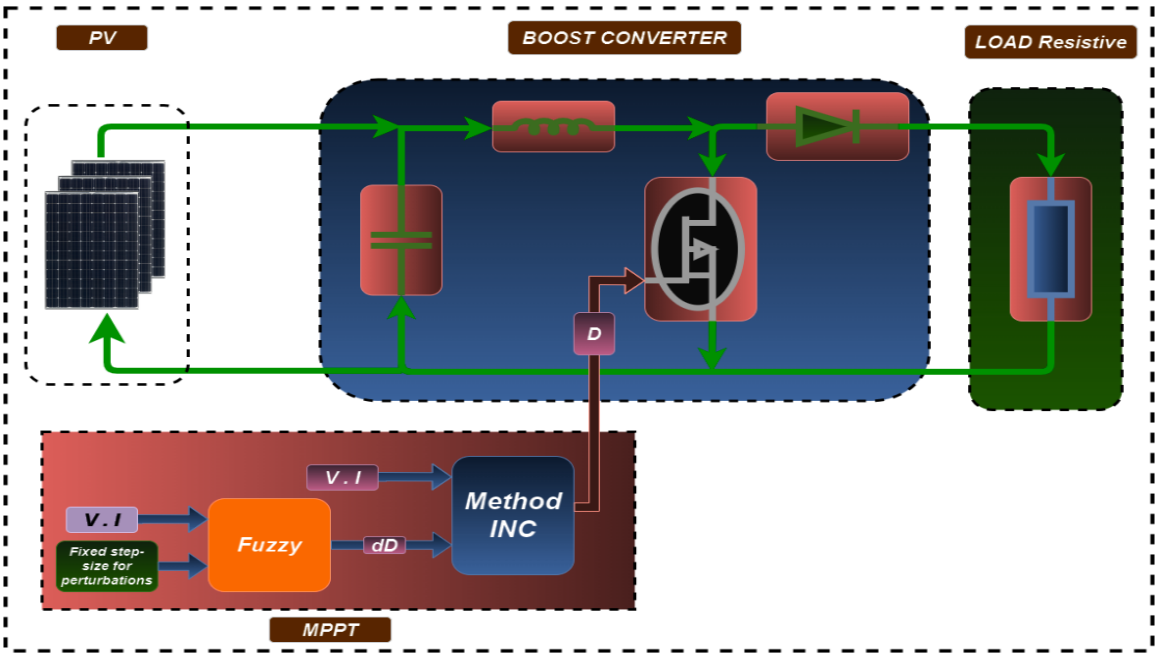

Fig.4.11. Block diagram of the MPPT algorithm testing experiment setup

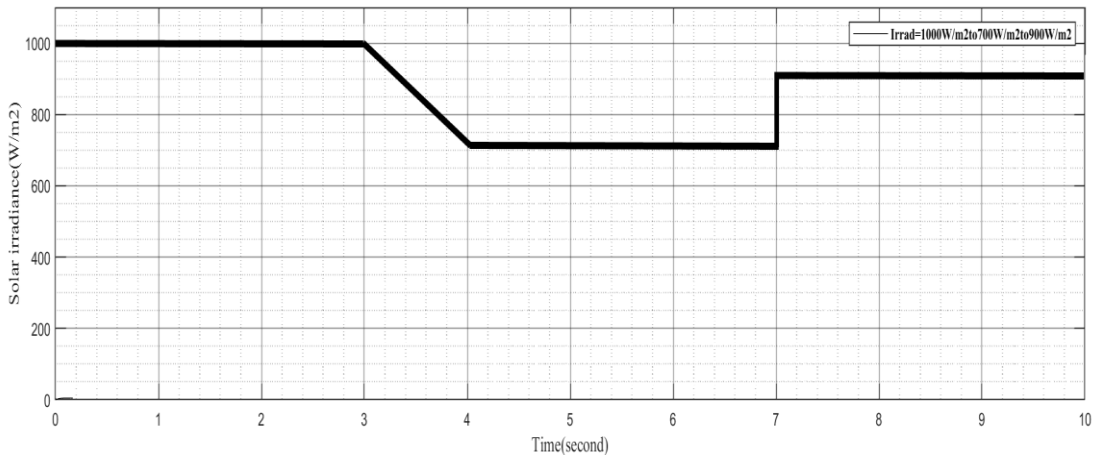

Fig.4.12. Change in solar irradiance (1000, 700 ,900 W/m2)

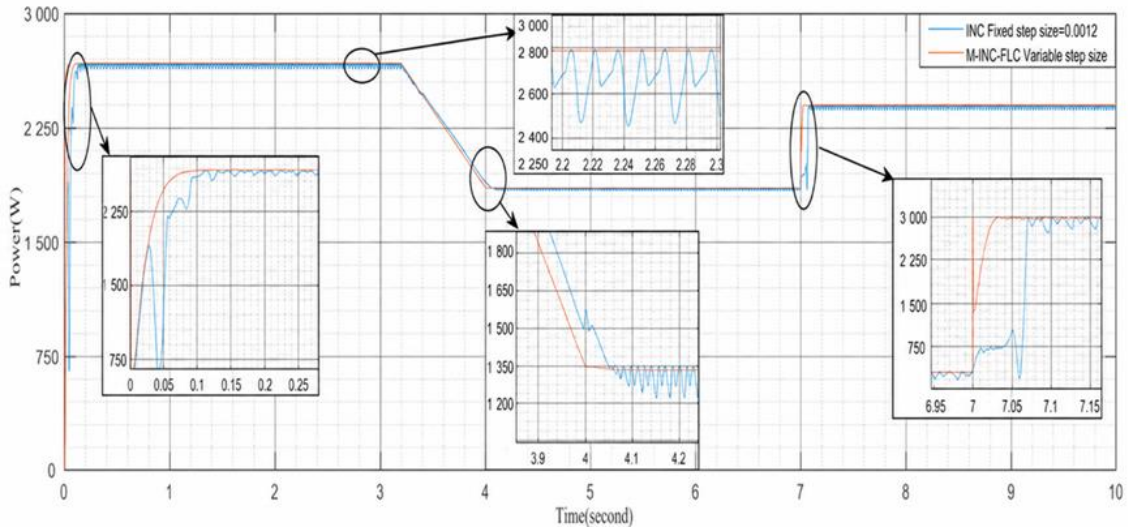

Fig.4.13. Output power under the two investigated methods.

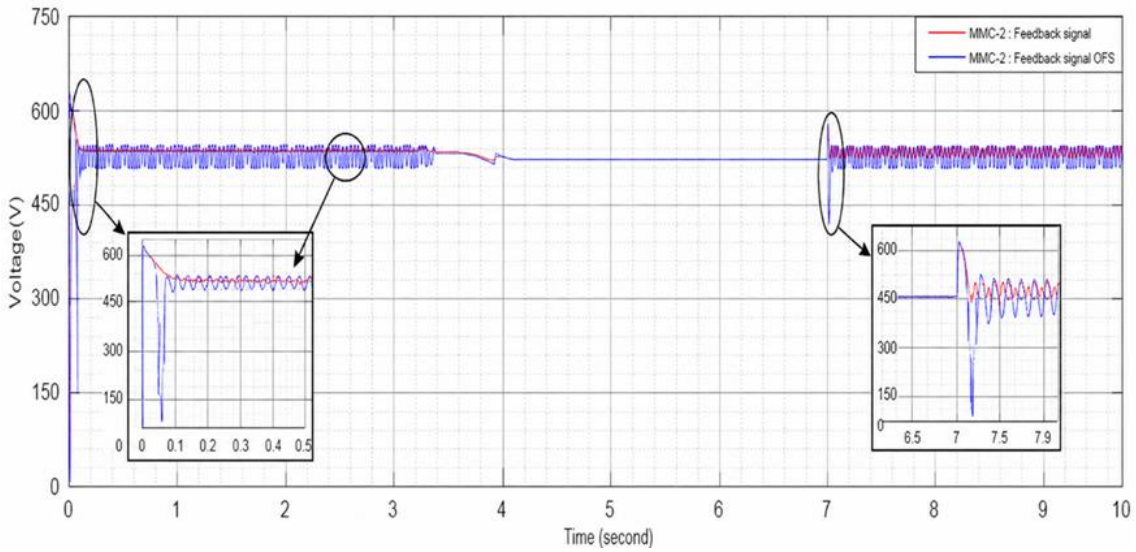

Fig.4.14. Output voltage under the two investigated methods.

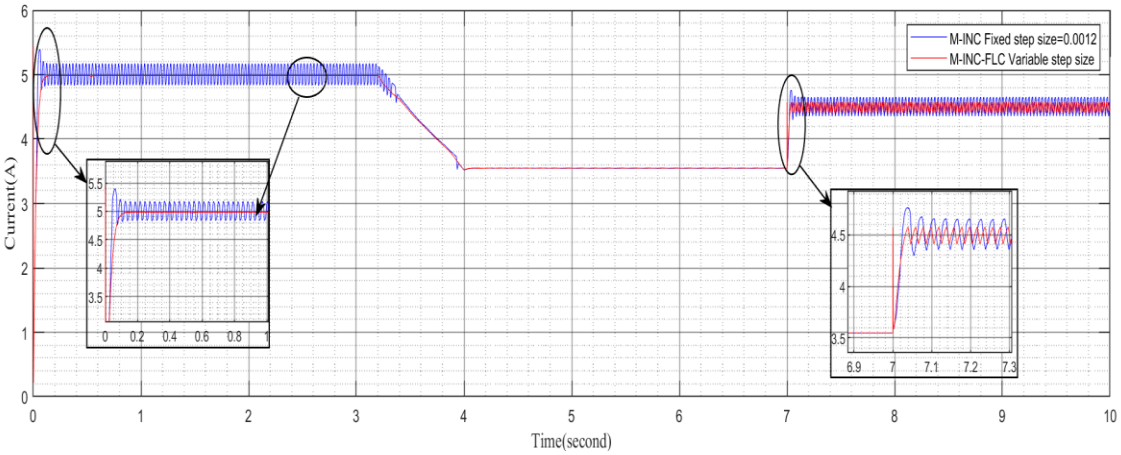

Fig.4.15. Output current under the two investigated methods.

Table.4.3. Comparison of several methods to determine the MPP

Methods / Standards	Traditionnel Methods		Improuve traditionnel Methods	
	P&O[8]	**INC** [9]	**P&O-Fuzzy** [10, 11]	**INC-Fuzzy (proposed)**
Working principle	It relies on a fixed step in changing the voltage	It relies on a fixed step in changing the voltage	It is based on a variable step in changing the voltage ΔV(k)	It is based on a variable step in changing the ΔD(k)
tracking time	Slow response	Slow response	Quick response	Quick response
Oscillation	Significant	Significant	Low	Very low
Work in shade control	Does not work /	Does not work /	It responds Indirect control	It responds Direct control

These data were gathered using SMA Sunny WebBox from the PEARL laboratory. The data was collected between 12:00 am and 12:55 pm. The data for this study was collected from 7:00 am to 7:00 pm. A actual sample's lighting intensity fluctuations over time are displayed in Table 5 below. The illumination intensity level corresponding to each time unit is represented by the parameter G in this system, while time intervals, represented by the letter T, are fixed at five minutes each. Fig. 4.13 shows actual changes in irradiance over time that have been studied.

The output power using the suggested method is shown over time in Fig. 4.14, where it successfully tracks the input irradiance.

Table.4.4. Historical irradiance data from PEARL grid-connected PV system

T	G	T	G	T	G	T	G	T	G	T	G
1	1	23	63.4	45	284	67	1000.06	89	493.5	112	11.56
2	1	24	63.62	46	327.19	68	953.65	90	699.56	113	11
3	1	25	66.64	47	471.75	69	1070.37	91	629.25	114	15.38
4	1.63	26	72.96	48	481.29	70	1066.48	92	643.16	115	21.96
5	2.31	27	73.56	49	506.63	71	971	93	678.97	116	28.04
6	5.41	28	76.35	50	586.7	72	412.76	94	845.81	117	38.36
7	11.46	29	232.79	51	627.81	73	421.33	95	736.59	118	47.46
8	16.76	30	380.19	52	644.32	74	584.52	96	824.97	119	58.15
9	21.65	31	395.44	53	451.31	75	424.31	97	521.42	120	54.5
10	25.56	32	382.5	54	357.23	76	418.77	98	234.28	121	54.12
11	28.96	33	363.9	55	476.41	77	437.44	99	190.1	122	51.35
12	31.2	34	404.16	56	762.65	78	332.84	100	154.52	123	37.42
13	33.36	35	494.69	57	812.56	79	281.71	101	68.66	124	39.88
14	37.08	36	502.32	58	799.55	80	336	102	38.7	125	41.44
15	42.12	37	526.78	59	709.53	81	375.73	103	20.22	126	40.88
16	49.32	38	557.32	60	564.22	82	406.23	105	8.33	127	37.31
17	56.4	39	595.19	61	348	83	489.21	106	4.63	128	30.77
18	61.6	40	629	62	352.61	84	490.29	107	845.81	129	24.24
19	64.36	41	630.61	63	389.48	85	383.5	108	736.59	130	17.29
20	65.23	42	536.03	64	520.32	86	394.9	109	4.33	131	16.78
21	68	43	287.94	65	989.97	87	402.59	110	6.94	132	14.54
22	64.92	44	323.25	66	1065.25	88	405.26	111	11.46	133	13.42

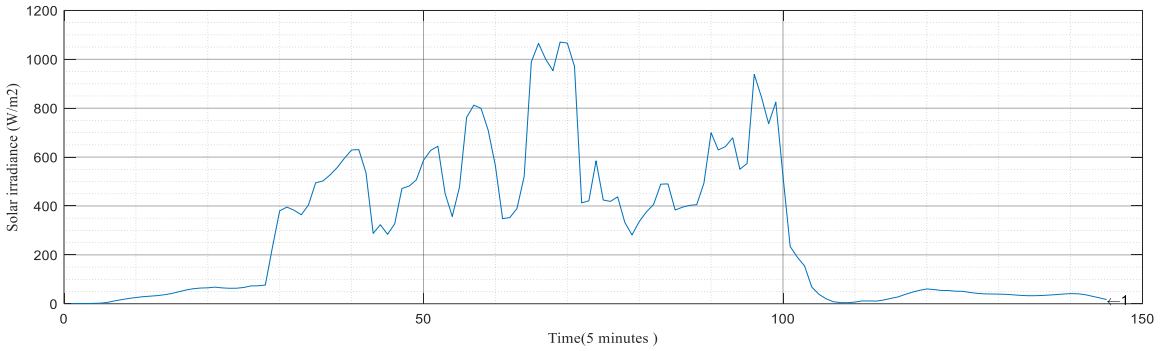

Fig.4.16. Changes in irradiance over time

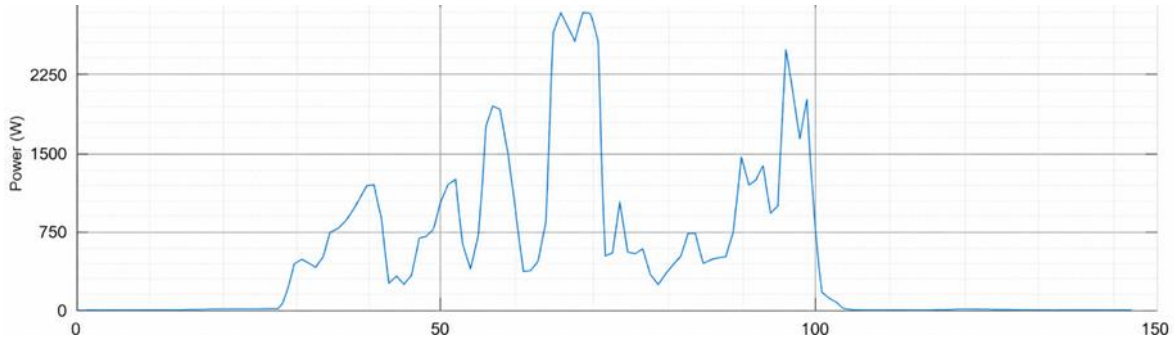

Fig.4.17. Output power over time with the proposed method

This work introduces M-INC, a unique MPPT algorithm implementation that uses the FL controller with variable step size. The goal is to overcome the limitations of traditional MPPT techniques, which are typified by preset step sizes. A simulation circuit has been used to validate the proposed M-INC MPPT approach. The simulation's findings indicate that the suggested approach provides a faster reaction time and less fluctuation around the MPP in a steady condition. The suggested FL-based Variable Step Size INC MPPT method may efficiently balance the trade-off between decreasing variability in PV array output power around the MPP and accelerating convergence to it. This eliminates many of the drawbacks of fixed step size MPPT techniques. The system is tested on an actual sample, and the outcomes are confirmed by contrasting how the system responds to the sample data.

NPC inverter with grid :

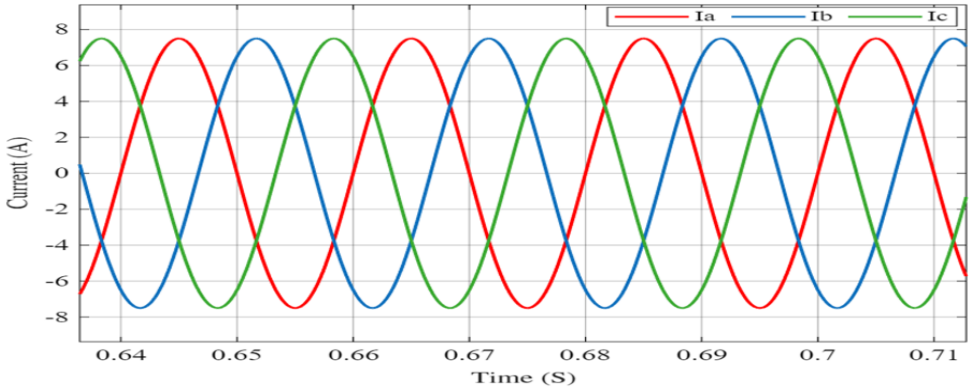

Fig.4.18. Source current reference 3 identical phases and a phase shift of 120 degrees

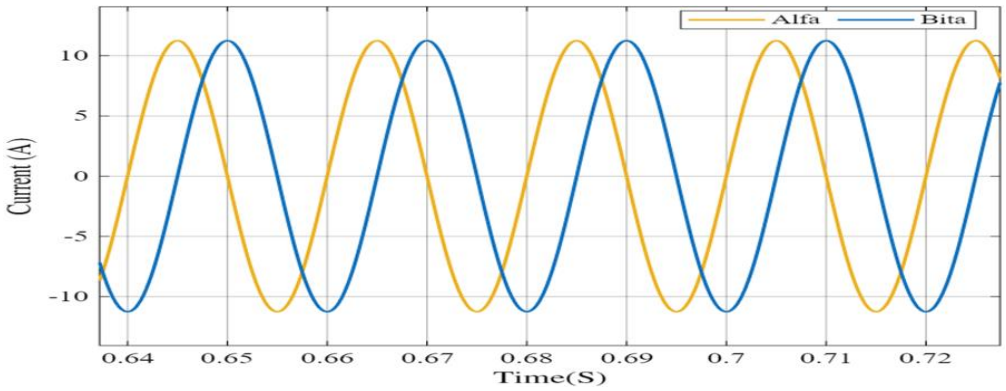

Fig.4.19. Clarke transformation reference (α, β)

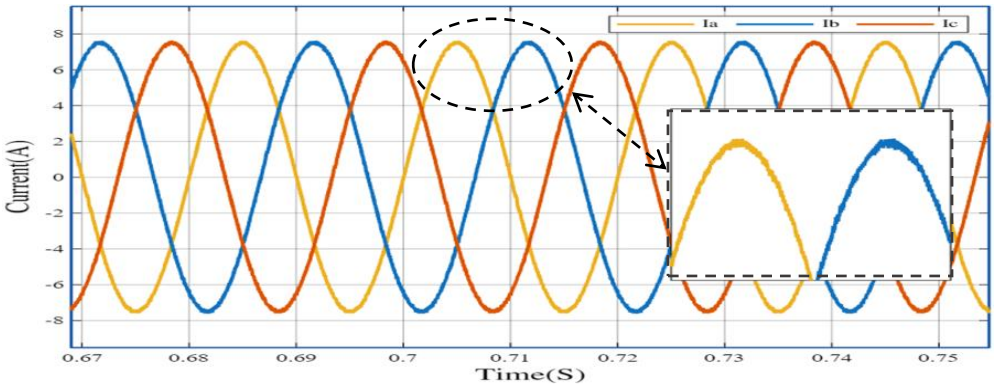

Fig.4.20. Source current 3 identical phases and a phase shift of 120 degrees

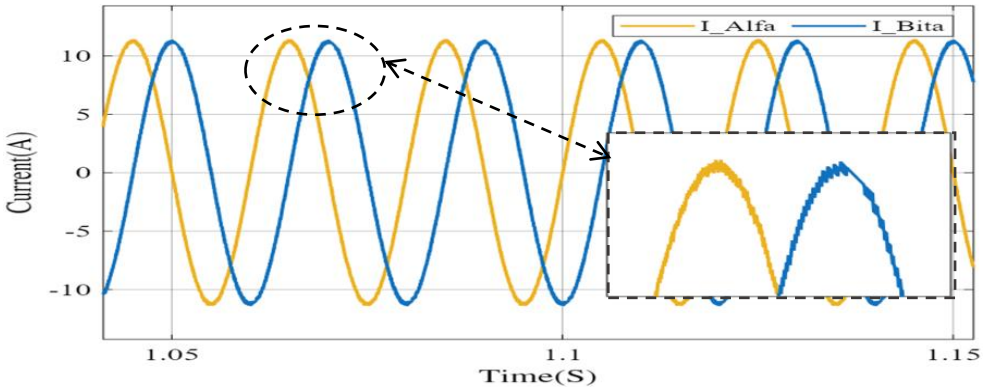

Fig.4.21. Clarke transformation (α, β)

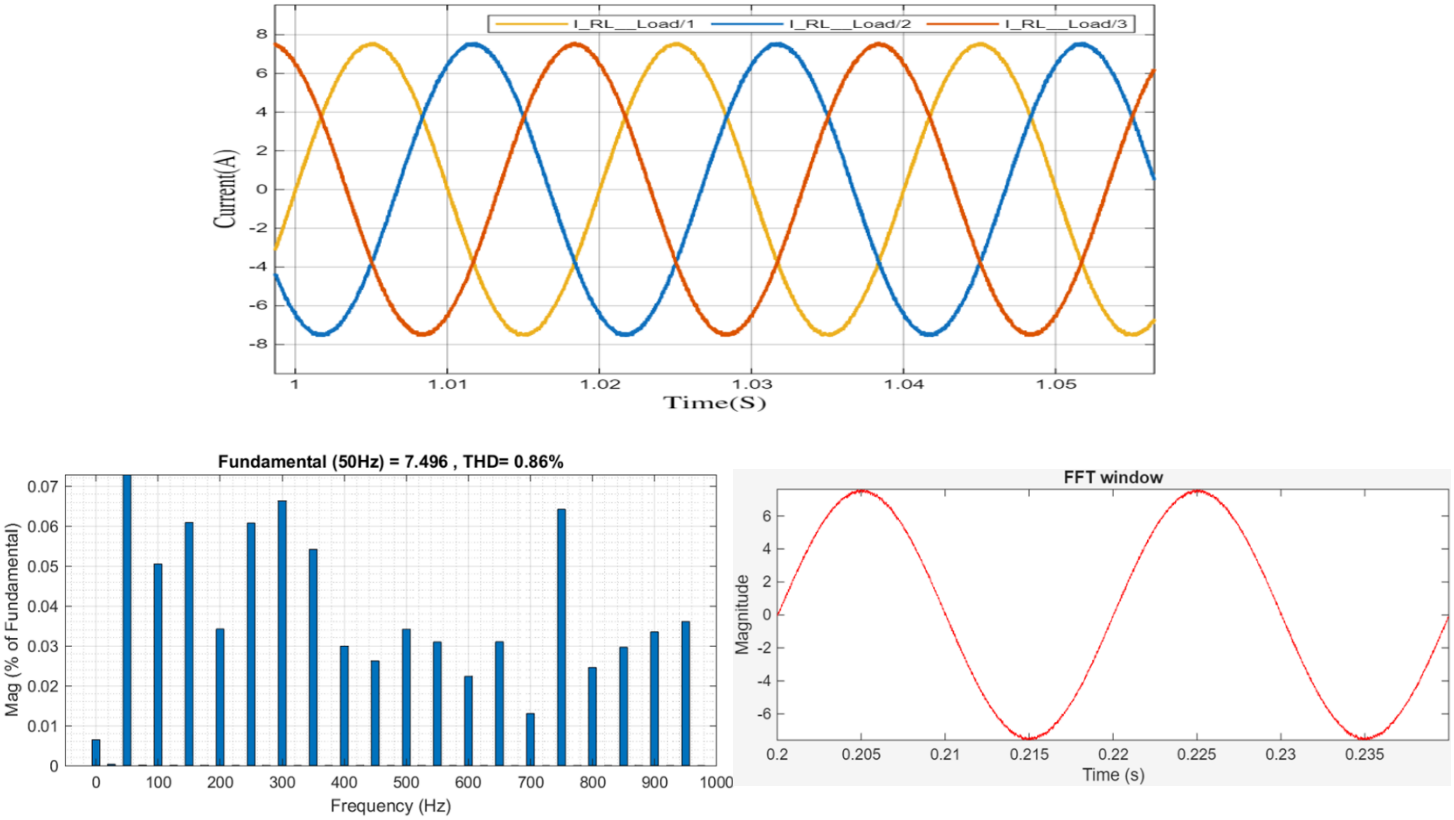

Fig.4.22. The current of a three-phase inverter

Current THD of 0.86%: Such a low THD indicates low harmonic distortion in the measured current. This

is generally considered a good result, as low harmonic distortion indicates a current waveform close to a

pure sine wave.

Maximum current value (Imax) of 7.5A: This indicates the highest peak reached by the current during the simulation.

Minimum current value (Imin) of -7.5A: This indicates the lowest peak reached by the current during the simulation.

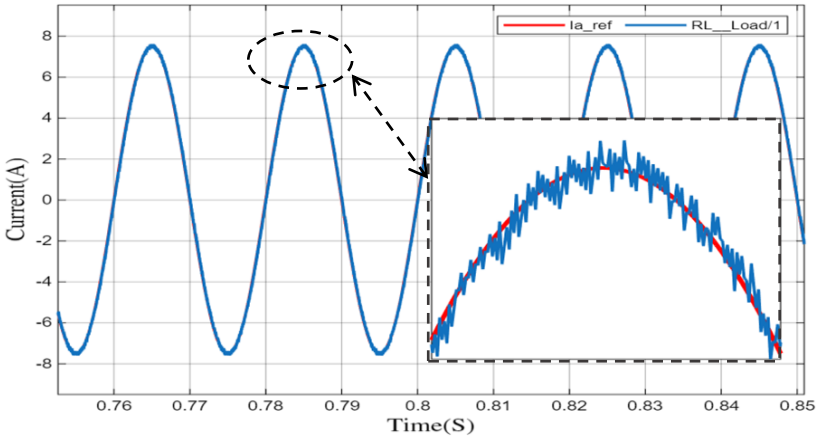

Fig.4.23. Converter Current Charge RL

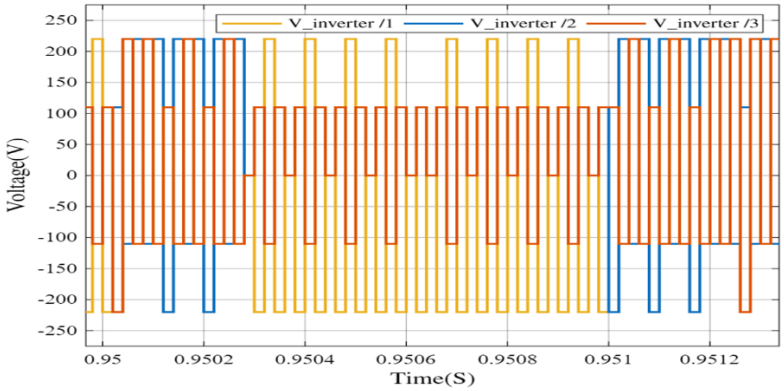

Fig.4.24. Inverter voltage

The detail performance of proposed MPPT under diverse temperature and illumination change, it can be noted

that the output power of the PV array, according to Fig.4.13 indicates proximity of the point of maximum power.

As see in Fig.4.18 the reference currents, the model predictive current control

has the ability of fast current regulation and guarantee the output currents to meet the grid requirements.

Furthermore, the currents (α, β) track their references with a very good performance in the steady state and in the transient in Fig.4.19

The numerical simulation results, driven by grid-connected photovoltaic inverters, ensure good dynamic tracking of peak power (MPP) and excellent quality of output current as shown in Fig.4.23.

5. Conclusion

A novel method for putting the MPPT algorithm into practice is presented in this chapter. The method made use of a FL controller known as M-INC, which has a configurable step size. The objective is to get over the fixed step size restrictions of conventional MPPT techniques. An FL-INC MPPT technique was proposed and validated using a simulation circuit. According to the results of the simulation, the recommended method reduces the steady-state oscillation around the MPP and offers a quicker reaction time. The Variable Step Size INC MPPT P&O algorithm based on FL, which has been supported, provides the opportunity to appropriately balance the trade-off between faster convergence to the MPP and reducing variability in PV array output power around it. This tactic successfully reduces some of the limitations of fixed step size MPPT techniques. The system is evaluated using a genuine specimen, and the accuracy of the system's response is verified by comparing it with the data from the sample. For the PEARL grid-connected PV system, a comparison of the suggested FL-INC MPPT method with three alternative MPPT techniques—P&O, INC, and P&O-fuzzy—was also carried out. The comparisons show that, as compared to the three other approaches, the proposed MPPT technique successfully monitored the MPP. In addition, the MPP was attained quickly and with little power variations.

Model Predictive Control (MPC) is a strong and adaptable control approach that provides a number of benefits for managing multivariable systems with restrictions. MPC allows for better performance, resilience, and constraint management than conventional control techniques by employing a dynamic model to forecast future system behavior and optimizing control actions over a finite horizon. It's particularly useful in complicated energy systems since it can adapt to changing conditions and include real-time feedback.

Reference

[1] G. Bayrak and D. Ghaderi, "An improved step-up converter with a developed real-time fuzzy-based MPPT controller for PV-based residential applications," *International Transactions on Electrical Energy Systems,* vol. 29, no. 12, p. e12140, 2019.

[2] R. Kumar and S. Singh, "Solar photovoltaic modeling and simulation: As a renewable energy solution," *Energy Reports,* vol. 4, pp. 701–712, 2018.

[3] S. M. Ebrahimi, E. Salahshour, M. Malekzadeh, and F. Gordillo, "Parameters identification of PV solar cells and modules using flexible particle swarm optimization algorithm," *Energy,* vol. 179, pp. 358–372, 2019.

[4] N. Femia, G. Petrone, G. Spagnuolo, and M. Vitelli, "Optimization of perturb and observe maximum power point tracking method," *IEEE transactions on power electronics,* vol. 20, no. 4, pp. 963–973, 2005.

[5] G.-I. Giurgi, L. A. Szolga, and D.-V. Giurgi, "Benefits of fuzzy logic on MPPT and PI controllers in the chain of photovoltaic control systems," *Applied Sciences,* vol. 12, no. 5, p. 2318, 2022.

[6] N. Mohan *et al.*, "Restructuring of first courses in power electronics and electric drives that integrates digital control," *IEEE Transactions on power electronics,* vol. 18, no. 1, pp. 429–437, 2003.

[7] J. Rodriguez *et al.*, "Predictive current control of a voltage source inverter," *IEEE transactions on industrial electronics,* vol. 54, no. 1, pp. 495–503, 2007.

[8] A. Harrison, N. H. Alombah, and J. de Dieu Nguimfack Ndongmo, "A new hybrid MPPT based on incremental conductance-integral backstepping controller applied to a PV system under fast-changing operating conditions," *International Journal of Photoenergy,* vol. 2023, no. 1, p. 9931481, 2023.

[9] J. Macaulay and Z. Zhou, "A fuzzy logical-based variable step size P&O MPPT algorithm for photovoltaic system," *Energies,* vol. 11, no. 6, p. 1340, 2018.

[10] O. Kukrer, "Discrete-time current control of voltage-fed three-phase PWM inverters," *IEEE Transactions on Power Electronics,* vol. 11, no. 2, pp. 260–269, 2002.

[11] P. Mutschler, "A new speed-control method for induction motors," in *Proc. Conf. Rec. PCIM*, 1998, pp. 131–136.

[12] H. Yang, M. Li, Y. Zhang, and A. Xu, "FCS-MPC for three-level NPC inverter-fed SPMSM drives without information of motor parameters and DC capacitor," *IEEE Transactions on Industrial Electronics,* vol. 71, no. 4, pp. 3504–3513, 2023.

[13] I. Harbi *et al.*, "Model-predictive control of multilevel inverters: Challenges, recent advances, and trends," *IEEE Transactions on Power Electronics,* vol. 38, no. 9, pp. 10845–10868, 2023.

[14] T. Mish-Al, K. K. Nanda, and K. R. V. Mahesh, "Modeling of fuzzy logic based MPPT for PV array in Simulink/MATLAB," in *AIP Conference Proceedings*, 2022, vol. 2452, no. 1: AIP Publishing LLC, p. 040007.

[15] K. Ullah, M. Ishaq, F. Tchier, H. Ahmad, and Z. Ahmad, "Fuzzy-based maximum power point tracking (MPPT) control system for photovoltaic power generation system," *Results in Engineering,* vol. 20, p. 101466, 2023.

[16] O. M. Lamine *et al.*, "A Combination of INC and Fuzzy Logic-Based Variable Step Size for Enhancing MPPT of PV Systems," *International Journal of Robotics & Control Systems,* vol. 4, no. 2, 2024.

General Conclusions

We presented in this thesis an improved Maximum Power Point Tracking (MPPT) method based on a Fuzzy Logic (FL) controller with a variable step size, referred to as the Modified Incremental Conductance (M-FL-INC) algorithm. Unlike conventional MPPT techniques that rely on fixed step sizes often resulting in either slow response times or significant oscillations around the Maximum Power Point (MPP) the proposed method dynamically adjusts the step size according to real-time system conditions. This adaptive approach aims to balance the trade-off between fast convergence to the MPP and minimal steady-state power fluctuations. Simulation results confirm that the M-FL-INC method achieves faster response times and reduces oscillations in the output power of the photovoltaic (PV) system, thereby increasing tracking efficiency. The system's performance is further validated using real-world sample data, against which the algorithm's behavior is compared. These improvements directly address one of the key challenges in PV systems: the inefficiency introduced by unstable or delayed MPPT responses, which can impair the inverter's ability to maintain high-quality DC-to-AC conversion. Although Space Vector Pulse Width Modulation (SVPWM) was initially used for inverter control, it failed to fully compensate for the fluctuations caused by fixed-step MPPT methods. To resolve this, the study integrates the enhanced M-FL-INC algorithm with Model Predictive Control (MPC) for the control of a Neutral Point Clamped (NPC) inverter. MPC is particularly well-suited to this application due to its predictive capabilities, which allow it to anticipate future system states and adjust control actions accordingly. Its flexibility in managing multiple inputs and constraints in real time ensures superior performance and grid compatibility, particularly in systems with high variability like those based on renewable energy. Together, the M-FL-INC algorithm and MPC-controlled inverter form a robust and adaptive control architecture that enhances overall system efficiency and stability in PV applications. Results from simulations using the MATLAB/Simulink software tools are used to confirm the accuracy and veracity of the modeling and management technique.

Future works

- Design and implementation of novel maximum power point tracking (MPPT) algorithms that account for the effects of partial shading conditions in photovoltaic (PV) systems.
- Extension and application of the proposed control methodologies to a range of advanced multilevel inverter topologies to enhance system performance.
- Comprehensive analysis and evaluation of DC-DC multilevel converter configurations for optimized integration in grid-connected PV systems.
- Development of advanced energy management and control strategies for hybrid energy systems comprising multiple sources in a grid-connected framework.
- Formulation of intelligent energy management techniques for effective grid interfacing, utilizing multilevel inverter architectures to improve reliability and efficiency.

Study of control techniques dedicated to micro-grid systems in the presence of renewable energy sources

Abstract

This thesis addresses the study of photovoltaic (PV) system topologies connected to the grid, along with energy management strategies for stand-alone PV systems. It also proposes a set of effective control strategies for grid-connected systems. However, these systems face several challenges, most notably the limitations associated with maximum power point tracking (MPPT) techniques, reduced accuracy in grid power control, and the decline in grid current quality.

To overcome these challenges, this work proposes an advanced strategy for MPPT control in order to regulate the performance of converters used in grid-connected PV topologies. A boost converter is employed to adjust and stabilize the input voltage to a three-level neutral-point-clamped inverter, ensuring efficient injection of the PV system's output current while maintaining capacitor voltage balance in the DC-link.

In this context, a simplified and effective algorithmic strategy has been developed by integrating fuzzy logic with a control algorithm for the converter. Simulation results demonstrated the accuracy and reliability of the proposed control strategies in enhancing the performance of the studied grid-connected PV topology.

Keywords: Grid-connected photovoltaic systems, multilevel converters, maximum power point tracking (MPPT), predictive control, fuzzy logic.

Etude des techniques de contrôle dédiées aux systèmes micro-réseaux en présence des sources d'énergies renouvelables

Résumé

Cette thèse porte sur l'étude des topologies des systèmes photovoltaïques (PV) raccordés au réseau, ainsi que sur les stratégies de gestion de l'énergie pour les systèmes photovoltaïques autonomes. Elle propose également un ensemble de stratégies de commande efficaces pour les systèmes connectés au réseau. Toutefois, ces systèmes sont confrontés à plusieurs défis, notamment les limites liées aux techniques de poursuite du point de puissance maximale (MPPT), la faible précision du contrôle de la puissance injectée au réseau, ainsi que la dégradation de la qualité du courant du réseau.

Afin de surmonter ces défis, ce travail propose une stratégie avancée de commande MPPT visant à réguler les performances des convertisseurs utilisés dans les topologies photovoltaïques raccordées au réseau. Un convertisseur élévateur est employé pour ajuster et stabiliser la tension d'entrée d'un onduleur multiniveaux à trois niveaux, fixé au point neutre, afin d'assurer une injection efficace du courant issu du système photovoltaïque, tout en maintenant l'équilibre des tensions des condensateurs du bus continu.

Dans ce cadre, une stratégie algorithmique simplifiée et efficace a été développée, intégrant la logique floue avec un algorithme de commande pour le convertisseur. Les résultats de simulation ont démontré la précision et la fiabilité des stratégies de commande proposées pour améliorer les performances de la topologie photovoltaïque raccordée au réseau étudié.

Mots-clés : Systèmes photovoltaïques raccordés au réseau, convertisseurs multiniveaux, poursuite du point de puissance maximale (MPPT), commande prédictive, logique floue.

دراسة تقنيات التحكم المخصصة لأنظمة الشبكات المصغّرة في وجود مصادر الطاقة المتجددة

الملخص

تتناول هذه الأطروحة دراسة طوبولوجيا الأنظمة الكهروضوئية المتصلة بالشبكة ، إلى جانب استراتيجيات إدارة الطاقة للأنظمة الكهروضوئية المستقلة .كما تقترح مجموعة من استراتيجيات التحكم الفعّالة الخاصة بالأنظمة المتصلة بالشبكة .ومع ذلك، تواجه هذه الأنظمة عدة تحديات، من أبرزها القيود المرتبطة بتقنيات التتبع الأقصى لنقطة القدرة ، وضعف دقة التحكم في طاقة الشبكة، إضافة إلى تراجع جودة تيار الشبكة.

وللتغلب على هذه التحديات، يقترح هذا العمل اعتماد استراتيجية متقدمة للتحكم في تتبع الأقصى لنقطة القدرة بغرض تنظيم أداء المحولات المستخدمة في الطوبولوجيا الكهروضوئية المتصلة بالشبكة .كما تم استخدامحول رافع لضبط و استقرار الجهد الداخل الى عاكس ثلاثي المستويات مثبت عند النقطة المحايدة لضمان حقن التيار الناتج عن النظام الكهروضوئي بكفاءة، مع المحافظة على توازن جهود مكثف وصلة التيار المستمر.

في هذا الإطار، تم تطوير استراتيجية خوارزمية مبسطة وفعّالة تعتمد على دمج المنطق الضبابي مع خوارزمية للتحكم في محول ، حيث أظهرت نتائج المحاكاة دقة وموثوقية استراتيجيات التحكم المقترحة في تحسين أداء الطوبولوجيا الكهروضوئية المتصلة بالشبكة قيد الدراسة.

الكلمات المفتاحية: الأنظمة الكهروضوئية المتصلة بالشبكة، المحولات متعددة المستويات، التتبع الأقصى لنقطة القدرة ، التحكم التنبؤي ، المنطق الضبابي